

**Preliminary evidence that prenatal maternal choline  
supplementation protects the white matter microstructure  
of infants born to heavy-drinking women**



by

Oreneile Maiphetho

MPHORE001

SUBMITTED TO THE UNIVERSITY OF CAPE TOWN

In fulfilment of the requirements for the degree

MSc in Biomedical Engineering

**Faculty of Health Sciences  
UNIVERSITY OF CAPE TOWN**

**Supervisor: Professor Ernesta Meintjes**

**Co-supervisor: Dr Fleur Warton**

The copyright of this thesis vests in the author. No quotation from it or information derived from it is to be published without full acknowledgement of the source. The thesis is to be used for private study or non-commercial research purposes only.

Published by the University of Cape Town (UCT) in terms of the non-exclusive license granted to UCT by the author.

# Declaration

I, Oreneile Maiphetlho, hereby declare that the work on which this dissertation/thesis is based is my original work (except where acknowledgements indicate otherwise) and that neither the whole work nor any part of it has been, is being, or is to be submitted for another degree in this or any other university.

I empower the university to reproduce for the purpose of research either the whole or any portion of the contents in any manner whatsoever.

Signed by candidate

Signature: .....

Date: 12/01/2024

# Acknowledgements

I would like to thank my supervisor, Professor Ernesta Meintjes, for her patience, support and encouragement throughout this process. I have appreciated all the assistance and guidance I have received, and I am truly grateful for everything I have learned. Your constant availability and reassurance made it easier for me to approach with any questions that may have seemed simplistic. I would also like to thank my co-supervisor, Dr Fleur Warton, for her assistance and advice in areas of anatomy I did not understand. I am also utterly grateful for your support and availability. This project would not be what it is without either of you.

I would like to thank everyone in the MRI group for their assistance and encouragement. An enormous thanks to Ndivhuwo Magondo for all her time and guidance through the processing steps, troubleshooting and coding. Thank you to everyone in the group for keeping my spirits up and making each day better than the last.

I would like to thank all my friends for encouraging me and being there for me in some of the hardest times.

Finally, I would like to thank my family for motivating me throughout and providing me with the reassurance that I should “keep doing what I am doing”. Thank you for your undivided encouragement and patience, your support has meant the world.

## Abstract

Prenatal alcohol exposure (PAE) is the most widespread preventable cause of neurocognitive and neurodevelopmental disabilities worldwide, known collectively as fetal alcohol spectrum disorders. It has been shown in a small double-blind, randomized choline supplementation trial that prenatal maternal choline supplementation reduces PAE-related postnatal growth restrictions, cognitive deficits, and regional brain volume reductions in infants born to heavy-drinking women. The impact of prenatal maternal choline supplementation on white matter (WM) microstructure – an area particularly vulnerable to PAE – has not been assessed.

This project used diffusion tensor imaging (DTI) in 43 neonates born to heavy-drinking mothers enrolled in that choline supplementation trial to examine the effects of prenatal maternal choline supplementation on the microstructure of WM connecting select subcortical regions. Given that pre-myelination (at 30-40 weeks gestational age (GA)) and maturation of the axonal cytoskeleton are categorised by stable fractional anisotropy (FA), decreasing axial diffusivity (AD) and radial diffusivity (RD), we hypothesised that neonates with PAE whose mothers had received choline would demonstrate lower AD and RD than those in the placebo arm, and that lower AD and RD would be associated with better cognitive performance.

T1-weighted structural magnetic resonance (sMR) and diffusion tensor (DT) imaging (DTI) data were acquired for each neonate between 1-7 weeks postpartum on a 3T Siemens Allegra. Previously, 17 subcortical brain regions (ROIs) had been manually traced on sMR images in Freeview. After DTI pre-processing, the manually traced ROIs were transformed into the DTI space and used as seeds for full probabilistic tractography. FA, AD and RD were extracted for each identified connection. Visual recognition memory scores on the Fagen test of Infant Intelligence (FTII) assessed at 12 months were also available for 34 participants.

We examined differences in the DTI measures between the choline and placebo groups, as well as associations of DTI measures with choline dose and FTII scores using robust linear regression. Choline dose was approximated in 2 ways: (1) using maternal treatment adherence (in % packets consumed), with choline dose set to zero for infants in the placebo arm, and (2) computing the total choline (in grams) consumed by the mothers throughout participation in the study (enrolment through to delivery).

A total of 22 neonates (14 choline; 11 boys; mean GA (SD) = 41.8 (2.0) weeks) provided usable, non-biased DTI data and FTII scores were available for 14 of these neonates (8 choline). We examined treatment effects in 15 WM connections that were present in a least 85 % of the neonates. Three neonates in the choline arm whose mothers had low treatment adherence (< 50 %) were excluded from the group difference analyses. Additionally, one

choline-treated participant whose average AD value introduced bias was excluded from all analyses that included the DTI measures.

After controlling for confounders, FA in the WM connection between the caudate and pallidum on the left was lower in the choline group ( $p = 0.023$ ) and on the right was inversely associated with choline dose – both in % packets consumed ( $\beta (\epsilon) = -0.55 (0.20)$ ;  $p = 0.016$ ) and in grams ( $\beta (\epsilon) = -0.51 (0.20)$ ;  $p = 0.024$ ). Moreover, increasing choline dose – in % packets consumed and in grams – was associated with lower AD in 2 WM connections: between the right caudate and right putamen, and right putamen and right pallidum ( $|\beta|$ 's  $> 0.40$ ;  $p$ 's  $< 0.05$ ). Finally, better visual recognition memory on the FTII was associated with lower RD ( $\beta (\epsilon) = -0.62 (0.27)$ ;  $p = 0.038$ ) in the connection between the left and right thalami, and with higher RD ( $\beta (\epsilon) = 0.54 (0.18)$ ;  $p = 0.009$ ) in the WM connection between the right caudate and right putamen.

Although choline-related decreases in FA were observed in the connection between the right caudate and right pallidum, the choline-related decreases in AD in the caudate, putamen and pallidum on the right aligned with our hypothesis. Studies of participants with Williams syndrome and attention-deficit/hyperactivity disorder have speculated that the lower FA observed in their control groups may be accredited to higher levels of axonal branching. Given that choline promotes axonal growth and branching in rodent models, the lower FA observed here may be indicative of choline-related increases in axonal branching in the caudate to pallidum connections.

Studies of postnatal WM development have found that AD and RD decrease during the first postnatal year. Given that AD provides information on axonal integrity and organization, the age-related decreases for AD have been accredited to increases in axonal growth. Human studies have demonstrated increases in fibre cross-sections in the first 6 months of life and animal studies have shown the importance of choline in axonal growth and elongation. Thus, the choline-related reductions in AD in connections between the caudate, putamen and pallidum on the right suggest accelerated brain development through the promotion of axonal growth in these WM connections. Axonal pruning may also contribute to decreases in AD.

Growth-related increases in axonal diameter may explain the association of higher RD seen in the same connection, right caudate to right putamen, with better visual recognition memory. The negative association between visual recognition memory and RD in the connection between the left and right thalami aligns with our hypothesis and several studies conducted in infants, children and adults.

These results provide preliminary evidence that choline is associated with the microstructural properties of subcortical WM connections, specifically between the caudate, putamen and

pallidum, which are regions known to be affected by PAE. These findings need to be replication in a larger sample and with unexposed controls. Further research is required to examine the impact of prenatal maternal choline supplementation on cortical WM.

# Table of Contents

<b>1. Introduction</b>	<b>1</b>
1.1. Prenatal Alcohol Exposure (PAE)	1
1.1.1. Fetal Alcohol Spectrum Disorders (FASD)	1
1.1.2. Adverse effects of PAE	1
1.1.3. Interventions for PAE and FASD	3
1.2. Choline	4
1.2.1. Dietary choline intake	4
1.2.2. Beneficial effects of choline supplementation in the context of PAE	5
Animal studies	5
Human studies	5
1.2.3. Effects of choline on white matter (WM) integrity	6
1.3. Assessing neonatal white matter (WM) integrity	7
1.4. Aim & hypotheses	7
<b>2. Background</b>	<b>11</b>
2.1. Fetal alcohol spectrum disorders (FASD)	11
2.2. Fetal white matter (WM) development	11
2.3. Diffusion tensor imaging (DTI)	14
2.3.1. Principles of DTI	14
2.3.1. DTI measures	17
2.3.2. Challenges associated with analysing neonatal brain images	18
2.3.3. Analysing neonatal brain images	19
2.3.4. Tractography	20
2.3.5. Software packages used in this project	21
2.3.6. Early-developing WM detected with DTI and tractography	22
2.4. Assessments of infant cognitive performance	23
2.4.1. Eyeblick Conditioning (EBC)	23
2.4.2. Fagan Test of Infant Intelligence (FTII)	23
2.5. Statistical analyses	24
2.5.1. Analysis of group differences	24
2.5.2. Linear regression analysis	25
<b>3. Materials and Methods</b>	<b>27</b>
3.1. Study sample	27
3.2. MRI data acquisition	29
3.3. Structural MR image processing	30
3.3.1. Synthesising optimal contrast volumes	30
3.3.2. Manual tracing/segmentation of regions of interest (ROIs)	31

3.4. Diffusion tensor imaging (DTI) data .....	31
3.5. Tractography .....	34
3.5.1. Transforming the ROIs to the DTI space.....	34
3.5.2. Running the tractography.....	36
3.6. Statistical analyses.....	37
3.6.1. Potential confounders .....	39
Rational reasoning.....	40
Collinearity (Table B.1 in Appendix B).....	40
Associations with outcomes.....	41
3.6.2. Group differences .....	42
3.6.3. Regression analyses .....	43
<b>4. Results.....</b>	<b>44</b>
4.1. Sample characteristics .....	44
4.2. Additional exclusions due to potential bias on DTI measures .....	49
4.3. Potential confounders.....	49
4.4. Group differences in the total number of WM connections.....	51
4.5. Treatment effects on WM microstructure .....	51
4.5.1. Group differences .....	51
4.5.2. Associations with choline dose .....	57
Choline dose approximated by treatment adherence .....	57
Choline dose approximated by total grams consumed from enrolment through delivery .....	62
4.5.3. Summary of WM connections showing choline treatment effects.....	62
4.6. Associations of WM integrity with visual recognition memory on the FTII .....	62
<b>5. Discussion.....</b>	<b>66</b>
5.1. Treatment effects on WM microstructure .....	66
5.1.1. Effects of prenatal alcohol exposure (PAE).....	68
5.1.2. Connections between the caudate & pallidum .....	70
5.1.3. Previous studies examining effects of choline on WM.....	71
5.1.4. Connections between the putamen & caudate and putamen & pallidum ..	71
5.2. Associations of WM integrity with visual recognition memory on the FTII .....	72
5.2.1. Connection between the left & right thalami .....	73
5.2.2. Connection between the caudate & putamen.....	74
5.3. Limitations and future work.....	75
<b>6. Conclusion .....</b>	<b>76</b>
<b>Appendix A: Sample characteristics .....</b>	<b>77</b>
Comparing the included (n = 22) and excluded (n = 21) participants.....	77
Comparing the included (n = 21) and excluded (n = 22) participants.....	81

Comparing the choline- and placebo-treated groups for the 21 included participants .....	85
<b>Appendix B: Potential confounders .....</b>	<b>89</b>
<b>Appendix C: Treatment effects .....</b>	<b>90</b>
Choline dose approximated by treatment adherence .....	90
Choline dose approximated by total grams consumed from enrolment through delivery .....	91
<b>References .....</b>	<b>96</b>

# List of illustrations

## List of tables

<b>Table 1:</b> The damaging effects of PAE. ....	2
<b>Table 2:</b> Summary of studies that have shown effects of PAE on the subcortical regions of interest (ROIs).....	8
<b>Table 3:</b> Summary of functional domains showing PAE-related deficits.....	8
<b>Table 4:</b> Functional domains showing PAE-related deficits and PAE-affected subcortical regions involved in these functions.....	9
<b>Table 5:</b> Functional domains where choline-related improvements were observed in the RCT by Jacobson and colleagues and the PAE-affected subcortical regions involved in these functions. ....	10
<b>Table 6:</b> Primary diffusion tensor imaging (DTI) measures used to categorise WM microstructural integrity. ....	17
<b>Table 7:</b> The assumptions that need (✓) or do not need (x) to be met for different tests that compare the means between 2 independent groups.....	25
<b>Table 8:</b> Imaging parameters of the scanning sequences utilised for each neuroimaging modality. ....	30
<b>Table 9:</b> All the sample characteristics.....	39
<b>Table 10:</b> Maternal characteristics (n = 22).....	45
<b>Table 11:</b> Maternal substance use (n = 22).....	46
<b>Table 12:</b> Neonatal birth characteristics and FASD diagnosis (n = 22). ....	47
<b>Table 13:</b> Neonatal scan characteristics (n = 22).....	48
<b>Table 14:</b> The number of WM connections in which each potential confounder showed a weak association (at $p < 0.1$ ) with the different WM outcomes being examined (FA, AD or RD in each of the 15 WM connections). Infant sex, postnatal age at scan and TIV each showed weak associations with at least 14 (> 30 %) of the WM outcomes being assessed (in bold).....	50
<b>Table 15:</b> Comparison by treatment group of fractional anisotropy (FA) in the 15 WM connections present in $\geq 85$ % of participants. ....	52
<b>Table 16:</b> Comparisons by treatment group of the mean axial diffusivity (AD) in the 15 WM connections present in $\geq 85$ % of participants. ....	54
<b>Table 17:</b> Comparisons by treatment group of the mean radial diffusivity (RD) in the 15 WM connections found in $\geq 85$ % of participants. ....	56
<b>Table 18:</b> Associations of fractional anisotropy (FA) in each WM connection with choline treatment adherence (in % choline packets consumed) as a proxy for choline dose while controlling for potential confounding by infant sex and postnatal age at scan, total intracranial volume (TIV), and a possible dose-by-sex interaction effect.....	58

**Table 19:** Associations of axial diffusivity (AD) in each WM with maternal choline treatment adherence (in % packets consumed as a proxy for choline dose), controlling for infant sex, postnatal age at scan , total intracranial volume (TIV) and after and a dose-by-sex interaction effect..... 60

**Table 20:** Associations of microstructural measures in each WM connection with visual recognition memory on the FTII. .... 64

## Appendix tables

**Table A.1.1 :** Maternal characteristics between the 22 included and 21 excluded participants.

**Table A.1.2:** Maternal substance use between the 22 included and 21 excluded participants.

**Table A.1.3:** Neonatal birth characteristics and FASD diagnosis between the 22 included and 21 excluded participants.

**Table A.1.4:** Neonatal scan characteristics between the 22 included and 21 excluded participants.

**Table A.2.1:** Maternal characteristics compared between the 21 participants who had usable DTI data and did not introduce bias on the DTI measures, and the 22 participants who were excluded.

**Table A.2.2:** Maternal substance use compared between the 21 participants who had usable DTI data and did not introduce bias on the DTI measures, and the 22 participants who were excluded.

**Table A.2.3:** Comparison of the neonatal birth characteristics and FASD diagnosis between the included 21 participants with usable DTI data and did not introduce bias on the DTI measures, and the excluded 22 participants.

**Table A.2.4:** Comparing the neonatal scan characteristics between the 21 participants who had usable DTI data and did not introduce bias on the DTI measures, and the 22 participants who were excluded.

**Table A.3.2:** Maternal substance use between the treatment groups after excluding the one choline-treated participant for whom using only AP data resulted in bias on the DTI measures (n = 21).

**Table A.3.3:** Neonatal birth characteristics and FASD diagnosis between the treatment groups excluding the one choline-treated for whom using only AP data resulted in bias on the DTI measures (n = 21).

**Table A.3.4:** Neonatal scan characteristics between the treatment groups excluding the one choline-treated for whom using only AP data resulted in bias on the DTI measures (n = 21).

**Table B.1:** The process of removing linearly dependent variables.

**Table C.1.1:** Associations of radial diffusivity (RD) in each WM connection with choline dose (proxied by maternal choline treatment adherence in % packets consumed) while controlling for infant sex, total intracranial volume (TIV) and postnatal age at scan; and after including a dose-by-sex interaction effect.

**Table C.2.1:** Associations of fractional anisotropy (FA) in each WM connection with choline dose approximated by total grams consumed from enrolment through delivery, controlling for infant sex, postnatal age at scan, total intracranial volume (TIV) and dose-by-sex interactions.

**Table C.2.2:** Associations of axial diffusivity (AD) in each WM connection with the amount of choline (in grams) consumed in grams from enrolment through delivery, controlling for infant sex, postnatal age at scan, total intracranial volume (TIV), and dose-by-sex interactions.

**Table C.2.3:** Associations of radial diffusivity (RD) in each WM connection with cumulative choline dose (in grams) consumed from enrolment through delivery while controlling for infant sex, postnatal age at scan, total intracranial volume (TIV) and dose-by-sex interactions.

## List of figures

<b>Figure 1:</b> T1-weighted structural magnetic resonance (sMR) image of a neonatal brain showing inverted signal intensities for grey and white matter compared to adult images.....	13
<b>Figure 2:</b> T1 (left) and T2 (right) relaxation curves for white matter (WM) and cerebral spinal fluid (CSF). $M_z$ denotes the longitudinal magnetisation; $M_0$ denotes the maximum magnetisation; $M_{xy}$ denotes the transverse magnetisation; TR denotes the repetition time and TE denotes the echo time. Adapted from Aaron and Daniel (2016).....	14
<b>Figure 3:</b> Illustration of anisotropic diffusion where the $\epsilon$ 's are the eigenvectors and the $\lambda$ 's are the eigenvalues. Adapted from Jellison et al. (2004) .....	16
<b>Figure 4:</b> Axial views of a neonatal (a) T1-weighted magnetic resonance (MR) image, (b) a non-diffusion weighted ( $b_0$ ) image, (c) a DW image, and (d) a fractional anisotropy (FA) map generated from DTI data. Bright regions on the FA map correspond to regions with anisotropic water diffusion characteristic of white matter. ....	16
<b>Figure 5:</b> Flowchart of the number of participants from maternal recruitment through to infant enrolment. GA denotes gestational age. Adapted from Jacobson et al. (2018a; 2018b).....	28
<b>Figure 6:</b> The manually traced subcortical regions of interest (ROIs) on T1-weighted structural MR (sMR) images for one of the neonates.....	31
<b>Figure 7:</b> The pre-processing steps performed on the DT and sMR image data.....	32
<b>Figure 8:</b> Example images with signal dropout slices, motion artefacts and poor quality. ..	33
<b>Figure 9:</b> A Fractional Anisotropy (FA) map for one participant. ....	34
<b>Figure 10:</b> A flowchart of the processing steps performed before tractography was conducted. All the tools that were used in these steps (except for Freeview) are found in AFNI.....	35
<b>Figure 11:</b> (a) Axial, (b) sagittal and (c) coronal views showing the manually traced ROIs successfully co-registered to the DTI data. Each colour represents a different manually segmented subcortical region. ....	36
<b>Figure 12:</b> A visual illustration in the (a) sagittal, (b) axial and (c) anterior views of the WM connections between manually traced subcortical regions in one infant. The colours represent the principal diffusion directions in each WM tract; red: right-left direction, green: anterior-posterior direction and blue: superior-inferior direction. ....	37
<b>Figure 13:</b> Zoomed-in axial view of the 15 WM connections between manually traced subcortical regions found in $\geq 85\%$ of participants. L = Left-hand side of the brain; R = Right-hand side of the brain.....	38
<b>Figure 14:</b> Flowchart illustrating the statistical test used to evaluate group differences. The bold red arrow is the pipeline that was followed for continuous dependent variables.....	42
<b>Figure 15:</b> Choline-treated neonates demonstrated lower fractional anisotropy (FA) than the placebo-treated neonates in the WM connection between the L thalamus and L caudate...	53

**Figure 16:** Choline-treated neonates demonstrated lower fractional anisotropy (FA) than the placebo-treated neonates in the WM connection between the L caudate and L pallidum. This difference remained significant after controlling for postnatal age at scan and total intracranial volume (TIV). ..... 53

**Figure 17:** Participants in the choline-treated group demonstrated lower axial diffusivity (AD) than those in the placebo-treated group in the WM connection between the R putamen and R pallidum. This difference remained significant after adjusting for potential confounding by total intracranial volume a (TIV) and postnatal age at scan. .... 55

**Figure 18:** Neonates in the choline group demonstrated significantly lower radial diffusivity (RD) than those in the placebo group in the WM connection between the L putamen and L pallidum. .... 57

**Figure 19:** Increasing choline dose was associated with lower FA in the WM connection between the R caudate and R pallidum. The correlation coefficient shown is Pearson r. .... 59

**Figure 20:** Increasing choline dose was associated with lower axial diffusivity (AD) in the WM connection between the R caudate and R putamen. The correlation coefficient shown is Pearson r. .... 61

**Figure 21:** Increasing choline dose was associated with lower axial diffusivity (AD) in the WM connection from the R putamen to the R pallidum. The correlation coefficient shown is Pearson r. .... 61

**Figure 22:** A zoomed-in axial view of the WM connections where choline-treated neonates demonstrated either lower FA or lower AD. L denotes the left-hand side of the brain and R denotes the right-hand side of the brain. .... 62

**Figure 23:** Lower radial diffusivity (RD) in the WM connection between the L and R thalami was associated with better visual recognition memory on the FTII.  $\beta$  is the standardized regression coefficient and  $\epsilon$  is the standardized standard error. .... 65

**Figure 24:** Increasing radial diffusivity (RD) in the WM connection between the R caudate and R putamen with better visual recognition memory on the FTII.  $\beta$  denotes the standardized regression coefficient and  $\epsilon$  denotes the standardized standard error. .... 65

**Figure 25:** The WM connections showing choline-related reductions in either axial diffusivity (AD) or fractional anisotropy (FA). L denotes the WM connections on the left-hand side of the brain and R on the right-hand side. .... 66

## Appendix figures

**Figure C.2.1:** Increasing cumulative choline dose (estimated by total grams consumed from enrolment through delivery) was associated with lower fractional anisotropy (FA) in the WM connection between the R caudate and R pallidum. Pearson  $r$  is the correlation coefficient shown.

**Figure C.2.2:** Increasing cumulative choline dose (approximated as the total grams consumed from enrolment through deliver) was associated with lower axial diffusivity (AD) in the WM connection between the R caudate and R putamen connection. The correlation coefficient shown is Pearson  $r$ .

**Figure C.2.3:** Increasing cumulative choline dose (estimated by total grams consumed from enrolment through delivery) was associated with lower axial diffusivity (AD) in the WM connection from the R putamen to the R pallidum connection. Pearson  $r$  is the correlation coefficient shown.

## List of abbreviations

AA	absolute alcohol
AD	axial diffusivity
AFNI	analysis of functional neuroimages
AP	anterior-posterior
BG	basal ganglia
CR	conditioned response
CS	conditioned stimulus
CSF	cerebral spinal fluid
CUBIC	Cape Universities Brain Imaging Centre
DICOM	digital imaging and communications in medicine
DT	diffusion tensor
DTI	diffusion tensor imaging
DWI	diffusion weighted imaging
EBC	eyeblick conditioning
EPI	echo-planar imaging
FA	fractional anisotropy
FACTID	fibre assessment by continuous tracking including the diagonals
FAS	fetal alcohol syndrome
FASD	fetal alcohol spectrum disorders
FATCAT	functional and tractographic connectivity toolbox
FTII	Fagan Test of Infant Intelligence
GA	gestational age
GM	grey matter
HE	non-syndromal heavily exposed
IQR	interquartile range
L	left hand side of the brain
MD	mean diffusivity
MEF	multi-echo FLASH
MRI	magnetic resonance imaging
NIFTI	neuroimaging informatics technology initiative
PA	posterior-anterior
PAE	prenatal alcohol exposure
PE	phase-encoding
PFAS	partial fetal alcohol syndrome
R	right hand side of the brain

RCT	randomized clinical trial
RD	radial diffusivity
ROI	region of interest
SD	standard deviation
SES	socioeconomic status
sMR	structural magnetic resonance
SUMA	surface mapping
TE	echo time
TIV	total intracranial volume
TORTOISE	tolerably obsessive registration and tensor optimization indolent software ensemble
TR	repetition time
TRSE	twice refocused spin-echo
TWV	total cerebral white matter volume
US	unconditioned stimulus
VB	voxel-based
VBM	voxel-based morphometry
WM	white matter

# 1. Introduction

## 1.1. Prenatal Alcohol Exposure (PAE)

### 1.1.1. Fetal Alcohol Spectrum Disorders (FASD)

Prenatal alcohol exposure (PAE) is the most widespread preventable cause of neurocognitive and neurodevelopmental disabilities worldwide, known collectively as fetal alcohol spectrum disorders (FASD) (Hoyme et al., 2005). Globally, FASD are prevalent at incident rates of 7.70 per 1 000 population (Lange et al., 2018). Compared to other countries such as Belarus (FASD rate of 36.6 per 1 000 population), Italy (FASD rate of 45.0 per 1 000 population) and Ireland (FASD rate of 47.5 per 1 000 population), certain high-risk communities in South Africa have the highest number of reported cases of FASD worldwide with incidence rates of 111 per 1 000 population (Lange et al., 2018).

Several environmental factors have been found to contribute to high rates of PAE, however, the main risk factor is lower socioeconomic status (Bingol et al., 1987, Abel and Hannigan, 1995). Such communities are characterised by adverse living conditions, high levels of stress, poor nourishment for the women, and high levels of alcohol misuse (i.e. regular binge drinking on weekends) (May and Gossage, 2011).

In addition, certain high-risk communities in the Western Cape province in South Africa have been found to have the highest reported cases of FASD in the country of 310 per 1 000 population in the province (May et al., 2022). May et al. (2019) suggest that the Dop system – where farm workers were paid in the form of alcohol in the Western Cape for over two centuries and into the 1990s – is an environmental factor that may have contributed to the high prevalences of PAE and, in turn, high FASD rates in these communities (London, 1999, Williams, 2016).

Research has shown that the specific consequences of drinking during pregnancy depend on both the amount and pattern of drinking, with binge-like drinking, such as is typically seen in high-risk communities in South Africa, being more harmful to the fetus and leading to FASD (Maier and West, 2001). Notably, heavy drinking during pregnancy is typically defined as an average consumption of  $\geq 2$  standard drinks (1.00 oz or 29.5 ml absolute alcohol (AA)) per day or at least 2 incidents of binge drinking ( $\geq 4$  drinks per occasion) (Jacobson et al., 2018b).

### 1.1.2. Adverse effects of PAE

Several studies have been conducted to advance understanding of the damaging effects of PAE on physical, behavioural, and cognitive development. These effects are summarized in Table 1.

**Table 1: The damaging effects of PAE.**

Domain affected	Adverse effect
Physical	<ul style="list-style-type: none"> <li>• Growth restrictions (both height and weight) and microcephaly.</li> <li>• Distinct facial features/anomalies such as a thin vermilion, smooth or flattened philtrum, reduced palpebral fissure, and a concaved nose, to name a few.</li> </ul>
Behavioural	<ul style="list-style-type: none"> <li>• Attention deficits, hyperactivity, self-injury and aggression, to name a few.</li> <li>• Disorders such as attention deficit hyperactivity disorder (ADHD) and mood disorders (depression, bipolar disorder, etc.).</li> </ul>
Cognitive	<ul style="list-style-type: none"> <li>• Speech/language, academic difficulties (learning and reading), memory (spatial and verbal), motor functions, hearing, executive functions (including working memory), visuospatial ability, postural balance, co-ordination (bimanual and hand-and-eye), information processing, and eyeblink conditioning.</li> </ul>

**References for Physical:** (Jones and Smith, 1973, Hoyme et al., 2005, Del Campo and Jones, 2017); **for Behavioural:** (Mattson and Riley, 2000, O'Connor et al., 2002, Burd et al., 2003) **and for Cognitive:** (Kyllerman et al., 1985, Jacobson et al., 1993, Streissguth et al., 1994, Mattson et al., 1996a, Olson et al., 1997, Mattson et al., 1998, Olson et al., 1998, Roebuck et al., 1998, Adnams et al., 2001, Rasmussen et al., 2007, Jacobson et al., 2008, Willoughby et al., 2008).

In addition to these, PAE also causes neurological damage. Neuroimaging studies have, for example, shown PAE-related changes in regional brain structures, including volume reductions in the basal ganglia (caudate nucleus, putamen and pallidum), hippocampus, corpus callosum and cerebellum (Mattson et al., 1996b, Mattson et al., 2001, Willoughby et al., 2008, Biffen et al., 2018), changes in cortical morphology (Lebel et al., 2011, De Guio et al., 2014, Moore et al., 2014) and altered brain growth trajectories (Moore and Xia, 2022). Archibald et al. (2001) and Roussotte et al. (2012) demonstrated overall brain volume reductions. Other studies have also illustrated that PAE results in changes in the microstructure of the white matter (WM) in the brain (Wozniak et al., 2006, Donald et al., 2015, Taylor et al., 2015).

WM alterations are among the most well-replicated neuroimaging findings in PAE and have been associated with poor performance in various cognitive domains (Wozniak et al., 2009, Lebel et al., 2010, Treit et al., 2013, Biffen et al., 2022). Specifically diffusion tensor imaging (DTI) has shown that PAE causes unhealthy, degenerated, less orientated and less insulated WM (for a review see Ghazi Sherbaf et al. (2019)). Damaged WM in individuals exposed to alcohol prenatally is typically characterised by:

- Lower fractional anisotropy (FA), the directionality of water diffusion in the WM tract (Ma et al., 2005, Alexander et al., 2007, Lebel et al., 2008, Sowell et al., 2008, Fryer et al., 2009, Li et al., 2009, Wozniak et al., 2009, Santhanam et al., 2011, Spottiswoode et al., 2011, Treit et al., 2013, O'Conaill et al., 2015, Fan et al., 2016, Paolozza et al., 2017);
- Lower axial diffusivity (AD), water diffusion parallel to the WM tract (Alexander et al., 2007, Donald et al., 2015, Taylor et al., 2015, Fan et al., 2016, Kar et al., 2021);
- Higher mean diffusivity (MD), the average movement of water in the WM tract (Ma et al., 2005, Wozniak et al., 2006, Alexander et al., 2007, Fryer et al., 2009, Li et al., 2009, Santhanam et al., 2011, Paolozza et al., 2014, O'Conaill et al., 2015, Fan et al., 2016, Paolozza et al., 2017); and/or
- Higher radial diffusivity (RD), water diffusion perpendicular to the WM tract (Alexander et al., 2007, Li et al., 2009, Santhanam et al., 2011, Spottiswoode et al., 2011, Fan et al., 2016).

These findings were in infants (Donald et al., 2015, Taylor et al., 2015), children (Wozniak et al., 2006, Lebel et al., 2008, Sowell et al., 2008, Fryer et al., 2009, Wozniak et al., 2009, Spottiswoode et al., 2011, Treit et al., 2013, Paolozza et al., 2014, Fan et al., 2016, Paolozza et al., 2017, Kar et al., 2021), adolescents (Sowell et al., 2008, Fryer et al., 2009, Treit et al., 2013, Paolozza et al., 2014, O'Conaill et al., 2015, Paolozza et al., 2017) and adults (Ma et al., 2005, Li et al., 2009, Santhanam et al., 2011). In contrast, some studies have reported:

- Higher FA (Fryer et al., 2009, Kar et al., 2021);
- Higher AD (Paolozza et al., 2014); and/or
- Lower MD (Lebel et al., 2008, Fryer et al., 2009, Kar et al., 2021, Gomez et al., 2022)

in children (Lebel et al., 2008, Fryer et al., 2009, Paolozza et al., 2014, Kar et al., 2021) and adolescents (Fryer et al., 2009, Paolozza et al., 2014) with PAE. Nonetheless, all these studies demonstrate that WM is an area in the brain that is significantly affected by PAE. Given the multitude of adverse effects caused by PAE, substantial effort has been invested in interventions aimed at reducing maternal drinking during pregnancy.

### **1.1.3. Interventions for PAE and FASD**

Within the South African healthcare system, reducing the prevalence of PAE includes regular screening of pregnant women to gain information on their alcohol use, using interviews and screening instruments; counselling and referral services to assist mothers in reducing alcohol intake (as specified in the 'Guidelines for Maternity Care in South Africa' manual ([www.knowledgehub.health.gov.za](http://www.knowledgehub.health.gov.za))); and increased awareness and education around consequences of PAE (such as programs set up by FASfacts ([www.fasfacts.org.za](http://www.fasfacts.org.za))).

Between 2009 and 2011, an intervention study, in South Africa, employing the Comprehensive Prevention Approach developed by the United States Institution of Medicine, successfully reduced overall alcohol consumption in the sample of pregnant women enrolled using one-on-one case management activities (Life Management, Motivational Interviews and Community Reinforcement Approach) (De Vries et al., 2016). However, to date, no specific policies have been implemented in South Africa for FASD management (Adebisi et al., 2021).

Globally, despite psychosocial interventions, heavy drinking during pregnancy continues, resulting in continued high incidence rates of FASD in at-risk communities (Popova et al., 2017, Lange et al., 2018). This has led to growing interest in prenatal maternal pharmacological or nutritional interventions that may mitigate the damaging effects of PAE on the fetus. One method currently being studied that has demonstrated promising preliminary results is choline supplementation.

## **1.2. Choline**

Choline is a fundamental nutrient that plays an important role in the human body. It is essential in the production of phospholipids involved in cell membranes, axonal growth and myelination (Zeisel, 2011, Fagone and Jackowski, 2013, Bekdash, 2019); it is a methyl group donor essential for metabolism and influences DNA methylation and gene expression (Krzysztof Blusztajn and J Mellott, 2012, Akison et al., 2018, Sarkar et al., 2019); and it is a constituent of acetylcholine (an important neurotransmitter) (Zeisel, 2013). Various foods such as milk, eggs, fish, chicken, beef and certain vegetables contain choline and provide more than 10% of the adequate dietary choline intake per serving (Zeisel et al., 2018). Due to its importance in the human body, adequate choline intake during pregnancy is essential for healthy fetal development.

### **1.2.1. Dietary choline intake**

It was established by the US Institute of Medicine's Food and Nutrition Board that the recommended adequate dietary intake (AI) of choline for pregnant women is 450 mg/day (Institute of Medicine Standing Committee on the Scientific Evaluation of Dietary Reference Intakes and its Panel on Folate, 1998). However, the majority of pregnant women around the world tend to have dietary choline intake levels below this recommended value. For example, in the randomised clinical trial (RCT) conducted in South Africa – the trial from which the participants for the current neuroimaging sub-study were recruited – only 9.70% of the 62 pregnant women in the trial met the AI of choline (Jacobson et al., 2018b); in a 24-hour dietary recall study performed in Canada from 2009 - 2010, only 23.0% of the 600 pregnant women in the study met the AI of choline (Lewis et al., 2014); and in a 2001 - 2014 study made up of

7 survey cycles in the United States, only 7.70% of the 533 pregnant women whose dietary choline intake levels were available met the AI of choline (Bailey et al., 2019).

Given that a rodent study by Idrus et al. (2017) found that low choline intake levels can intensify some of the adverse effects caused by PAE and may increase the risk for FASD, studies have been examining whether choline supplementation during critical times of brain development can limit the damaging effects of PAE.

### **1.2.2. Beneficial effects of choline supplementation in the context of PAE**

Various human and animal studies have been conducted to determine the efficacy of choline supplementation on reducing the damaging effects of PAE.

#### **Animal studies**

For the animal studies, it is important to note that the early postnatal period in rodents is equivalent to the third trimester in humans (observe <http://www.translatingtime.net>) (Patten et al., 2014). A rodent study conducted by Schneider and Thomas (2016) found that adolescent choline supplementation improved spatial memory (Schneider and Thomas, 2016). Other rodent studies have shown that early postnatal choline supplementation improved working memory, hyperactivity and eyeblink conditioning (Thomas et al., 2000, Thomas et al., 2004, Tran and Thomas, 2007), benefits persisted after the supplementation was stopped (i.e. the effects of choline were long-lasting) (Thomas et al., 2000, Thomas et al., 2004), and that administration earlier in pregnancy was more effective (Meck and Williams, 2003). Moreover, rodents receiving earlier choline supplementation (i.e. before birth) demonstrated improvements in reflex development, birth weight and brain weight (Thomas et al., 2009).

#### **Human studies**

Prior to the randomised clinical trial (RCT) from which the participants in the current study were recruited, three human studies had been conducted to examine the effects of choline supplementation on reducing the adverse effects of PAE. Of these, two trials involved postnatal supplementation in childhood (Wozniak et al., 2013, Wozniak et al., 2015, Nguyen et al., 2016), and one conducted in Rivne, Ukraine, involved prenatal maternal supplementation (Coles et al., 2015, Kable et al., 2015).

Children in the choline group of the postnatal study that involved 9 months of daily choline intake by children ages 2.5 to 5 years (Wozniak et al., 2015), demonstrated age-related improvements, at the 4-year follow-up, in learning and memory compared to the placebo group, as well as improved nonverbal intelligence, visual-spatial skills, working and verbal memory, and fewer symptoms of attention deficit hyperactivity disorder (ADHD) (Wozniak et

al., 2020). In contrast, the postnatal study by Nguyen and colleagues, which involved 6 weeks of choline supplementation to children with PAE ages 5 to 10 years of age found no treatment-related differences (Nguyen et al., 2016).

In the Ukraine prenatal supplementation study, 119 alcohol-drinking and 136 non-alcohol-drinking pregnant women were supplemented with either no multivitamins, multivitamins only or multivitamins with choline (750 mg of choline) (Kable et al., 2015). In this study, the combination of multivitamins with choline resulted in improvements, at 12 months of age, in cardiac orienting responses (COR) to visual stimuli in infants born to both alcohol-drinking and non-alcohol-drinking women, indicating improved memory and encoding of events in the environment (Kable et al., 2015). No beneficial effects of choline were seen in newborn growth, or on 6-month cognitive or psychomotor performance (Coles et al., 2015).

In the RCT by Jacobson et al. (2018a) from which the participants for the current neuroimaging sub-study were recruited, 62 heavy-drinking pregnant women in Cape Town, South Africa were prenatally supplemented daily with 2 g of either choline or placebo (31 choline-treated, 31 placebo-treated) (Jacobson et al., 2018a, Jacobson et al., 2018b). In this trial, although the infants were similar at birth, the choline-treated infants showed increased growth over the first postnatal year (assessed at 6.5 and 12 months) (Jacobson et al., 2018b). The choline-treated infants also showed improvements in eyeblink conditioning performance at 6.5 months and better recognition memory on the Fagan Test of Infant Intelligence (FTII) at 12 months (Jacobson et al., 2018b). This RCT had a higher choline dosage and started supplementation earlier in gestation than the Ukraine study.

In the neuroimaging sub-study of the RCT that was conducted on 52 neonates (28 choline-treated, 24 placebo-treated) born to women enrolled in the trial, within their first postnatal month, neonates born to choline-treated mothers demonstrated larger bilateral thalami, bilateral caudate nuclei, corpus callosum and right putamen (Warton et al., 2021). It was also found that the larger right putamen and corpus callosum partially mediated the choline-related improvements in recognition memory on the FTII at 12 months (Warton et al., 2021).

Given the role of choline in phospholipid synthesis, myelination and axonal growth, choline supplementation may protect fetal WM from the damaging effects of PAE. However, to date, the effect of maternal prenatal choline supplementation on the microstructure of WM – an area particularly vulnerable to PAE (Ghazi Sherbaf et al., 2019) – has not been assessed.

### **1.2.3. Effects of choline on white matter (WM) integrity**

To the author's knowledge, only two previous studies have examined the effects of choline on WM: a long-term follow-up (on average 7 years post-trial) of children with PAE who

participated in the 9-month postnatal choline supplementation trial described above (Wozniak et al., 2013, Wozniak et al., 2015, Gimbel et al., 2022) and a study examining the effects of varying prenatal choline intake levels in non-alcohol-exposed pigs (Mudd et al., 2018). In both studies, choline was associated with positive outcomes, namely, more coherent WM with less bending in the corpus callosum of alcohol-exposed children (Gimbel et al., 2022) and greater WM 'density' in the internal capsule, WM of the right cortex, and the connection between the putamen and pallidum of pigs with prenatally sufficient choline intake levels (Mudd et al., 2018). These positive outcomes suggest that, in addition to improving cognition, postnatal growth and regional brain volumes, prenatal choline supplementation may also benefit WM development in the presence of PAE.

The current study, therefore, aimed to examine the potential benefits of prenatal maternal choline supplementation on WM development using the neonatal DTI data that had been acquired as part of the neuroimaging sub-study of the RCT conducted by Jacobson and colleagues (Jacobson, 2018a, 2018b). Neonatal imaging data provides a unique opportunity to examine the effects of an intervention before potential confounding by environmental factors.

### **1.3. Assessing neonatal white matter (WM) integrity**

Widely used DTI analysis methods include voxel-based (VB) comparisons of DTI measures (FA, MD, AD and RD), analysis within WM regions of interest (ROIs) defined either manually or using atlases, and comparison of DTI measures averaged within tracts defined using fibre-tracking/tractography (Caan, 2016, Froeling et al., 2016, Van Hecke et al., 2016).

Co-registering poorly myelinated neonatal brain images of participants to each other or to a standardised atlas/template for VB group comparisons is challenging. Moreover, only a few anatomical neonatal or infant atlases are available (Dai et al., 2013, Makropoulos et al., 2018, Zöllei et al., 2020, Wang et al., 2022), the regions that can be parcellated are limited, and accuracies are variable (for a review see Oishi et al. (2019)). The infant FreeSurfer atlas, for example, does not sub-parcellate the cerebral cortex. Additionally, delineating WM on these poorly myelinated images decreases the accuracy of DTI measures acquired from ROI-based analyses. In contrast to ROI-based and VB approaches, tractography can be performed in native space between pre-selected GM seed regions and is the preferred method for analysing neonatal WM integrity.

### **1.4. Aim & hypotheses**

Since limited parcellations of the neonatal brain are possible with available atlases, manual tracing remains the gold standard for accurate labelling of brain regions on neonatal structural

magnetic resonance (sMR) images (Morey et al., 2009). As part of the neuroimaging sub-study of the Jacobson et al. (2018a, 2018b) RCT mentioned previously, 17 subcortical regions (8 bilateral regions: caudate, nucleus accumbens, putamen, pallidum, thalamus, amygdala, hippocampus, cerebellar hemispheres; and 1 medial region: cerebellar vermis) were manually traced on sMR images (Warton et al., 2021). Given that these 17 subcortical regions have both been implicated in PAE (Table 2) and play a role in the functional domains showing PAE-related deficits (Tables 3, 4 and 5), it is likely that the WM connections between these regions are also affected by PAE and may show choline treatment-related benefits.

**Table 2:** Summary of studies that have shown effects of PAE on the subcortical regions of interest (ROIs).

Subcortical grey matter ROI	References
Caudate	(Mattson et al., 1996b, Archibald et al., 2001)
Nucleus accumbens (NA)	(Blanchard et al., 1993)
Putamen	(Treit et al., 2013, Long and Lebel, 2022)
Pallidum	(Lebel et al., 2008, Treit et al., 2013)
Thalamus	(Lebel et al., 2008, Treit et al., 2013)
Hippocampus	(Willoughby et al., 2008)
Amygdala <sup>a</sup>	(Kozanian et al., 2018)
Cerebellar hemispheres (CH)	(Archibald et al., 2001, Bookstein et al., 2006)
Vermis	(O'Hare et al., 2005)

<sup>a</sup>Rodent model

**Table 3:** Summary of functional domains showing PAE-related deficits.

Functional domain affected by PAE	References
Language	(Adnams et al., 2001, Willoughby et al., 2008)
Learning	(Streissguth et al., 1994, Mattson et al., 1996a, Olson et al., 1997)
Spatial memory	(Willoughby et al., 2008)
Verbal memory	(Mattson et al., 1996a, Willoughby et al., 2008)
Reading	(Olson et al., 1998)
Visuospatial ability	(Olson et al., 1998)
Eyeblink conditioning	(Jacobson et al., 2008)
Motor functions	(Kyllerman et al., 1985)
Hearing	(Adnams et al., 2001)
Coordination	(Kyllerman et al., 1985, Adnams et al., 2001)
Executive functions (incl. working memory)	(Rasmussen et al., 2007)
Postural balance	(Roebuck et al., 1998)
Attention	(Olson et al., 1998)
Visual recognition memory and information processing	(Jacobson et al., 1993, Kable and Coles, 2004)

**Table 4:** Functional domains showing PAE-related deficits and PAE-affected subcortical regions involved in these functions.

Functional domain	Subcortical regions of interest that play a role in affected functional domains	Relevant references
Language	Putamen, Thalamus, CH	(Booth et al., 2007, Llano, 2013, Klein et al., 2016, Viñas-Guasch and Wu, 2017)
Learning	Caudate, Putamen, Hippocampus, Vermis, NA Thalamus	(Setlow, 1997, O'Hare et al., 2005, Seger and Cincotta, 2005, Anand and Dhikav, 2012, Mitchell, 2015, Viñas-Guasch and Wu, 2017)
Spatial memory	Caudate, Hippocampus, NA <sup>a</sup> , Thalamus <sup>a</sup>	(Mattson et al., 2001, Mitchell and Dalrymple-Alford, 2005, Rinaldi et al., 2012, Mobley, 2019)
Verbal memory	Vermis, Putamen, Hippocampus, Caudate, Thalamus	(O'Hare et al., 2005, Coles et al., 2011, Bonner-Jackson et al., 2015)
Reading	Putamen, Vermis, Thalamus	(Price et al., 1994, Moretti et al., 2002, Booth et al., 2007)
Visuospatial ability	Hippocampus, Thalamus, Caudate, CH	(Rafal and Posner, 1987, Klein et al., 2016, Rosen et al., 2018, Hauser et al., 2020)
Motor functions	Putamen, Pallidum, Vermis, Thalamus, CH	(Chambers and Sprague, 1955, Alexander et al., 1986, Manto et al., 2012)
Hearing	Putamen <sup>a</sup> , Caudate <sup>a</sup> , Thalamus <sup>a</sup> , Amygdala <sup>a</sup> , Pallidum <sup>a</sup>	(Chavez and Zaborszky, 2017)
Coordination	Putamen, Pallidum, Thalamus, Vermis	(Miall et al., 2000, Debaere et al., 2004)
Executive functions (incl. Working memory)	Caudate, Hippocampus, Amygdala, Thalamus <sup>a</sup> , Putamen, Pallidum, CH	(Menon et al., 2000, Van der Werf et al., 2003, Lewis et al., 2004, Mitchell and Dalrymple-Alford, 2005, Moore et al., 2013, Ross et al., 2013, Rubin et al., 2014, Klein et al., 2016, Xuan et al., 2016, Blair, 2017)
Postural balance	Vermis, Putamen, Pallidum, Thalamus	(Ouchi et al., 1999, Visser and Bloem, 2005)
Attention	Thalamus, Putamen, Caudate, Vermis	(Xuan et al., 2016)

NA nucleus accumbens; CH cerebellar hemispheres

<sup>a</sup>The studies were based on animal research for these regions.

**Table 5:** Functional domains where choline-related improvements were observed in the RCT by Jacobson and colleagues and the PAE-affected subcortical regions involved in these functions.

Functional domain	Subcortical regions of interest that play a role in affected function domains	Relevant references
Eyeblink conditioning	Hippocampus <sup>a</sup> , Amygdala <sup>a</sup> , Thalamus <sup>a</sup> , CH, Vermis <sup>a</sup>	(Logan and Grafton, 1995, Lee and Kim, 2004, Gerwig et al., 2007, Halverson et al., 2008)
Visual recognition memory	Thalamus <sup>b</sup> , Putamen <sup>b</sup> , Hippocampus	(Bakker et al., 2008, Merkow et al., 2015, Warton et al., 2021)

CH cerebellar hemispheres

<sup>a</sup>The studies were based on animal research for these regions.

<sup>b</sup>Regions that Warton et al. (2021) found to have mediated the choline-related improvements on the FTII (assesses visual recognition memory) observed in the Jacobson et al. (2018b) trial.

In this study, we aimed to examine whether prenatal maternal choline supplementation reduced the effects of PAE on WM microstructure in connections between these subcortical seeds. Since choline reduced the impact of PAE on the volume of the caudate, thalamus and putamen, we hypothesised that choline would normalise WM development.

Given that brain development from 30 to 40 weeks gestational age (GA) includes pre-myelination of WM fibres (Oishi et al., 2019) and, at the same stage, the maturation of the axonal cytoskeleton (Dubois et al., 2008), which is characterised by stable FA and decreasing radial and axial diffusivities (Dubois et al., 2006, Dubois et al., 2008, Oishi et al., 2019), we hypothesised that neonates born to mothers who received choline supplementation would demonstrate lower AD and RD than those in the placebo group. Based on this, we also hypothesised that lower AD and RD would be associated with improved visual recognition memory on the FTII at 12 months of age – this is the cognitive domain in which choline-related improvements were observed in the RCT by Jacobson and colleagues (Jacobson et al., 2018b).

## **2. Background**

### **2.1. Fetal alcohol spectrum disorders (FASD)**

FASD is an umbrella term that encompasses different diagnoses of PA based on the severity of the symptoms displayed. FASD diagnoses are made by dysmorphologists according to the revised Institute of Medicine (IOM) (Hoyme et al., 2005).

Fetal Alcohol Syndrome (FAS), the most severe form of FASD, is characterised by distinct craniofacial anomalies (reduced palpebral fissure, flattened philtrum and thin vermilion), growth restrictions (weight or height), small head circumference and cognitive problems that relate to specific brain abnormalities (Jones and Smith, 1973, Hoyme et al., 2005). An FAS diagnosis does not require confirmed maternal drinking during pregnancy. Partial FAS (PFAS) is diagnosed in individuals who exhibit 2 of the 3 facial dysmorphologies characteristic of FAS, who had microcephaly (small head circumference), growth restrictions, or neurobehavioral impairment and with confirmed prenatal alcohol exposure due to heavy drinking (Hoyme et al., 2005).

In studies performed in our lab in Cape Town, South Africa, children whose mothers confirmed heaving drinking (at least 14 drink/week and/or partook in regular binge drinking) during pregnancy but who did not display any facial features associated with FASD, are denoted as non-syndromal heavily exposed (HE).

### **2.2. Fetal white matter (WM) development**

White matter (WM) is an arrangement of neural networks found beneath the grey matter (GM) regions of the brain. It is composed of axons that connect these GM regions. WM tracts (also known as WM fibres) begin forming by (1) organizing into fibre bundles, (2) increasing in density and pre-myelinating by the proliferation of the axonal cytoskeleton, and (3) fully myelinating (Dubois et al., 2006, Dubois et al., 2008).

The most common fibre bundles that form in the cerebrum are categorised into 3 groups: association, commissural and projection fibres (De Reuck, 2014). The cerebellum is a region found at the back of the brain that also contains WM. This region contains two hemispheres joined by the vermis at the midline (Drake et al., 2023).

Association fibres connect adjacent or distant parts of the brain in the same hemisphere (the largest being the superior longitudinal fasciculus), commissural fibres connect the left and right hemispheres (the largest being the corpus callosum) and projection fibres connect subcortical GM, the brainstem and spinal cord with cortical GM (with fibres being highly concentrated in the internal capsule) (Mendoza, 2011, De Reuck, 2014, Haines and Mihailoff, 2018, Janelle

et al., 2022). The WM in the cerebellum is made up of the vermis and fibres that connect to the deep GM nuclei found in the cerebellar hemispheres (Drake et al., 2023). By observing the development of these large and prominent WM regions, a general understanding of WM development in the fetal and infant brain has been gained.

Fibre pathways start developing as early as 9-15 weeks GA (Dubois et al., 2016) with the cerebellum emerging between 12-13 weeks GA (du Plessis et al., 2018). By 11-12 weeks GA there is evidence of the largest commissural fibres, the corpus callosum, and by 13 weeks GA these fibres could be identified on a dissected brain (Horgos et al., 2020, Yu and Tubbs, 2023).

At 13 weeks GA, the vertical fibres of the internal capsule (which is separated into the anterior and posterior limb) – contains several projection fibres – could be identified on a dissected brain, with more consistent and correctly positioned fibre bundles only being identified by 17 weeks GA (Haines and Mihailoff, 2018, Horgos et al., 2020). Between 14 and 23 weeks GA the largest association fibre – superior longitudinal fasciculus – increases in width, length, fibres and layers in dissected brains (Horgos et al., 2020).

During the development of these bundles, axons mature by increasing in size and density, and become surrounded by myelin (pre-myelination) which acts as insulators to increase stimulus velocity and conduction speed along the axon (Morell, 2013, Dubois et al., 2014).

Axonal size and density are increased by the maturation and proliferation of the cytoskeletal components: actin filaments, microtubules and neurofilaments (Kevenaar and Hoogenraad, 2015). The actin filaments are responsible for axonal initiation, elongation and branching (Letourneau, 2009), microfilaments for proliferation and migration of axons (Lasser et al., 2018) and neurofilaments regulate the axonal diameter or calibre size (Xu et al., 1996).

The maturing axons are then surrendered by myelin which is what creates the white colour of WM. Myelination begins later in gestation (20-22 weeks GA) and continues throughout development (Inder and Huppi, 2000, Barkovich, 2002, Prayer et al., 2006, Dubois et al., 2014, Yu and Tubbs, 2023). Due to incomplete myelination in neonatal and infant brains, sMR images in the period 0-6 months are characterised by varying WM signal intensities and a reversal of normal adult GM and WM contrasts (Figure 1; lower WM than GM signal intensity) (Li et al., 2019, Dubois et al., 2021).



**Figure 1:** T1-weighted structural magnetic resonance (sMR) image of a neonatal brain showing inverted signal intensities for grey and white matter compared to adult images.

Myelination is regulated by axon calibre size, where axons with larger diameters myelinate first and become fully myelinated while those with smaller diameters may remain partially or never myelinated (Stadelmann et al., 2019). Myelin development begins (1) centrally/subcortically and proceeds peripherally and (2) posteriorly and proceeds anteriorly (Welker and Patton, 2012, Dubois et al., 2014).

For example, the posterior limb of the internal capsule – which separates the thalamus from the putamen and pallidum (Haines and Mihailoff, 2018) – is a central and posterior WM region whose myelin can be discerned microscopically (using immunochemical staining) from 24-25 weeks GA (Hasegawa et al., 1992). This WM region becomes fully myelinated within the first three postnatal months by which time mature myelin has extended to the anterior limb (Hasegawa et al., 1992, Welker and Patton, 2012, Dubois et al., 2014). In contrast, myelin in the anterior limb of the internal capsule – separates the caudate from the putamen and pallidum (Haines and Mihailoff, 2018) – can only be seen microscopically (using immunochemical staining) by 37 weeks GA and mature myelin can only be observed in the entire anterior limb by the sixth postnatal month (Hasegawa et al., 1992, Dubois et al., 2014).

Myelin in the cerebellar vermis is visible at 27 weeks GA (Salomon and Garel, 2007). Myelin in the deep cerebellar WM is detectable by 2 postnatal months and in the entire cerebellum at 4 postnatal months (Welker and Patton, 2012). The corpus callosum begins myelinating at approximately 4 postnatal months (Yu and Tubbs, 2023), while the more peripheral superior longitudinal fasciculus – which connects the major cortical lobes – matures more slowly with myelin and/or axonal maturation taking up to 5 years (Zhang et al., 2007).

Given that myelination is dependent on calibre size and predominantly occurs postnatally and varies by region (as per some of the largest fibre bundles and cerebellar WM), the degree of pre-myelination and matured axons in neonatal WM will also be variable.

## 2.3. Diffusion tensor imaging (DTI)

### 2.3.1. Principles of DTI

Magnetic resonance imaging (MRI) is a non-invasive imaging technique that uses radio frequency and well-controlled magnetic fields to produce images of specific body parts at high resolutions (Katti et al., 2011). MRI measures the signal from the hydrogen nuclei (spins) found in water molecules in the body (Feldman et al., 2010). Compared to most of the other imaging modalities, MRI is highly versatile because the contrast in the images can be varied using magnetic field gradients and radiofrequency pulses applied at different times during acquisition.

The contrast in an image is highly dependent on the repetition time (TR) and echo time (TE) of the imaging sequence. TR is the time between successive radiofrequency pulses while TE is the time between the radiofrequency pulse and the measured signal (Van Geuns et al., 1999, Buxton, 2009). While varying TR affects the contrast arising from differences between the longitudinal magnetization ( $M_z$ ) relaxation rates of different tissues, known as T1, varying TE affects the contrast arising from differences in the transverse magnetization ( $M_{xy}$ ) relaxation rates, known as T2 (Gibby, 2005). T1 is defined as the time when the longitudinal magnetisation has regrown to 63 % of its maximum value, and T2 as the time when the transverse magnetisation has decayed by 63 %. Figure 2 shows how TR and TE can be chosen to maximise the signal contrast due to T1 (left) or T2 (right) relaxation effects, respectively.

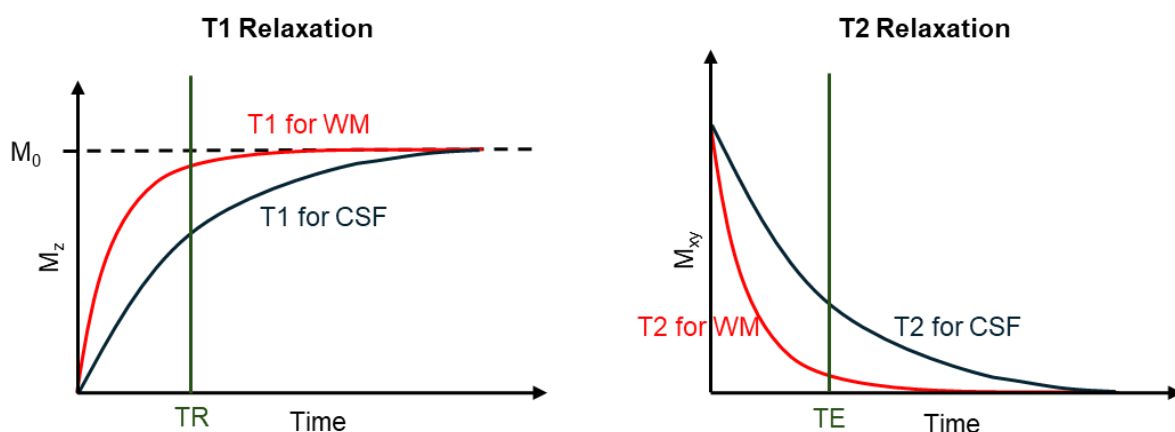


**Figure 2:** T1 (left) and T2 (right) relaxation curves for white matter (WM) and cerebral spinal fluid (CSF).  $M_z$  denotes the longitudinal magnetisation;  $M_0$  denotes the maximum magnetisation;  $M_{xy}$  denotes the transverse magnetisation; TR denotes the repetition time and TE denotes the echo time. Adapted from Aaron and Daniel (2016).

The most widely used structural MR (sMR) acquisitions are either T1-weighted, meaning most of the contrast is due to differences in T1 between tissues, or T2-weighted, where most of the

contrast is due to differences in T2 (see Figure 2) (Van Geuns et al., 1999, Gibby, 2005). T1-weighted sMR images are commonly used for brain segmentation (Lemieux et al., 1999, Mikheev et al., 2008, Warton et al., 2021).

In diffusion weighted (DW) imaging (DWI), at its simplest, an additional pair of gradient pulses is applied after a single excitation. While stationary spins will be fully re-phased by the gradient pair, spins that have 'diffused' along the gradient direction either during the application of a pulse or between the application of the gradient pair, will not be fully re-phased, leading to signal loss. The amount of attenuation depends on the amount of diffusion along the gradient direction – diffusion perpendicular to the gradient direction will not result in any dephasing and signal loss – as well as the strength of the diffusion/phase encoding direction. It should be noted that this is the simplest implementation of diffusion encoding. Many more complex encoding schemes exist.

The b-value is a factor that reflects the strength and duration of the diffusion-sensitising gradients (Huisman, 2010, Baliyan et al., 2016); the higher the b-value, the stronger the image's diffusion contrast. Notably, images can be sensitised to diffusion along different directions by applying encoding gradients in different directions.

Diffusion tensor imaging (DTI) is an extension of DWI where the acquisition is repeated for at least 6 different DW directions (Huisman, 2010), allowing the diffusion tensor (DT) to be solved in every voxel. The DTI is a 3 by 3 matrix that fully characterises both the rate and direction of diffusion in each voxel (Mori and Zhang, 2006). Transforming to a coordinate system with axes centred parallel and perpendicular to the principle direction of diffusion in a voxel, results in the off-diagonal elements in the matrix becoming zero. The diffusion ellipsoid (Figure 3) now comprises of three mutually orthogonal eigenvectors ( $\epsilon_1, \epsilon_2, \epsilon_3$ ) with magnitudes given by eigenvalues ( $\lambda_1, \lambda_2, \lambda_3$ ) which together describe the direction and rate, respectively, of water diffusion in each voxel (Mori and Zhang, 2006, Huisman, 2010).

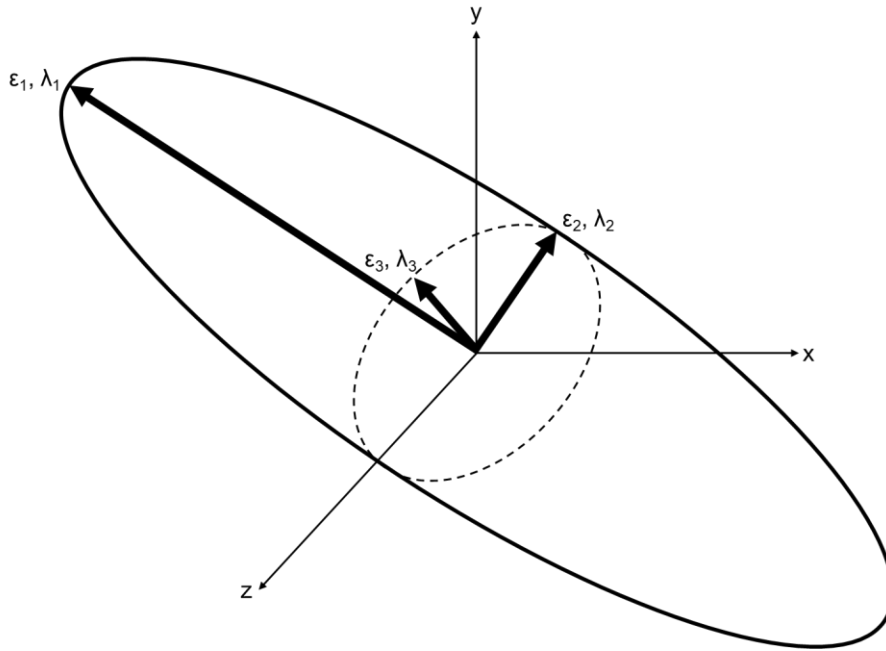


**Figure 3:** Illustration of anisotropic diffusion where the  $\epsilon$ 's are the eigenvectors and the  $\lambda$ 's are the eigenvalues. Adapted from Jellison et al. (2004)

In contrast to GM and cerebrospinal fluid (CSF), WM is characterised by anisotropic diffusion (refer to Figure 3), and greater anisotropy reflects healthier and better myelinated WM (Feldman et al., 2010). Since this WM microstructure cannot be characterised using conventional MRI, DTI is widely used to provide insights regarding WM integrity and structural brain connectivity (Mori et al., 2005, Feldman et al., 2010). Figure 4 shows a comparison of a neonatal T1-weighted sMR, non-diffusion weighted and DW images, and a fractional anisotropy (FA) map generated from the DTI data.

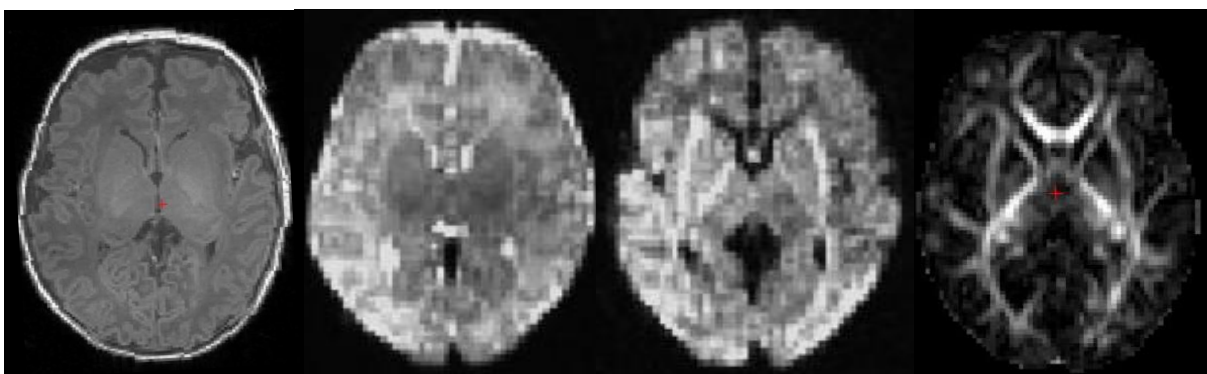


**Figure 4:** Axial views of a neonatal (a) T1-weighted magnetic resonance (MR) image, (b) a non-diffusion weighted ( $b_0$ ) image, (c) a DW image, and (d) a fractional anisotropy (FA) map generated from DTI data. Bright regions on the FA map correspond to regions with anisotropic water diffusion characteristic of white matter.

### 2.3.1. DTI measures

DTI allows for a three-dimensional analysis of molecular water diffusion within WM in the brain, providing information on the microstructure of WM (Basser et al., 1994, Feldman et al., 2010). The microstructural properties of the WM are represented by four key measures that are computed from the diffusion tensor (Basser et al., 1994), namely, fractional anisotropy (FA), axial diffusivity (AD), radial diffusivity (RD) and mean diffusivity (MD). The information reflected by each of these parameters is summarised in Table 6.

**Table 6:** Primary diffusion tensor imaging (DTI) measures used to categorise WM microstructural integrity.

DTI measures	Units	Formula (symbols refer to Figure 3)	What it measures	Interpreting the parameters <sup>a</sup>	
				Higher/increasing values	Lower/decreasing values
Mean diffusivity (MD)	mm <sup>2</sup> /s	$\frac{\lambda_1 + \lambda_2 + \lambda_3}{3}$	Average diffusion of water molecules in a region, irrespective of the direction.	Higher brain water content (e.g. cerebral edema).	High cell densities (e.g. in GM and WM regions)
Fractional anisotropy (FA)	Unitless	$\sqrt{\frac{(\lambda_1 - \lambda_2)^2 + (\lambda_2 - \lambda_3)^2 + (\lambda_1 - \lambda_3)^2}{2(\lambda_1^2 + \lambda_2^2 + \lambda_3^2)}}$ where $0 \leq FA \leq 1$	The directional reliance and degree of regularity of water diffusion in a certain direction.	Healthy WM microstructure, increased packing density or myelination.	Impaired WM microstructure.
Axial diffusivity (AD)	mm <sup>2</sup> /s	$\lambda_1$	Water diffusion parallel to the WM tracts.	Densely packed and well-orientated axons.	Degenerated or damaged axons.
Radial diffusivity (RD)	mm <sup>2</sup> /s	$\frac{\lambda_2 + \lambda_3}{2}$	Water diffusion perpendicular to the WM tracts.	De- or dysmyelination, or larger axonal diameter.	Highly myelinated axons.

**References:** (Basser et al., 1994, Basser and Pierpaoli, 1996, Le Bihan et al., 2001, Beaulieu, 2002, Alexander et al., 2007, Salat et al., 2009, Harkins et al., 2021)

<sup>a</sup>These are the conventional interpretations for changes in these DTI measures. It is important to note these are not all the possible interpretations.

Generally, AD and RD are used as explanatory parameters for changes in MD and FA. Increases in FA are usually attributed to increases in AD and/or decreases in RD. Increases in MD are usually accredited to increases in AD, RD or both. Conversely, decreases in FA and MD indicate the opposite.

### **2.3.2. Challenges associated with analysing neonatal brain images**

Neonatal brains are relatively small which increases the chances of several tissue types occupying a single voxel resulting in blurred boundaries between tissues, known as partial voluming artefacts (Vos et al., 2011). These artefacts can be remedied by increasing spatial resolutions, however, given that neonates are usually in natural sleep and not sedated during scanning, sequence duration and spatial resolutions are limited (Dubois et al., 2021). Additionally, given that healthy neonates have almost 3 times faster breathing rates than the average healthy adult, neonatal brain images are more susceptible to motion artefacts (Heemskerk et al., 2013, Coleman et al., 2022). These artefacts can alter the DTI measures generated, thus, visual inspection is an essential step in identifying and excluding images with extreme motion artefacts, while algorithms (such as those found in the Tolerably Obsessive Registration and Tensor Optimization Indolent Software Ensemble (TORTOISE)) are additionally employed in correcting for motion artefacts (Irfanoglu et al., 2017).

Neonatal brains have a relatively higher water content of about 85-90 % as compared to adult brains with 75 % (Dobbing and Sands, 1973, Ann-Christine and Rima Sestokas, 2015). This increased water content results in reduced anisotropy (FA) and altered diffusivity (MD, AD and RD) (Bastiani et al., 2019, Dubois et al., 2021). When running tractography, an FA threshold is applied during tracking to prevent areas that are not WM from being included. The default for adults is 0.2, however, due to the reduced anisotropy in neonatal brains, the FA threshold is set to 0.1 as this is the conventional threshold applied for infants (Dubois et al., 2014).

As mentioned previously, neonatal brains are largely unmyelinated. This, coupled with the high water content, causes inverted contrasts between GM and WM in neonatal images compared to adult brain images (Li et al., 2019). Due to this and the poor quality of neonatal brain images caused by partial voluming and motion artefacts, automatic segmentation methods are difficult to implement, thus, manual segmentation has been considered the 'gold standard' (Morey et al., 2009).

The rapid development of neonatal brains in the first years of life results in T1 and T2 relaxation times of WM decreasing by about 1 100 ms (within the first two years of life) and 100 ms (birth to adulthood), respectively (Heemskerk et al., 2013), with T2-weighted images having better contrast than T1 weighted images (Li et al., 2019). DTI is said to be supported by the longer

T2 relaxation times observed at birth since, at a similar TE, more residual signal is present allowing for pre-myelination and WM development to be detected (Heemskerk et al., 2013).

### **2.3.3. Analysing neonatal brain images**

As mentioned previously, three main DTI analysis methods are typically employed to examine the microstructure of WM. These include voxel-based (VB) analysis, ROI-based analysis, and fibre tracking/tractography (Caan, 2016, Froeling et al., 2016, Van Hecke et al., 2016). While all these methods perform well in child, adolescent and adult brains, some are challenging in the rapidly developing and poorly myelinated neonatal brain (Girault et al., 2019).

VB analysis estimates and compares changes in the DTI measures found in each voxel of a brain image (Van Hecke et al., 2016). Co-registering to an atlas or template is required during pre-processing to ensure that DTI measures in voxels with identical anatomical locations are compared between participants (Abe et al., 2010, Van Hecke et al., 2016). An atlas is a brain image that provides the location and shape of brain regions in a common coordinate space (Dickie et al., 2017). Infant atlases are limited and very few are publicly available, with one of the largest atlas databases (Johns Hopkins University MRICloud database) having no atlases for 0.5- to 3-year-olds (Oishi et al., 2019). Of the few atlases that have been developed for infants, all have been based on healthy brains and none have been created for brains with disorders or neurological deficits (Oishi et al., 2019). Additionally, other issues have arisen in the use of these atlases, including inaccurate co-registration due to the lack of contrast as a result of poor myelination (Oishi et al., 2019).

The ROI-based analysis estimates the DTI measures found in predetermined WM areas (WM ROIs) that have been manually or automatically (semi or full) delineated (Froeling et al., 2016), and an atlas may or may not be used during the analysis to define the WM ROIs (Froeling et al., 2016). Even without the use of an atlas, the delineation of WM ROIs is required and is reliant on the ability to accurately identify WM regions. However, the lack of myelination in neonatal brains poses a problem as there are higher chances of GM and/or CSF erroneously being segmented with WM ROIs, resulting in inaccurate findings (Snook et al., 2007).

Tractography analysis uses the DTI tensors in each voxel to generate WM pathways between grey matter (GM) regions and eventually estimates the average values of the DTI measures (FA, MD, AD and RD) for each pathway (Basser et al., 2000, Behrens et al., 2014). Delineation of WM ROIs is not required, and an atlas may or may not be used to define the GM ROIs. Since GM ROIs can be identified more accurately in neonatal brains, tractography is an attractive approach for analysing the microstructure of WM in neonates. Instead of performing tractography between two GM ROIs, known as seed- or ROI-based tractography, there is also an option to perform tractography across the entire brain, known as whole-brain tractography

(Jeurissen et al., 2019). Both methods require the specification of seeds – voxels where the initiation and/or termination of fibre tracking occurs (Conturo et al., 1999, Caan, 2016).

The seeds for whole-brain tractography can be defined as either (1) all the WM voxels or (2) all voxels close to the GM-WM boundary (Jeurissen et al., 2019). The tracking is initiated from these seeds and generates all WM pathways across the entire brain. The disadvantage with seeding from all the WM voxels is that it may result in large WM bundles being over-defined, while seeding from voxels close to the GM-WM boundary may result in errors of longer pathways (Jeurissen et al., 2019).

Seed-based tractography avoids these challenges by defining specific GM seed regions from which tracking is initiated and terminated. Atlases can also be used to specify these GM seeds, however, based on limitations of neonatal atlases, manual segmentation of seeds may provide more accurate results (Caan, 2016).

#### **2.3.4. Tractography**

Whole-brain and seed-based tractography can be performed using two main methods: deterministic tractography and probabilistic tractography. The main difference between these algorithms is how they estimate the pathway between two specific regions of interest (also known as seeds) (Sotiropoulos and Zalesky, 2019).

Deterministic tractography estimates the WM tracts in the following manner: firstly, the desired seeds are identified and specified; secondly, a single direction of the WM tract is estimated between those seed points; thirdly, a small distance of movement occurs in that direction; fourthly, re-evaluation of the direction takes place; and finally, the latter three processes are repeated until the entire tract is fully developed (Alexander et al., 2007).

Probabilistic tractography, which is subdivided into full and mini-probabilistic tractography, uses Monte Carlo simulations to estimate the WM tracts (Taylor et al., 2016). After the desired seeds have been specified, the Monte Carlo simulation performs several predetermined iterations which, firstly, consider all the uncertainties in the direction of the WM tracts connecting the desired seeds, secondly; measures the probability of each possible WM tract direction, and lastly, provides the WM tract path with the highest likelihood (Behrens et al., 2003, Sotiropoulos and Zalesky, 2019). Due to this, probabilistic is deemed more accurate than deterministic tractography.

Of the two types of probabilistic tractography, full probabilistic tractography is more commonly used for estimating the DTI parameters while mini-probabilistic tractography is used for visualising the WM tracts between seed points. The difference between these tractography methods is the number of iterations performed of the Monte Carlo simulations that are

performed; mini-probabilistic tractography performs substantially fewer iterations compared to full probabilistic tractography (Taylor et al., 2016).

Tractography can be conducted automatically using various algorithms and software packages that have been developed (Fillard et al., 2011).

### **2.3.5. Software packages used in this project**

Structural MR (sMR) and DT images can be pre-processed and processed using various software package's. The sMR images are typically used to define the ROIs that are used as seeds for tractography, while the DT images are used to compute the DTs. The available software package's allow for brain segmentation, tractography and the estimation of the DTI measures.

FreeSurfer is a software package used to analyse, visualise and process magnetic resonance images of humans (<https://surfer.nmr.mgh.harvard.edu>). This software can be used for pre-processing sMR image data before segmentation/parcellation (Warton et al., 2021). Freeview is a tool in FreeSurfer that is used for visualizing and examining pre-processed data (<https://surfer.nmr.mgh.harvard.edu>). This tool can also be used to manually parcellate brain and compute regional brain volumes.

Analysis of Functional Neuroimages (AFNI) is a software package that contains tools which are used for the analysis of various MRI modalities including DTI data (<https://afni.nimh.nih.gov>) (Cox, 1996). While this software processes image data in the Neuroimaging Informatics Technology Initiative (NIFTI) or AFNI format (Larobina and Murino, 2014, Li et al., 2016), image data from the scanner are stored in a format known as the Digital Imaging and Communications in Medicine (DICOM) (<http://medical.nema.org/standard.html>) format (Li et al., 2016). Due to this, the first pre-processing steps typically involve converting the images from DICOM to NIFTI or AFNI format (Li et al., 2016). The following tools found in AFNI are widely used in the pre-processing and processing of DTI data.

Firstly, a 3D visualisation tool called AFNI Surface Mapping (SUMA) allows for volumetric data to be viewed on 3D cortical regions (Saad et al., 2004, Saad and Reynolds, 2012). Only outputs obtained from mini-probabilistic tractography, and not full probabilistic tractography, can viewed in SUMA. Secondly, the Tolerably Obsessive Registration and Tensor Optimization Indolent Software Ensemble (TORTOISE) are used for pre-processing and processing DTI data (Pierpaoli et al., 2010, Irfanoglu et al., 2017). Thirdly, the Functional and Tractographic Connectivity Toolbox (FATCAT) is used to perform tractography and contains various programs that integrate efficiently with other AFNI tools (Taylor and Saad, 2013). For tractographic analysis, this toolbox uses the Fibre Assessment by Continuous Tracking

Including the Diagonals (FACTID) algorithm to track the whole brain and estimate the WM connections between two target ROIs (Taylor and Saad, 2013).

All these software packages allow for efficient processing of DTI data thereby permitting assessment of WM microstructure.

### **2.3.6. Early-developing WM detected with DTI and tractography**

It has been shown previously that the largest fibres of the most common fibre bundles (projection, commissural and association fibres) and cerebellum can be detected pre- and postnatally using DTI and/or tractography.

For example, the internal capsule (anterior and posterior limb) – concentrated with projection fibres – was identified on DTI by 13 weeks GA and projection fibres passing through this area were visualised using tractography at 19 weeks GA (Huang et al., 2006, Huang et al., 2009). Using DTI, Khan et al. (2019) detected anisotropy in the internal capsule at 22 weeks GA and increased anisotropy was detected in this area at birth (Welker and Patton, 2012)

The corpus callosum (one of the largest commissural fibre bundles) was identified on DTI by 15 weeks GA (Huang et al., 2009) and anisotropy was detectable on DTI by the 22<sup>nd</sup> week GA (Khan et al., 2019) with increases being evident at birth (Welker and Patton, 2012). In addition, by 24-37 weeks GA, the WM tracts of regions of the corpus callosum (genu and splenium) could be visualised using tractography (Gregor et al., 2008).

In contrast to the internal capsule and corpus callosum, some studies were unable to identify the largest association fibre (superior longitudinal fasciculus) prenatally using tractography; the authors were only able to visualise this tracts in a 5 year old participant (Huang et al., 2006). However, others observed anisotropy in this region by 27 weeks GA (Khan et al., 2019) and increases in anisotropy at 12 postnatal months (Welker and Patton, 2012).

Using tractography, the WM in the cerebellar vermis was detected from 17 weeks GA and the WM connecting to the deep GM nuclei of the cerebellum at 38 weeks GA (Takahashi et al., 2014). The ability of DTI to detect WM, including WM that develops early and late in gestation, indicates the applicability of DTI and tractography in the characterization and analyses of neonatal WM microstructure.

While higher FA and AD, and lower RD and MD, typically characterise healthier and more myelinated WM in children, adolescents and adults, this may not be the case in the partially myelinated neonatal brain. It has been shown, for example, that pre-myelination of WM fibres occurring from 30-40 weeks GA is characterised by stable FA and decreasing RD and AD (Dubois et al., 2008, Oishi et al., 2019). In neonates, lower AD and RD may, therefore, reflect more optimal WM development, but this may also vary regionally, complicating the

interpretation of neonatal DTI findings. Moreover, since most algorithms to process DTI data have been developed based on adult data, analysing neonatal data is challenging.

## **2.4. Assessments of infant cognitive performance**

The primary cognitive performance measures on which choline-related improvements were observed in the RCT from which the participants for the current sub-study were recruited were Eyeblink Conditioning (EBC) at 6.5 months and the Fagan Test of Infant Intelligence (FTII) at 12 months (Jacobson et al., 2018b). Each of these tests are described below.

### **2.4.1. Eyeblink Conditioning (EBC)**

EBC provides information on the development of associative learning in infants (Kehor, 2012). EBC utilises a conditioned stimulus (CS) that can be a auditory, tactical or visual and a somatosensory unconditioned stimulus (US) to test conditioned response (CR) (Kehor, 2012).

In the delay EBC test administered to infants in the RCT, an auditory CS in the form of a tone was played through speakers to the infant for a predefined period (750 ms), the somatosensory US was a short air puff administered to the right eye in the last 100 ms of the CS period, and the CR was the blinking action of the infant in anticipation of the US. For the eyeblink to be classified as a CR, it needed to occur before the US (air puff) was applied, i.e. 300-650 ms after the onset tone (Jacobson et al., 2018b). Each session consisted of 51 trials (on average 1 trial every 12s); sessions were repeated on 3 separate days. The infants were entertained by a research assistant while the EBC trials were administered.

On EBC, the occurrence of associative learning is decided based on the CR criteria set by the study. For example, in the Jacobson et al. (2018b) RCT, an infant met criterion for conditioning (i.e. learned) if he/she exhibited CRs in  $\geq 50\%$  of the trials performed on at least 1 of the testing days. More CRs reflect greater associative learning.

### **2.4.2. Fagan Test of Infant Intelligence (FTII)**

The FTII is a cognitive test to assess visual recognition memory and information processing speed in infants (Fagan and Singer, 1983). This test was administered to infants in the Jacobson et al. (2018b) RCT were tested at 6.5 months and 12 months. The FTII is based on the idea that infants tend to fixate/gaze longer at unfamiliar stimuli compared to familiar stimuli (Fagan and Singer, 1983, Fagan III and Detterman, 1992).

During the FTII test, infants are initially presented with two identical photographs for a set period, whereafter a novel photograph is paired with the familiar (Fagan and Singer, 1983, Fagan III and Detterman, 1992). The periods that the infant fixate on each stimulus is recorded. Preference for the novel stimulus indicates that the infant can recall the familiar one and discriminate it from the novel one. The stimuli are then removed, and the test is repeated

(for a predefined number of trials) using the same pair of familiar stimuli and a different unfamiliar stimulus (Fagan III and Detterman, 1992, Jacobson et al., 2018b). To prevent the preference of fixating on one side (right- or left-hand side), the position of the familiar and novel stimuli are swapped midway between each trial (Fagan III and Detterman, 1992). For each trial, a score (FTII score in %) is generated using the following equation (Fagan III and Detterman, 1992, Jacobson et al., 2018b):

$$FTII \text{ score} = \frac{\text{Amount of time focused on novel stimulus}}{\text{Total amount of time focused on familiar and novel stimulus}} \times 100 \quad (1)$$

Scores are averaged across trials. Higher the FTII scores (%) reflect better visual recognition memory (Jacobson et al., 2018b). Interestingly, studies by Fagan and colleagues have found that this test accurately predicted future intellectual ability in high-risk infants – these were infants who had been exposed to any substances including alcohol (a summary of the studies is presented by Fagan III and Detterman (1992)).

## **2.5. Statistical analyses**

### **2.5.1. Analysis of group differences**

The current study focuses on comparing independent groups. The analyses used to compare the means of these groups are reliant on the type of variable: categorical or quantitative variables. Categorical variables are composed of nominal and ordinal variables while quantitative variables are composed of continuous and discrete variables. Nominal variables have two or more groups/categories that are not in a particular order, ordinal variables have 2 or more groups/categories that can be placed in an order/rank, continuous variables can take on any value and discrete variables are finite integer values (not categories) (Elenbaas et al., 1983, Kaliyadan and Kulkarni, 2019).

For discrete or nominal dependent variables, the means of 2 independent groups are compared using the chi-squared test for larger sample sizes. While Fisher's exact test is used for sample sizes between 20 - 40 and where at least one of the expected values in the contingency table is < 5 (Elenbaas et al., 1983, De Muth, 2009). Interestingly, this test directly calculates a p-value instead of a test statistic.

For ordinal dependent variables, the means between 2 independent groups are compared using a rank-order test, the Mann-Whitney U test (Gaddis and Gaddis, 1990, Parab and Bhalerao, 2010).

For continuous dependent variables, there are four main statistical tests that can be used to compare means between 2 independent groups: Independent samples T-test, Welch's T-test, Yuen's test and Mann-Whitney U test. The differences between these tests are their

robustness or sensitivity to violations of two main assumptions: normally distributed data and homogeneity of variances between groups. The different tests and their assumptions are summarised in Table 7.

**Table 7:** The assumptions that need (✓) or do not need (x) to be met for different tests that compare the means between 2 independent groups.

Statistical test	Assumptions		Reference
	Normally distributed data	Homogeneity of variances between groups	
Independent samples T-test	✓	✓	(Student, 1908)
Welch's T-test	✓	x	(Welch, 1947)
Mann-Whitney U test	x	✓	(Mann and Whitney, 1947)
Yuen test	x	x	(Yuen, 1974)

Generally, the Shapiro-Wilk's test is used to test the normality assumption since it is the most powerful normality test – it has the highest likelihood of rejecting the null hypothesis and detecting skewness (Yap and Sim, 2011). The results from this allow for parametric tests to be used for normally distributed data and non-parametric tests for skew data. The homogeneity of variances assumption can then be tested using either the F-test (parametric test) or the Levenes test (non-parametric test) (Gastwirth et al., 2009).

Additionally, for continuous dependent variables, the analysis of variance (ANOVA) test is used to compare means between 3 or more independent groups (Mishra et al., 2019), while the rank-ordered version – Kruskal-Wallis ANOVA test – is used to compare means between 3 or more independent ordered groups (Gaddis and Gaddis, 1990).

### 2.5.2. Linear regression analysis

Linear regression is used to observe the strength and direction of a relationship between two variables. When sample sizes are relatively small, the removal of outliers can limit statistical power and ordinary linear regression is sensitive to the occurrence of outliers (Hazra and Gogtay, 2016). Robust linear regression is a statistical technique that addresses this by accounting for the presence of outliers (Alma, 2011).

One of the most common robust regression estimators used in robust linear regression is the maximum likelihood type or M-estimator introduced by Huber (1964). This estimator accounts for outliers by applying an alternative function ( $\rho$ -function) to points with standard errors – difference between the observed and estimated values – that surpass a threshold known as

the tuning constant ( $1.345\sigma$ ; where  $\sigma$  is the standard deviation of the standard errors) (Huber, 1964, Fox and Weisberg, 2002, Alma, 2011, Khan et al., 2021). This is the tuning constant that allows for a 95 % efficiency in Huber's M-estimator (Fox and Weisberg, 2002).

Similar to normal linear regression, robust linear regression generates regression coefficients, standard errors and p-values. The magnitude of the regression coefficients can easily be compared using their standardized form (as per equation 2):

$$\beta^* = \beta \frac{S_x}{S_y} \quad (2)$$

where  $\beta^*$  is the standardized regression coefficient,  $\beta$  is the unstandardized regression coefficient,  $S_x$  is the sample standard deviation of the independent variable and  $S_y$  is the sample standard deviation of the dependent variable. The standard error is standardized in the same way.

## **3. Materials and Methods**

### **3.1. Study sample**

Participants were infants born to heavy-drinking mothers enrolled in the Cape Town choline supplementation RCT from 2012 to 2015 (Jacobson et al., 2018a; 2018b). For the RCT, women initiating antenatal care approximately before 23 weeks GA at one of the two midwife obstetrics units serving disadvantaged communities in Cape Town known to have high prevalences of maternal drinking during pregnancy, were screened regarding their alcohol consumption. Detailed drinking histories were obtained using a timeline follow-back interview. Eligible mothers were randomised to be supplemented daily with 2g of either choline or a placebo from enrolment through delivery. Sixty-two infants born to mothers who completed the entire supplementation trial were enrolled (Jacobson et al., 2018a; 2018b). Figure 5 is a flowchart detailing participant numbers from maternal recruitment through to infant enrolment.

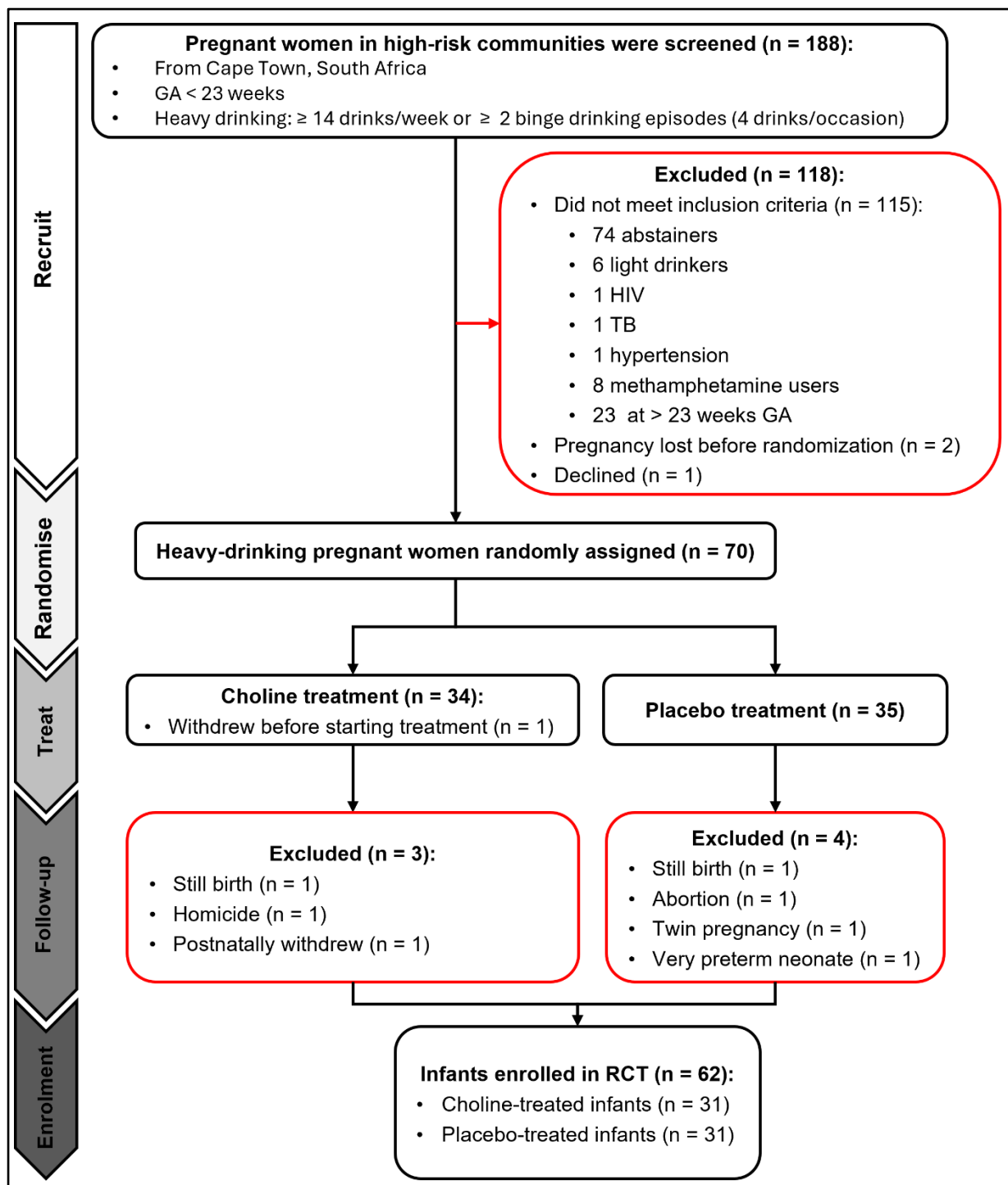


**Figure 5:** Flowchart of the number of participants from maternal recruitment through to infant enrolment. GA denotes gestational age. Adapted from Jacobson et al. (2018a; 2018b).

Of the 62 infants, neuroimaging data were acquired in 52 infants within their first postnatal month. All 52 provided sMRI data. Given that the neonates were scanned in natural sleep and DTI was performed later in the protocol, only 43 provided DTI data (Warton et al., 2021).

Protocols of both the RCT and neuroimaging sub-study were approved by the human research ethics committees of all the collaborating institutions, and the RCT by the then Medicines

Control Council (MCC). All mothers provided written informed consent. To maintain confidentiality, participants were assigned numerical IDs at the time of enrolment, and study staff were blinded to treatment status. In the present sub-study, the investigator remained blinded to the treatment arm until the data had been visually assessed in the pre-processing steps.

### **3.2. MRI data acquisition**

Neonates between 1-7 weeks postpartum were scanned during natural sleep (as per Warton et al., 2021) at the Cape Universities Brain Imaging Centre (CUBIC) on a 3T Allegra MRI (Siemens, Erlangen, Germany) using a circularly polarised birdcage coil that was custom built for imaging neonates (170.9 mm inner diameter) (Taylor et al., 2015, Jacobson et al., 2017, Warton et al., 2021). Table 8 summarizes the imaging parameters of the sMRI and DTI acquisitions. The multi-echo FLASH (MEF) acquisition for the sMRI was repeated twice with flip angles of 5° and 20°, respectively, and the DT acquisition was repeated twice with opposite phase encoding directions. The two MEF acquisitions allowed a volume with optimal contrast to be synthesized, while the acquisitions with opposite phase encoding directions were combined to correct echo-planar imaging (EPI) distortions.

**Table 8:** Imaging parameters of the scanning sequences utilised for each neuroimaging modality.

Image type	Sequences			
	Sequence type	Matrix size (voxels)	Voxel size (mm <sup>3</sup> )	Other
<b>sMRI<sup>a</sup></b>	Multi-echo FLASH (MEF) sequence (TE's 1.46, 3.14, 4.82, 6.5, 8.18, 9.86, 11.54, 13.22 ms; TR 20 ms)	144 x 144	1 x 1 x 1	128 sagittal slices
<b>DTI<sup>b</sup></b>	Twice refocused spin-echo (TRSE) echo planar imaging (EPI) sequence (TE 86 ms; non-navigated sequence TR 9 500 ms; navigated sequence TR 10 026 ms)	80 x 80	2 x 2 x 2	<ul style="list-style-type: none"> <li>- 50 slices</li> <li>- 4 or 5 reference volumes with <math>b = 0</math> s/mm<sup>2</sup></li> <li>- 30 DT volumes with <math>b = 1\ 000</math> s/mm<sup>2</sup></li> </ul>

TE: Echo time; TR: Reptation time; DT: Diffusion tensor

<sup>a</sup>Repeated with flip angles of 5° and 20°, respectively

<sup>b</sup>Repeated with opposite phase encoding (PE) directions (anterior-posterior [AP] and posterior-anterior [PA])

It is important to note that in Table 8 the navigated sequence refers to a DTI sequence that detects and corrects motion occurring during the scanning process in real time (Alhamud et al., 2012). Six of the neonates (4 placebo-treated; 2 choline-treated) had been scanned with the non-navigated DTI sequence. The DTI data of 4 of these neonates (2 placebo-treated; 2 choline-treated) did not meet the quality control criteria for inclusion and were among the 19 excluded participants. As such, there were only 2 DTI data sets (both placebo-treated neonates) acquired with the non-navigated sequence among our final set analysed. To avoid bias, these two participants were excluded from the sample.

### 3.3. Structural MR image processing

#### 3.3.1. Synthesising optimal contrast volumes

Previously, Warton et al. (2021) used FreeSurfer to synthesise volumes with optimal contrast for manual tracing (Warton et al., 2021). Firstly, the echoes from each of the MEF acquisitions were separated and proton density and T1 were estimated (Taylor et al., 2015, Warton et al., 2021). Subsequently, image volumes were generated for different flip angles to determine the synthetic volume with optimal contrast. Finally, volumes were synthesised for the optimal flip angle of 24° and TE 0 ms (Warton et al., 2021).

### 3.3.2. Manual tracing/segmentation of regions of interest (ROIs)

Freeview in FreeSurfer was used by Warton et al. (2021) to manually segment the 9 subcortical regions of interest (8 bilateral and 1 medial) on a Lenovo ThinkPad x220 tablet (Warton et al., 2021). The segmentation used the tracing procedures outlined in the Infant Brain Segmentation Manual (developed by the HST/MGH Martinos Center) (Warton et al., 2021). Visual inspection was used to exclude participants whose images had extreme motion or other artefacts before manual tracing (Warton et al., 2021).

The following regions of interest (ROIs) were bilaterally traced on T1-weighted structural MR (sMR) images: cerebellar hemispheres, putamen, caudate, hippocampus, nucleus accumbens, thalamus, amygdala and pallidum, and the cerebellar vermis on medial slices (see Figure 6) (Warton et al., 2021). The tracing primarily occurred in the coronal view while the axial and sagittal views were utilised for regions that were not distinctly visible in the coronal view (Warton et al., 2021).

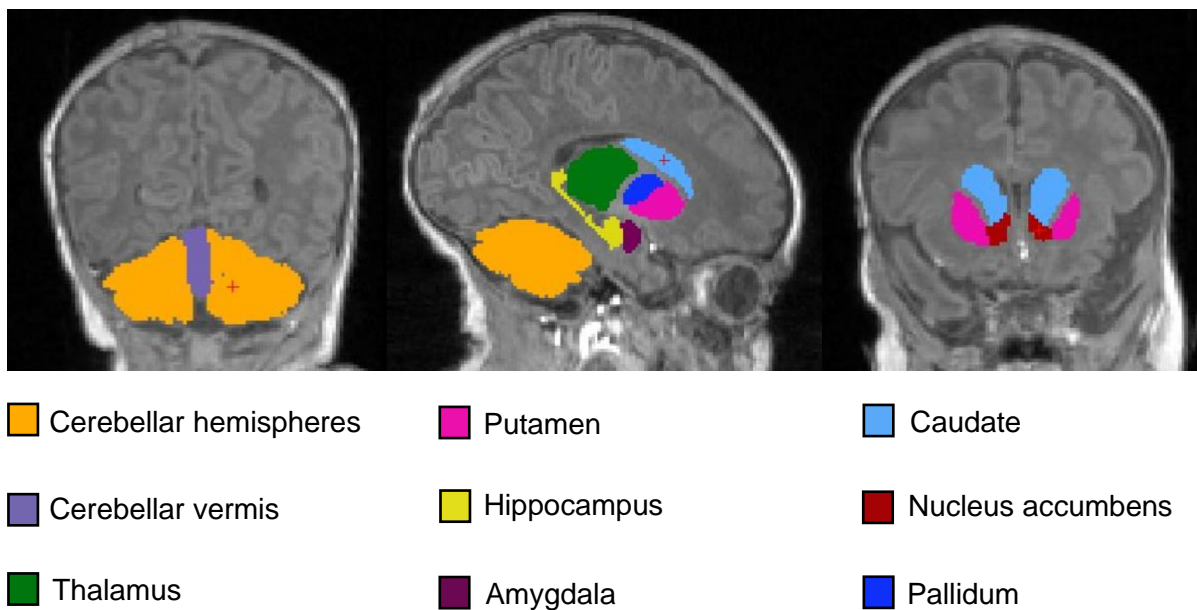


**Figure 6:** The manually traced subcortical regions of interest (ROIs) on T1-weighted structural MR (sMR) images for one of the neonates.

### 3.4. Diffusion tensor imaging (DTI) data

In the present study, the Analysis of Functional Neuroimages (AFNI) software was used to pre-process the DTI data. The pre-processing steps are summarized in Figure 7.

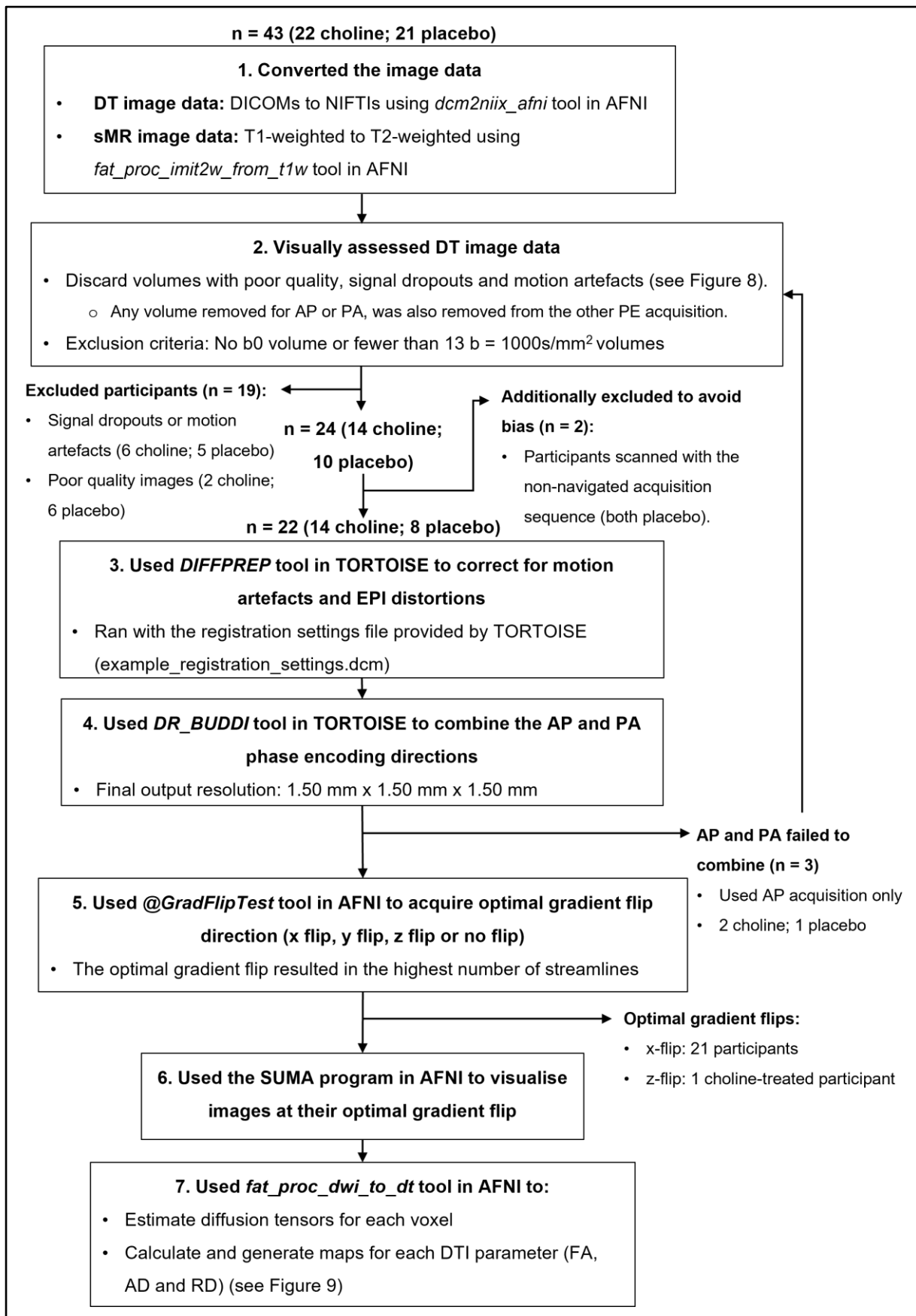


**Figure 7:** The pre-processing steps performed on the DT and sMR image data.

For step 2 in Figure 7, the visual assessment was done separately in volumes acquired with phase encoding in the AP and PA directions. Any volume discarded in the AP acquisition was also discarded in the PA acquisition, and vice versa.

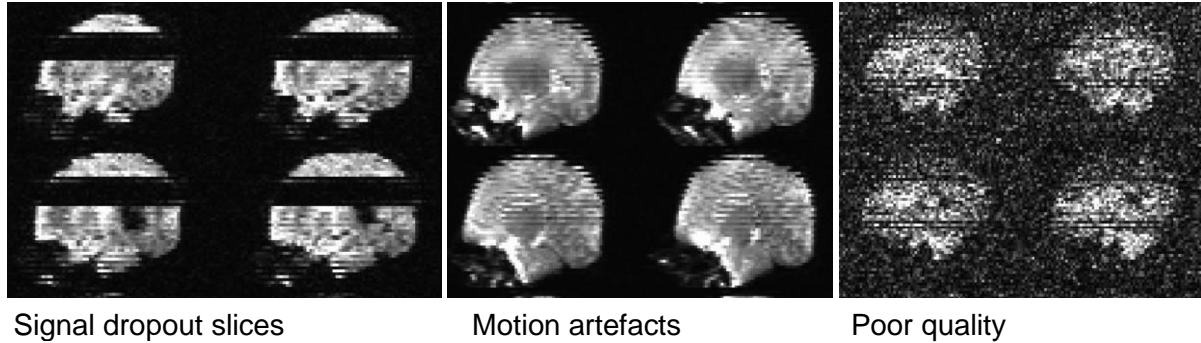


**Figure 8:** Example images with signal dropout slices, motion artefacts and poor quality.

The DIFFPREP tool in step 3 of Figure 7 generates output files (\*\_transformations.txt) for both the AP and PA acquisitions that can be used to calculate the average head motion of each participant.

To do this, each text file was used in the *do\_read\_tort\_transformations.py* script ([link to: AFNI code](#)) to estimate the position of each volume relative to one reference volume and generate 6 alignment parameters for each volume. These alignment parameters were comprised of translation values in the right-left, anterior-posterior and inferior-superior directions (in mm) as well as rotation values around the x, y and z axes (in degrees) ([link to: AFNI code](#)).

Using the differences between the alignment parameters of successive volumes, the framewise displacement (3 translational and 3 rotational motion parameters) of each volume was calculated ([link to: AFNI handout](#)) and subsequently the Euclidean Norm (Enorm) of each volume. The Euclidean norm is defined as the square root of the sum of squares of the motion parameters (equation 3) (Burnham and Anderson, 2004, Szabo, 2015). It should be noted that 1 degree of rotation is approximately equivalent to 1 mm of translation at the edge for the human brain ([link to: AFNI handout](#)).

$$Enorm(i) = \sqrt{\sum_{j=1}^6 |x_{i,j} - x_{(i-1),j}|^2} \quad \text{where } x \in \mathbb{R} \quad (3)$$

In equation 3,  $Enorm(i)$  is the Euclidean Norm of a single volume  $i$  (in mm), and  $x_{i,j}$  (with  $j = 1$  to 6) are the 6 alignment parameters for volume  $i$ .

These Euclidean Norm values were first averaged across volumes separately for the AP and PA acquisitions of each participant. These averaged values were then averaged across the AP and PA acquisitions to obtain an estimate of the average head motion per participant.

As seen after step 4 in Figure 7, the AP and PA acquisitions failed to combine for 3 participants (2 choline-treated; 1 placebo-treated). This was due to the large differences between the AP and PA coordinates of these participants. Due to this, steps 2 and 3 were repeated for each of these participants using their AP acquisition only – the default acquisition for the Siemens scanner we used. None of these participants were excluded after the visual assessment. Figure 9 shows an example of an FA map (for step 7) generated for one neonate.

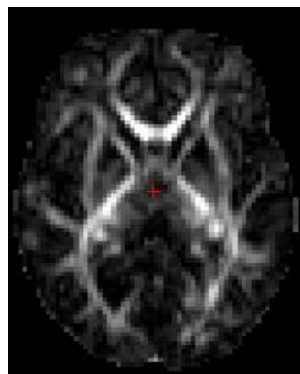


**Figure 9:** A Fractional Anisotropy (FA) map for one participant.

### **3.5. Tractography**

The current study used the manually segmented regions (ROIs) from Warton et al. (2021) as seeds for tractography.

#### **3.5.1. Transforming the ROIs to the DTI space**

Figure 10 is an illustration of the processing steps that occurred before tractography was performed.

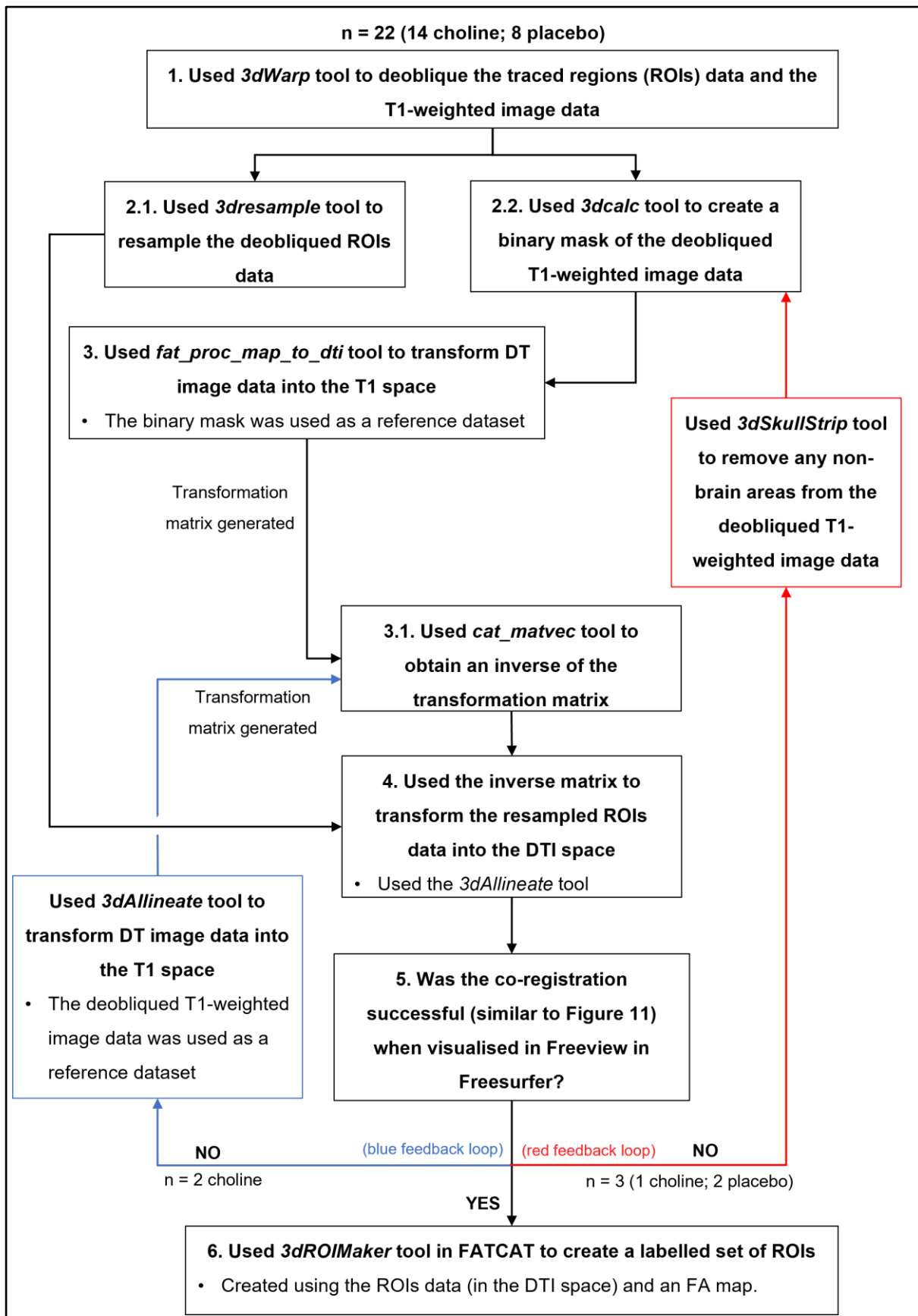


**Figure 10:** A flowchart of the processing steps performed before tractography was conducted. All the tools that were used in these steps (except for Freeview) are found in AFNI.

In step 1 in Figure 10, deobliquing was used to convert the datasets from oblique to cardinal. To ensure that the deobliqued ROIs and T1-weighted image data had the same resolution, the deobliqued ROIs were resampled to match the deobliqued T1-weighted resolution in step 2.1..

In step 5, co-registration was unsuccessful in 5 participants. Successful co-registrations were achieved after alterations were made to their processing steps as per the red and blue feedback loops shown in Figure 10. Figure 11 shows manually traced ROIs overlaid on DTI data for a single participant.

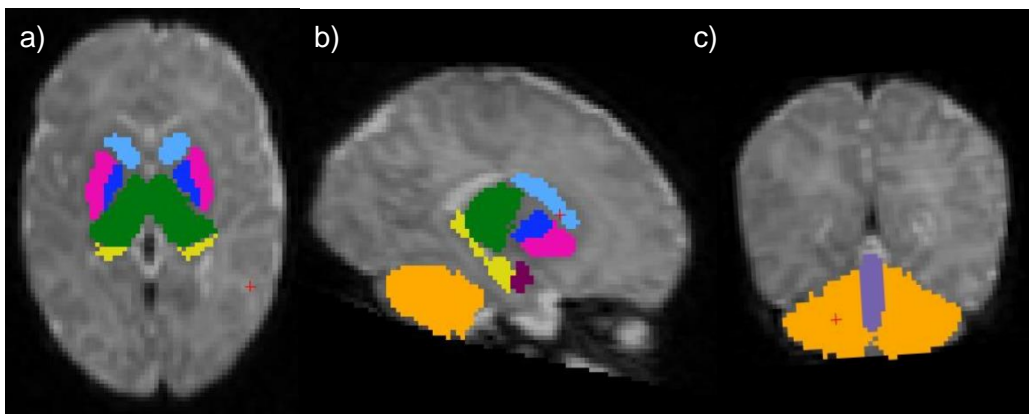


**Figure 11:** (a) Axial, (b) sagittal and (c) coronal views showing the manually traced ROIs successfully co-registered to the DTI data. Each colour represents a different manually segmented subcortical region.

### 3.5.2. Running the tractography

Probabilistic tractography was performed using the *3dTrackID* tool in the FATCAT software (Taylor et al., 2012, Taylor and Saad, 2013).

Mini-probabilistic tractography was first performed to visualise the WM connections for each participant in SUMA (Figure 12). This was executed using five iterations of the FACTID algorithm and the following parameters (Saad et al., 2004, Saad and Reynolds, 2012, Taylor and Saad, 2013, Taylor et al., 2016):

- Minimum tract length: 20 mm
- Maximum propagation angle for each proceeding voxel: 60°
- FA threshold: 0.1 – conventional FA threshold for imaging WM in infants (Dubois et al., 2014)
- Number of seed points per voxel in the x, y and z direction: 1 seed/voxel for each direction.

- The total number of seed points placed and distributed equally throughout each 3D voxel during tracking was the product of the number of seed points per voxel in each direction (i.e.  $1 \times 1 \times 1 = 1$  seed point per voxel during tracking) (<https://afni.nimh.nih.gov>).

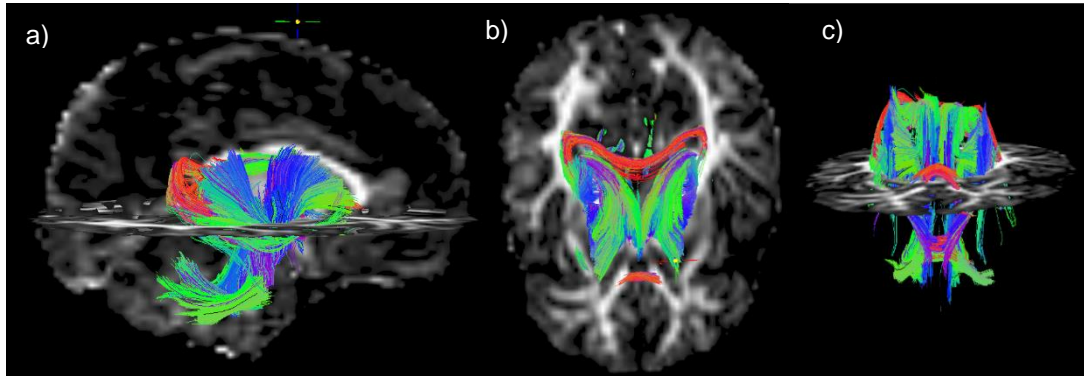


**Figure 12:** A visual illustration in the (a) sagittal, (b) axial and (c) anterior views of the WM connections between manually traced subcortical regions in one infant. The colours represent the principal diffusion directions in each WM tract; red: right-left direction, green: anterior-posterior direction and blue: superior-inferior direction.

After visualising the WM connections, full probabilistic tractography was performed to attain the DTI measures and other output variables. To this end, we performed 1000 iterations of the FACTID algorithm using the same minimum tract length, maximum propagation angle and FA threshold as described for mini-probabilistic tractography. Additionally, the minimum number of tracts per voxel for each connection was 5 streamlines/voxel/connection. This value is the product of the number of iterations (1000 iterations/seed), the number of seeds per voxel per iteration (AFNI default of 5 seeds/voxel/iteration) and the minimum number of tracts passing through each voxel for each connection (AFNI default of 0.001 streamlines/connection) (Taylor et al., 2012, Taylor and Saad, 2013).

The FATCAT tracking function automatically calculated the mean and standard deviation of the DTI measures (FA, MD, AD and RD) for each WM connection. The *fat\_mvm\_prep.py* function in AFNI was used to generate a readable output of the results obtained from *3dTrackID*. In the current study, we used FA, AD and RD to examine WM integrity.

### 3.6. Statistical analyses

The results obtained from full probabilistic tractography were used to evaluate treatment effects on WM microstructure. We also examined whether the total number of WM connections generated between our subcortical seeds differed between the choline and placebo groups.

Statistical analyses were conducted using R software. All analyses, except those comparing the total number of WM connections between treatment groups, were conducted on the subset of WM connections found in  $\geq 85\%$  of the neonates. Of the 78 WM connections generated using full probabilistic tractography, 15 WM connections were present in  $\geq 85\%$  of the participants (Figure 13). Due to the small sample size, which limited statistical power, we did not perform correction for multiple comparisons.

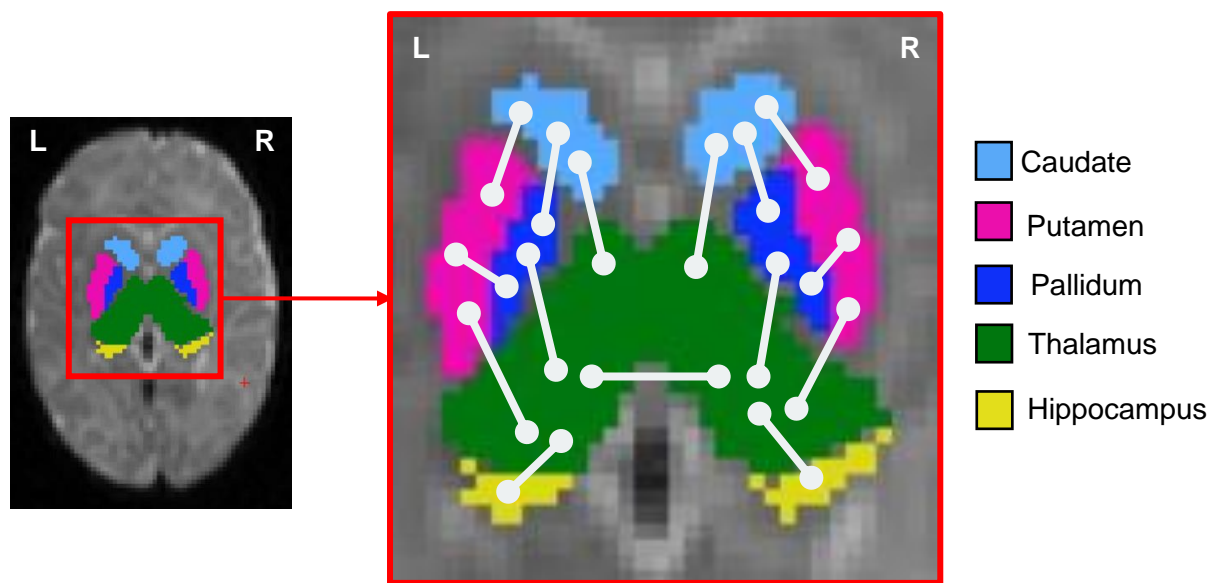


**Figure 13:** Zoomed-in axial view of the 15 WM connections between manually traced subcortical regions found in  $\geq 85\%$  of participants. L = Left-hand side of the brain; R = Right-hand side of the brain.

We checked for bias on the DTI measures for the 3 participants (2 choline-treated; 1 placebo-treated) whose AP acquisition was used due to their AP and PA acquisitions failing to combine; the 6 participants (5 choline-treated, 1 placebo-treated) exposed to marijuana during pregnancy; and the 1 choline-treated participant exposed to methamphetamine during pregnancy. This was performed by computing each participant's average FA, AD and RD across all 15 WM connections and comparing these to the rest of the sample means. If their mean, on at least one DTI measure, was 1.5 times the IQR above or below the upper or lower quartiles, respectively, the participant was excluded from all analyses that included the DTI measures.

Treatment effects on WM microstructural integrity were assessed using group differences, as well as associations with choline dose. Two different estimates of choline dose were used for these analyses: (1) maternal choline treatment adherence (in % packets consumed) was used as a proxy for choline dose with choline dose set to zero for infants born to mothers in the placebo arm, and (2) computing the total choline (in grams) consumed by the mother from

enrolment through delivery (cumulative choline dose). For the latter, we used the product of maternal treatment adherence (in % packets consumed), the number of treatment weeks from enrolment to delivery, and weekly choline dosage (2 grams/day x 7 days/week = 14 grams/week).

Given that visual recognition memory on FTII demonstrated choline-related improvements in the RCT (Jacobson et al., 2018b), we examined associations of WM microstructural integrity on visual recognition memory on the FTII and, if present, the degree to which improved WM microstructure mediates the effect of choline treatment on visual recognition memory.

### 3.6.1. Potential confounders

Potential confounders included both maternal and infant characteristics and are summarised in Table 9.

**Table 9:** All the sample characteristics.

Maternal sample characteristics		Neonatal sample characteristics	
Age at delivery (years)	Frequency of drinking at conception (days/week)	Infant sex	Length at scan (cm)
Education level	oz AA/day during pregnancy*	Gestational age (GA) at birth (weeks)	Head circumference at scan (cm)
Marriage status	oz AA/drinking day during pregnancy*	Birthweight (g)	Total intracranial volume (TIV) (mm <sup>3</sup> )
Socioeconomic status	Frequency of drinking during pregnancy (days/week)	Birth length (cm)	Average head motion (mm)
Parity	Smoking (cigarettes/day)	Birth head circumference (cm)	FASD diagnosis
Treatment adherence (%)	Marijuana (days/month)	Postnatal age at scan (weeks)	Acquisition sequence (navigated or non-navigated)
oz AA/day at conception*	Methamphetamine (days/month)	Gestational age (GA) equivalent at scan (weeks)	Total cerebral white matter volume (TWV) (mm <sup>3</sup> )
oz AA/drinking day at conception*	Number of mandrax users	Weight at scan (g)	

\*oz AA is ounces of absolute alcohol consumed

The number of potential confounders was reduced by employing rational reasoning, removing variables that were not linearly independent, and examining associations with the outcomes. These steps are described below.

### **Rational reasoning**

Since oz AA/day during pregnancy (Table 9) summarises the mother's daily alcohol consumption throughout pregnancy, this was the only alcohol exposure variable we retained to control for potential confounding by different levels of prenatal alcohol exposure. Notably, this measure, which is computed from the mother's frequency of drinking and the amount she drank per occasion, also encapsulates her drinking around the time of conception.

Marijuana and methamphetamine usage were excluded from the list of potential confounders as only a few mothers reported using these substances. Six mothers reported using marijuana during pregnancy (5 choline-treated, 1 placebo-treated) and 1 choline-treated mother reported using methamphetamine. We confirmed that the averages of the DTI measures – across all 15 WM connections – of the neonates born to these mothers did not introduce bias, thus, all these participants were included in subsequent analyses. There were no mandrax users.

Given that infant length is notoriously inaccurate and related to weight, we instead included weight measures to control for potential confounding by the size of the neonate.

Remaining potential confounders included 8 maternal characteristics (age at delivery, education, marital status, socioeconomic status (SES), parity, smoking, treatment adherence and oz AA/day during pregnancy) and 11 neonatal characteristics (infant sex, gestational age (GA) at birth and scan, weight at birth and scan, head circumference at birth and scan, postnatal age at scan, average head motion during scan, total intracranial volume (TIV) and total cerebral WM volume (TWV)). In contrast to maternal *choline* treatment adherence which will be used as a proxy for choline dose in our analyses of treatment effects, maternal treatment adherence (in both choline and placebo groups) was used here to control for potential confounding by 'maternal health'. It is assumed that a mother who is more consistent in taking her treatment may also be healthier.

### **Collinearity (Table B.1 in Appendix B)**

The number of potential confounders were further reduced by examining collinearity between pairs of variables using either Pearson  $r$  (parametric test) or Spearman rank (non-parametric test) correlation. The Shapiro-Wilk's test was used to check normality. For pairs of variables with at least fair correlations ( $r \geq 0.4$ ) (Akoglu, 2018), the variable in each pair that demonstrated stronger correlations with FA and MD was retained as a potential confounder in subsequent analyses.

Based on collinearity, (1) parity was retained in favour of maternal age at delivery, (2) postnatal age at scan instead of weight and GA at birth and scan, and (3) both TIV and TWV instead of head circumference at birth and scan (Table B.1 in Appendix B).

After removing linearly dependent variables, the remaining potential confounders, therefore, included 7 maternal characteristics (education, marital status, SES, parity, smoking, treatment adherence and oz AA/day during pregnancy) and 5 neonatal sample characteristics (infant sex, postnatal age at scan, average head motion during scan, TIV, TWV).

### **Associations with outcomes**

Outliers on outcomes (FA, AD and RD; total number of WM connections; FTII scores) were removed before examining associations between the outcomes and nominal (e.g. infant sex, marital status), ordinal (e.g. education) or discrete (e.g. parity) potential confounders. Outliers were defined as any value at least 1.5 times the IQR above or below the upper or lower quartiles, respectively.

The Independent samples T-test, Yuen test and/or Welch's T-test were used to examine associations of nominal variables with the outcomes. The choice of test was dependent on the assumptions – normality assumption and homogeneity of variances assumption – that were or were not satisfied. Independent samples T-test required normally distributed data and homogeneous variances; Welch's T-test only required homogenous variances while the Yuen test required neither. Associations of discrete and ordinal independent variables with outcomes were evaluated using one-way ANOVA and Kruskal-Wallis ANOVA tests, respectively.

We did not remove outliers on outcomes when examining associations with continuous potential confounders but instead used robust simple regression, which accounts for the presence of outliers. Continuous variables with skewed data were logarithmically transformed prior to analyses, such as all maternal alcohol consumption measures, smoking and average head motion during scan, to name a few. The logarithmic form was only used if the transformation normalised the data.

Any variable even weakly associated (at  $p < 0.1$ ) with  $\geq 30\%$  of the 45 WM outcomes being examined (FA, AD and RD in each of the 15 WM connections) was retained as a potential confounder in analyses involving DTI measures as the outcome. Similarly, any variables weakly associated (at  $p < 0.1$ ) with FTII scores or the total number of WM connections, respectively, were retained as potential confounders in analyses involving those measures. The results for this can be seen in section **4.3. Potential confounders**.

### 3.6.2. Group differences

Sample characteristics, the total number of WM connections between subcortical seeds, as well as WM integrity in the 15 WM connections found in at least 85 % of participants, were compared between the two treatment groups using the pipeline illustrated in Figure 14. This pipeline was also used to compare sample characteristics between the 22 participants who provided usable DTI data and the 21 participants who were excluded due to acquisition with a different sequence (non-navigated sequence) or DT images with signal dropouts, motion artefacts or poor quality.

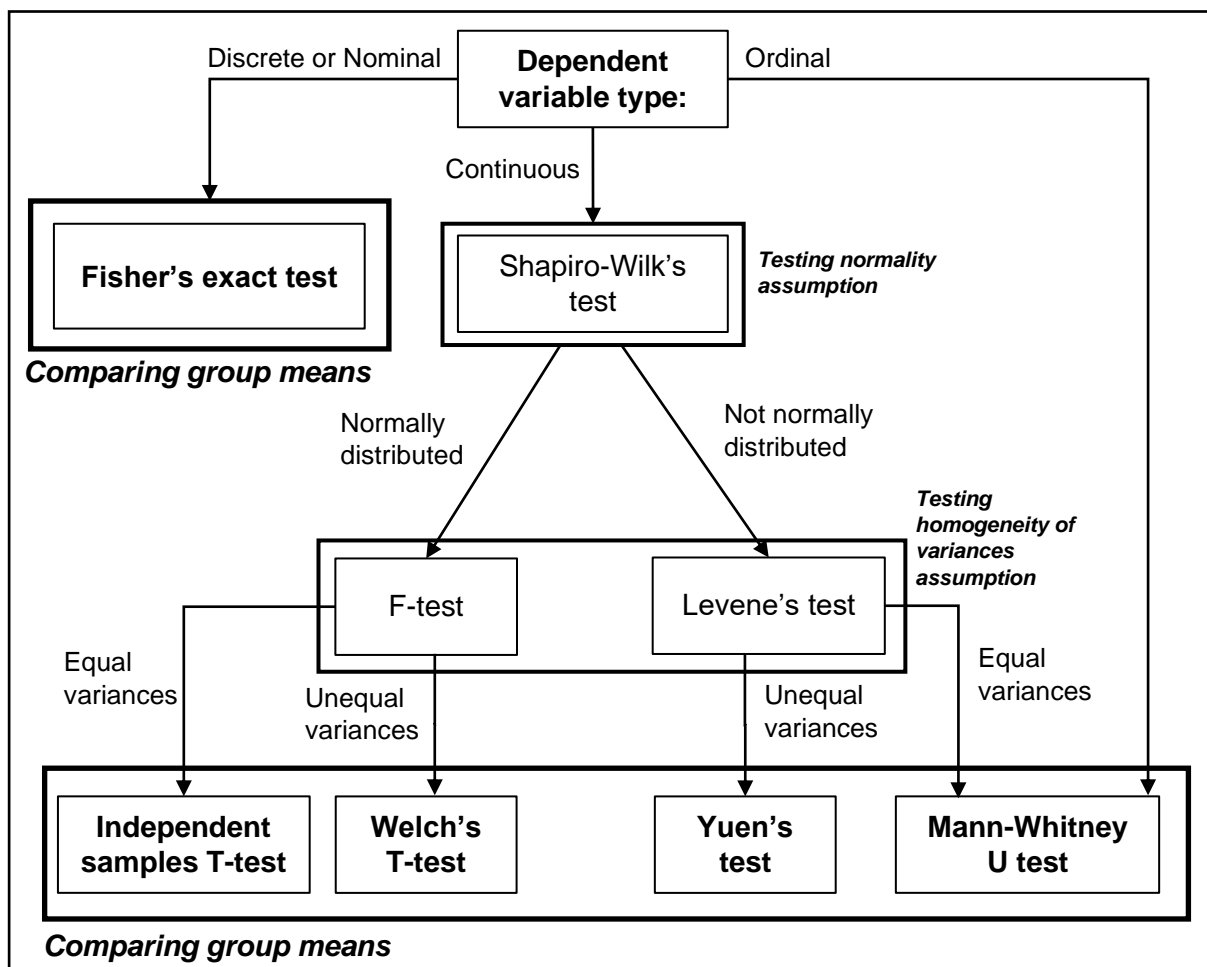


**Figure 14:** Flowchart illustrating the statistical test used to evaluate group differences. The bold red arrow is the pipeline that was followed for continuous dependent variables.

For each WM connection and each DTI measure, any value at least 1.5 times the IQR above or below the upper or lower quartile, respectively, was defined as an outlier. Outliers were excluded before performing group comparisons. Group comparisons of the sample characteristics were repeated with and without the 3 participants whose mothers had

treatment adherence < 50 %. We used analysis of covariance (ANCOVA) to control for potential confounding.

### **3.6.3. Regression analyses**

Robust linear regression (using Huber's M-estimator) was used to evaluate associations of choline dose with WM microstructure (DTI measures), and associations of WM microstructure with cognitive performance (FTII scores) controlling for potential confounding. Robust multiple regression was performed when potential confounders were present, otherwise, robust simple regression was conducted. With the knowledge that brain development tends to differ in males and females, we included a dose-by-sex interaction effect in all our multiple regression models. We report standardized regression coefficients ( $\beta$ ), standardized standard errors ( $\epsilon$ ) and p-values for each analysis with Pearson r coefficient demonstrating correlations in the scatter plots of significant findings.

## 4. Results

### 4.1. Sample characteristics

Of the 43 neonates, 24 neonates (14 choline-treated; 10 placebo-treated) provided usable DT imaging data but an additional 2 neonates from the placebo arm who had been scanned using the non-navigated sequence were excluded to avoid bias. We, therefore present data for 22 neonates (14 choline-treated; 8 placebo-treated).

Overall, sample characteristics of the 21 excluded neonates were similar to those included in our analyses, except that their mothers were less adherent to treatment ( $p = 0.025$ ), and they were, on average, 3 gestational weeks further along at enrolment ( $p = 0.002$ ) and received treatment (from enrolment through delivery) for 2.5 fewer weeks than the mothers of the participants who were included ( $p = 0.019$ ) (Table A.1.1 in Appendix A). Additionally, the excluded neonates were about 2 cm longer ( $p = 0.035$ ) and had slightly larger head circumferences at birth ( $p = 0.040$ ) (Table A.1.2 in Appendix A).

Tables 10 and 11 and Tables 12 and 13 summarise maternal and neonatal characteristics, respectively, of the 22 participants included in our analyses. Maternal characteristics did not differ between the treatment groups, except for treatment adherence. The mothers in the choline arm were less adherent to treatment than the mothers in the placebo arm, even after excluding the 3 choline-treated mothers with adherences < 50 % (Table 10). Removing these participants did not result in significant between-group differences being observed in any other sample characteristics (all  $p$ 's > 0.1). Notably, enrolment characteristics and levels of alcohol, smoking and drug use during pregnancy or around the time of conception were similar for mothers in both treatment arms (Tables 10 and 11). Infants in both treatment groups did not differ in terms of birth measures, nor their characteristics at scan (Tables 12 and 13).

**Table 10: Maternal characteristics (n = 22).**

Sample characteristics	Choline (n = 14)		Placebo (n = 8)		Statistics
	Mean (SD) or Median [IQR]	Range	Mean (SD) or Median [IQR]	Range	<i>p</i>
Maternal age at delivery (years)	27.8 (4.4)	19.1 - 33.8	28.8 (5.7)	20.7 - 37.1	0.6
Education (highest grade passed)	9 [8; 10]	5 - 12	9.5 [7; 10]	6 - 12	0.9 <sup>a</sup>
Number married	7 (50.0 %)		4 (50.0 %)		1.0 <sup>b</sup>
Socioeconomic status <sup>d</sup>	19.6 (6.7)	9.5 - 30.5	17.9 (4.5)	9.5 - 24.0	0.5
Parity	2.1 (1.7)	0 - 6	1.8 (1)	1 - 3	0.2 <sup>b</sup>
<b>Treatment adherence (%) (n = 22)</b>	<b>84.0 [49.7; 87.5]</b>	13.4 - 89.4	<b>94.3 [83.0; 98.9]</b>	75.3 - 99.6	<b>0.021<sup>c</sup></b>
<b>Treatment adherence (%) (n = 19)<sup>f</sup></b>	<b>86.3 [75.3; 87.6]</b>	56.3 - 89.4	<b>94.3 [83.0; 98.9]</b>	75.3 - 99.6	<b>0.028<sup>a</sup></b>
Gestational age (GA) at enrolment (weeks)	18.5 (3.1)	13.7 - 23.6	18.0 (4.3)	9.9 - 22.1	0.8
Duration from enrolment through delivery (weeks)	20.0 (3.6)	12.0 - 26.0	21.5 (5.3)	16.0 - 31.0	0.8
<b>Cumulative choline dose (grams)<sup>e</sup></b>	<b>189.4 [117.9; 251.7]</b>	43 - 307.2	<b>0</b>	0	<b>&lt; 0.0001<sup>c</sup></b>

Values are mean (SD) or Median [IQR]; SD: Standard deviation; IQR: Interquartile range

Independent samples T-test was used unless stated otherwise

<sup>a</sup>Mann-Whitney U test

<sup>b</sup>Fisher exact test

<sup>c</sup>Yuen test

<sup>d</sup>Hollingshead scale (Adams and Weakliem, 2011)

<sup>e</sup>Estimated as a product of maternal choline treatment adherence (with neonates in the placebo arm being set to 0), weeks from enrolment through delivery and weekly dosage (2 grams/day x 7 days/week = 14 grams/week)

<sup>f</sup>Excluding 3 mothers from the choline arm with adherences < 50.0 % (adherences of 13.4 %, 22.2 % and 29.9 %, respectively)

**Table 11: Maternal substance use (n = 22).**

Sample characteristics	Choline (n = 14)		Placebo (n = 8)		Statistics
	Mean (SD) or Median [IQR]	Range	Mean (SD) or Median [IQR]	Range	p
oz AA/day at conception <sup>d</sup>	1.1 [0.6; 2.2]	0 - 9.8	1.5 [0.7; 2.9]	0 - 3.2	0.9 <sup>c</sup>
oz AA/drinking day at conception <sup>d</sup>	4.5 (3.6)	0 - 13.7	5.1 (3.4)	0 - 9.6	0.6 <sup>c</sup>
Frequency of drinking at conception (days/week)	2 [2.0; 3.0]	0 - 5.0	2.0 [1.5; 2.8]	0 - 3.0	0.9 <sup>a</sup>
oz AA/day during pregnancy <sup>d</sup>	0.6 [0.2; 1.0]	0.04 - 2.8	0.7 [0.2; 0.9]	0.1 - 1.0	0.9 <sup>a, c</sup>
oz AA/drinking day during pregnancy <sup>d</sup>	3.1 [2.4; 4.4]	1.6 - 12.5	4.3 [2.6; 6.2]	2.5 - 7.0	0.3 <sup>c</sup>
Frequency of drinking during pregnancy (days/week)	1.6 [0.5; 1.8]	0.1 - 3.8	0.9 [0.4; 1.2]	0.1 - 1.5	0.2 <sup>b</sup>
Smoking (cigarettes/day) <sup>e</sup>	5.0 [4.2; 6.8]	2.3 - 20.0	5.0 [3.3; 11.7]	3.0 - 15.0	0.8 <sup>c</sup>
Marijuana use (days/month) <sup>e</sup>	11.0 (12.6)	0.1 - 30.1	5.0 (N/A)	N/A	N/A
Methamphetamine use (days/month) <sup>e</sup>	2.1 (N/A)	N/A	N/A	N/A	N/A
Number of mandrax users	0		0		N/A

Values are mean (SD) or Median [IQR]; SD: Standard deviation; IQR: Interquartile range

Independent samples T-test was used unless stated otherwise

<sup>a</sup>Mann-Whitney U test

<sup>b</sup>Yuen test

<sup>c</sup>Log transform was used for the statistics

<sup>d</sup>Ounces (oz) of absolute alcohol (AA) consumed

<sup>e</sup>Median, IQR, range and statistics are based only on participants who used the respective substances: Participants in the choline group who were smokers n = 14 (100 %), marijuana users n = 5 (36 %) and methamphetamine users n = 1 (7 %); participants in the placebo group who were smokers n = 7 (88 %), marijuana users n = 1 (13 %) and methamphetamine users n = 0 (0 %)

**Table 12:** Neonatal birth characteristics and FASD diagnosis (n = 22).

Sample characteristics		Choline (n = 14)		Placebo (n = 18)		Statistics
		Mean (SD) or Median [IQR]	Range	Mean (SD) or Median [IQR]	Range	p
FASD diagnosis (2019 clinic)	Number of FAS <sup>b</sup>	4 (28.6 %)		1 (12.5 %)		0.8 <sup>a</sup>
	Number of PFAS <sup>b</sup>	1 (7.1 %)		1 (12.5%)		
	Number of HE <sup>b</sup>	9 (64.3 %)		6 (75.0 %)		
Number of males		5 (35.7 %)		6 (75.0 %)		0.2 <sup>a</sup>
Gestational age (GA) at birth (weeks)		38.5 (1.3)	35.6 - 40.6	39.2 (1.7)	37.3 - 41.3	0.3
Birthweight (g)		2700 (369)	2180 - 3230	2672.5 (381.8)	2240 - 3360	0.9
Birth length (cm) <sup>c</sup>		46.9 (3.4)	40.0 - 53.0	48.1 (2.9)	43.0 - 52.0	0.4
Birth head circumference (cm)		32.1 (1.5)	30.0 - 34.0	33.1 (1.9)	30.0 - 36.0	0.2

Values are mean (SD) or Median [IQR]; SD: Standard deviation; IQR: Interquartile range

Independent samples T-test was used unless stated otherwise

<sup>a</sup>Fisher exact test

<sup>b</sup>FAS = Fetal Alcohol Syndrome, PFAS = Partial Fetal Alcohol Syndrome and HE = Non-syndromal Heavily Exposed

<sup>c</sup>Missing data for n = 1 placebo-treated neonate

**Table 13:** Neonatal scan characteristics (n = 22).

Sample characteristics	Choline (n = 14)		Placebo (n = 18)		Statistics
	Mean (SD) or Median [IQR]	Range	Mean (SD) or Median [IQR]	Range	p
Postnatal age at scan (weeks)	3.0 [2.8; 3.3]	1.6 - 5.1	2.7 [1.5; 3.3]	1.3 - 6.1	0.4 <sup>a</sup>
Gestational age (GA) equivalent at scan (weeks)	41.6 (1.6)	37.7 - 43.6	42.0 (2.6)	39.3 - 47.0	0.6
Weight at scan (g) <sup>b</sup>	3160 (445)	2340 - 3960	3198 (1104)	2280 - 5100	0.4 <sup>a</sup>
Length at scan (cm) <sup>b</sup>	48.6 (2.2)	45.5 - 52.2	48.5 (3.4)	45.0 - 53.4	0.9
Head circumference at scan (cm) <sup>b</sup>	35.0 (1.6)	31.8 - 37.7	35.6 (3.1)	32.8 - 39.0	0.6
Total intracranial volume (mm <sup>3</sup> )	492 250 (60 311)	393 000 - 579 400	494 188 (81 118)	420 000 - 655 300	0.9
Total cerebral white matter volume (mm <sup>3</sup> ) <sup>c</sup>	124 121 (18 463)	99 000 - 156 142	121 539 (23 953)	101 013 - 172 092	0.8
Average head motion (mm) <sup>d</sup>	0.3 [0.3; 0.5]	0.2 - 0.7	0.3 [0.2; 0.4]	0.2 - 0.6	0.2 <sup>e</sup>

Values are mean (SD) or Median [IQR]; SD: Standard deviation; IQR: Interquartile range

Independent samples T-test was used unless stated otherwise

<sup>a</sup>Mann-Whitney U test

<sup>b</sup>Missing data for n = 3 placebo-treated neonates

<sup>c</sup>Missing data for n = 1 choline-treated neonate

<sup>d</sup>Euclidean norm

<sup>e</sup>Log transform was used for the statistical analysis

## **4.2. Additional exclusions due to potential bias on DTI measures**

Of the 3 participants (2 choline-treated; 1 placebo-treated) whose AP acquisitions were used due to their AP and PA acquisitions failing to combine, one choline-treated participant was excluded due to their average AD value (across all 15 WM connections examined) being 1.5 times the IQR above the upper quartile. Thus, 21 participants (13 choline-treated; 8 placebo-treated) were included in all analyses that included the DTI measures.

The removal of this participant did not alter the significant differences in the sample characteristics between the included and excluded participants (Tables A.2.1-A.2.4 in Appendix A), except that the differences in the head circumferences at birth was no longer significant (Table A.2.3 in Appendix A).

In addition, among the neonates included in our analyses ( $n = 21$ ), maternal treatment adherence remained the only difference observed between the choline- and placebo-treated neonates and their mothers (Tables A.3.1-A.3.4 in Appendix A). In other words, before and after excluding the 3 choline-treated mothers with adherence  $< 50\%$ , median treatment adherences of mothers in the choline arm were  $83.5\%$  [43.1; 87.4] and  $85.3\%$  [64.6; 87.9], respectively, compared to  $94.3\%$  [83.0; 98.9] (Table A.3.1 in Appendix A).

## **4.3. Potential confounders**

As described previously, the variables assessed for potential confounding after removing collinearity included 7 maternal characteristics (parity, socioeconomic status (SES), marital status, oz AA/day during pregnancy, education, treatment adherence, and smoking) and 5 neonatal characteristics (infant sex, postnatal age at scan, total intracranial volume (TIV), total cerebral WM volume (TWV), average head motion during scan). Results from our analyses of assessing collinearity are presented in Table B.1 in Appendix B.

After removing the choline-treated participant that introduced bias on the DTI measures, only postnatal age at scan, infant sex and TIV were each weakly associated (at  $p < 0.1$ ) with at least 30 % of the 45 WM outcomes examined (FA, AD and RD in each of the 15 WM connections) (Tables 14).

None of the maternal characteristics considered were associated with at least 14 WM outcome measures. Subsequently, only postnatal age at scan, infant sex and TIV were controlled for in the analyses examining the effects of choline treatment on WM outcomes. However, given that there were only 2 girls (25 %) in the placebo arm, we could not control for potential confounding by infant sex when examining group differences (as seen in Tables 15-17). Moreover, none of the potential confounders considered showed any association with FTII

scores (all  $p$ 's > 0.2), and only infant sex was associated with the total number of WM connections ( $p < 0.05$ ).

**Table 14:** The number of WM connections in which each potential confounder showed a weak association (at  $p < 0.1$ ) with the different WM outcomes being examined (FA, AD or RD in each of the 15 WM connections). Infant sex, postnatal age at scan and TIV each showed weak associations with at least 14 (> 30 %) of the WM outcomes being assessed (in bold).

	FA	AD	RD	Total (%)
<b>Maternal characteristics</b>				
Marital status <sup>a</sup>	2	2	0	4 (9 %)
Education	1	0	0	1 (2 %)
Socioeconomic status (SES)	1	3	2	6 (13 %)
Parity <sup>b</sup>	1	2	7	10 (22 %)
Treatment adherence	2	0	0	2 (4 %)
oz AA/day during pregnancy	0	1	2	3 (7 %)
Smoking	0	0	0	0 (0 %)
<b>Neonatal characteristics</b>				
Postnatal age at scan	5	8	10	<b>23 (51 %)</b>
Infant sex	2 <sup>c</sup>	9 <sup>d</sup>	5 <sup>e</sup>	<b>16 (36 %)</b>
Total intracranial volume (TIV)	3	5	6	<b>14 (31 %)</b>
Total cerebral WM volume (TWV)	3	1	8	12 (27 %)
Average head motion	0	1	0	1 (2 %)

<sup>a</sup>Independent samples *T*-test was used: 0 and 3 outliers, respectively, were removed for the 2 WM connections showing associations with FA; 0 and 1 outliers, respectively, were removed for the WM connections showing associations with AD.

<sup>b</sup>One-way ANOVA was used: 3 outliers were removed for the WM connection showing associations with FA; 1 outlier for each WM connection showing associations with AD; 0 outliers for 4 WM connections and 1 outlier for 3 WM connections showing associations with RD.

<sup>c</sup>Independent samples *T*-test and Yuen test, respectively, were used: 0 and 3 outliers were removed, respectively.

<sup>d</sup>Independent samples *T*-test was used for 5 WM connections: 0, 1 and 3 outliers removed for 2, 2 and 1 WM connections, respectively; Welch's *T*-test was used for 4 WM connections: 0 and 2 outliers removed for 2 WM connections, respectively.

<sup>e</sup>Independent samples *T*-test was used: 0, 1 and 3 outliers removed for 1, 2 and 2 WM connections respectively.

Given that maternal choline treatment adherence was also used as a proxy for choline dose, in the choline-treated arm (however, with dose set to zero in the placebo arm), it is worth noting that maternal treatment adherence (as a proxy for 'maternal health') was associated with FA in only 2 WM connections (Table 14), namely between the L and R thalami (at  $p < 0.05$ ) and between the R putamen and the R pallidum (at  $p < 0.1$ ). Therefore, we did not control for 'maternal health' in any of our analyses.

#### **4.4. Group differences in the total number of WM connections**

A total of 78 WM connections were generated from full probabilistic tractography. Since this comparison did not rely on DTI outcomes (FA, AD, or RD) as measures of WM integrity, all 22 neonates in whom tractography had been performed were included in this analysis. After excluding the 3 choline-treated participants whose mothers had low treatment adherence (< 50 %), the Independent samples T-test did not reveal differences in the total number of WM connections between the choline- and placebo-treated neonates (choline mean (SD): 26 (7), 10-39 WM connections; placebo: 22 (6), 13-28 WM connections;  $p = 0.2$ ).

#### **4.5. Treatment effects on WM microstructure**

Given that these analyses examined effects on WM integrity, we excluded the choline-treated participant for whom using the AP data resulted in bias on the DTI measures. Therefore, the data from 21 neonates (13 choline-treated; 8 placebo-treated) were used in these analyses.

##### **4.5.1. Group differences**

The 3 choline-treated neonates whose mothers were poorly adherent (< 50 %) were excluded from all analyses investigating group differences in WM measures. Given that the 15 WM connections we examined were present in  $\geq 85$  % of participants, each connection was present in at least 15 participants.

After removing outliers, choline-treated neonates demonstrated lower FA in 2 WM connections (between L thalamus and L caudate; L caudate and L pallidum) (Table 15; Figures 15 and 16), lower AD in the connection between the R putamen and R pallidum (Table 16; Figure 17), and lower RD in the WM connection between the L putamen and L pallidum (Table 17; Figure 18). Lower FA in the L caudate and L pallidum connection, and lower AD in the R putamen and R pallidum connection remained significant after adjusting for potential confounding by postnatal age at scan and TIV.

**Table 15:** Comparison by treatment group of fractional anisotropy (FA) in the 15 WM connections present in  $\geq 85\%$  of participants.

WM connections	FA							
	Choline (n = 10)			Placebo (n = 8)			Statistics	
	n (% males)	Mean (SD)	Range	n (% males)	Mean (SD)	Range	p	p'
<b>L Thalamus – L Caudate<sup>a</sup></b>	7 (14.3 %)	<b>0.26 (0.007)</b>	0.22 - 0.35	8 (75.0 %)	<b>0.29 (0.03)</b>	0.25 - 0.33	<b>0.045</b>	0.1
L Thalamus – L Putamen <sup>b</sup>	9 (33.3 %)	0.32 (0.02)	0.31 - 0.40	8 (75.0 %)	0.35 (0.03)	0.29 - 0.38	0.08	
L Thalamus – L Pallidum	10 (40.0 %)	0.35 (0.03)	0.30 - 0.41	8 (75.0 %)	0.37 (0.04)	0.30 - 0.43	0.2	
L Thalamus – L Hippocampus <sup>c</sup>	9 (44.4 %)	0.32 (0.01)	0.31 - 0.36	7 (71.4 %)	0.32 (0.02)	0.25 - 0.38	0.9	
L Thalamus – R Thalamus <sup>d</sup>	9 (44.4 %)	0.34 (0.06)	0.24 - 0.44	5 (100 %)	0.33 (0.02)	0.25 - 0.39	0.7	
L Caudate – L Putamen <sup>e</sup>	9 (33.3 %)	0.32 (0.02)	0.30 - 0.35	6 (83.3 %)	0.32 (0.01)	0.30 - 0.38	0.9	
<b>L Caudate – L Pallidum<sup>b</sup></b>	8 (25.0 %)	<b>0.31 (0.01)</b>	0.29 - 0.35	6 (83.3 %)	<b>0.33 (0.02)</b>	0.31 - 0.36	<b>0.013</b>	<b>0.023</b>
L Putamen – L Pallidum <sup>b</sup>	9 (33.3 %)	0.30 (0.02)	0.28 - 0.36	8 (75.0 %)	0.30 (0.02)	0.26 - 0.36	0.7	
R Thalamus – R Caudate <sup>b</sup>	8 (25.0 %)	0.26 (0.02)	0.22 - 0.33	7 (71.4 %)	0.27 (0.03)	0.23 - 0.33	0.9	
R Thalamus – R Putamen	10 (40.0 %)	0.32 (0.02)	0.29 - 0.34	8 (75.0 %)	0.33 (0.01)	0.30 - 0.34	0.5	
R Thalamus – R Pallidum <sup>b</sup>	8 (25.0 %)	0.34 (0.02)	0.31 - 0.41	7 (71.4 %)	0.36 (0.03)	0.31 - 0.40	0.2	
R Thalamus – R Hippocampus <sup>d</sup>	10 (40.0 %)	0.32 (0.02)	0.28 - 0.35	5 (80.0 %)	0.33 (0.003)	0.29 - 0.38	0.3	
R Caudate – R Putamen	8 (25.0 %)	0.32 (0.02)	0.29 - 0.35	8 (75.0 %)	0.33 (0.02)	0.29 - 0.35	0.4	
R Caudate – R Pallidum	9 (33.3 %)	0.32 (0.02)	0.29 - 0.36	7 (71.4 %)	0.33 (0.02)	0.28 - 0.37	0.3	
R Putamen – R Pallidum <sup>e</sup>	9 (33.3 %)	0.31 (0.03)	0.26 - 0.34	6 (83.3 %)	0.29 (0.01)	0.29 - 0.36	0.3	

SD: Standard deviation; n: Total number of participants

Independent samples T-test was used (p)

ANCOVA was used to adjust for potential confounding by total intracranial volume (TIV) and postnatal age at scan (p')

No outliers were removed unless stated otherwise

<sup>a</sup>Two outliers were removed from the choline group

<sup>b</sup>One outlier was removed from the choline group

<sup>c</sup>An outlier was removed from each treatment group

<sup>d</sup>Two outliers were removed from the placebo group

<sup>e</sup>One outlier was removed from the placebo group



**Figure 15:** Choline-treated neonates demonstrated lower fractional anisotropy (FA) than the placebo-treated neonates in the WM connection between the L thalamus and L caudate.

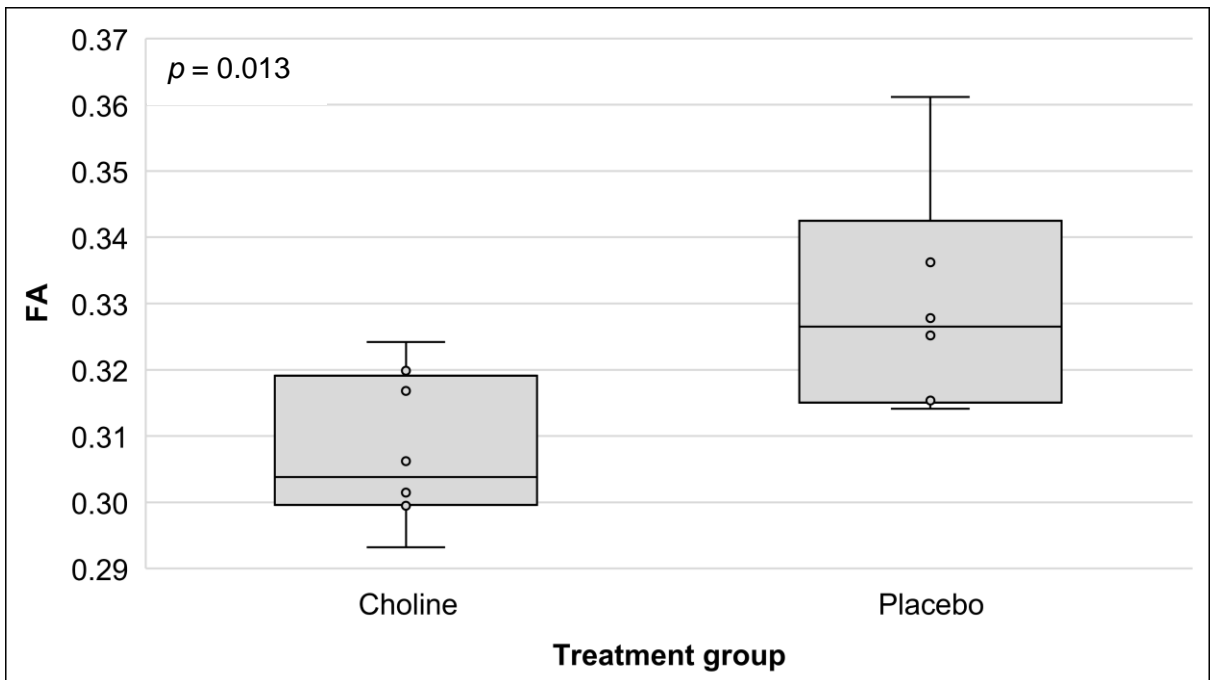


**Figure 16:** Choline-treated neonates demonstrated lower fractional anisotropy (FA) than the placebo-treated neonates in the WM connection between the L caudate and L pallidum. This difference remained significant after controlling for postnatal age at scan and total intracranial volume (TIV).

**Table 16:** Comparisons by treatment group of the mean axial diffusivity (AD) in the 15 WM connections present in  $\geq 85\%$  of participants.

WM connections	AD ( $10^{-3}$ mm <sup>2</sup> /s)							
	Choline (n = 10)			Placebo (n = 8)			Statistics	
	n (% males)	Mean (SD)	Range	n (% males)	Mean (SD)	Range	p	p'
L Thalamus – L Caudate <sup>a</sup>	8 (37.5 %) <sup>a</sup>	1.44 (0.10)	1.37 - 1.79	8 (75.0 %)	1.51 (0.20)	1.34 - 1.77	0.3	
L Thalamus – L Putamen	10 (40.0 %)	1.43 (0.05)	1.39 - 1.54	8 (75.0 %)	1.46 (0.06)	1.35 - 1.54	0.4	
L Thalamus – L Pallidum	10 (40.0 %)	1.42 (0.06)	1.34 - 1.59	8 (75.0 %)	1.46 (0.08)	1.32 - 1.52	0.3	
L Thalamus – L Hippocampus	10 (40.0 %)	1.52 (0.04)	1.48 - 1.58	8 (75.0 %)	1.52 (0.05)	1.47 - 1.78	0.9	
L Thalamus – R Thalamus <sup>d</sup>	9 (44.4 %)	1.84 (0.24)	1.58 - 2.30	6 (83.3 %)	1.83 (0.11)	1.35 - 2.01	0.9	
L Caudate – L Putamen	9 (33.3 %)	1.42 (0.04)	1.37 - 1.53	8 (75.0 %)	1.46 (0.06)	1.36 - 1.55	0.2	
L Caudate – L Pallidum	9 (33.3 %)	1.41 (0.06)	1.34 - 1.52	7 (71.4 %)	1.46 (0.06)	1.37 - 1.51	0.2	
L Putamen – L Pallidum <sup>b</sup>	8 (37.5 %)	1.40 (0.02)	1.32 - 1.50	8 (75.0 %)	1.40 (0.05)	1.34 - 1.49	1.0	
R Thalamus – R Caudate <sup>a</sup>	8 (37.5 %)	1.44 (0.05)	1.35- 1.71	7 (71.4 %)	1.45 (0.08)	1.33 - 1.55	0.8	
R Thalamus – R Putamen	10 (40.0 %)	1.42 (0.04)	1.37 - 1.52	8 (75.0 %)	1.44 (0.04)	1.39 - 1.51	0.2	
R Thalamus – R Pallidum <sup>c</sup>	6 (16.7 %)	1.38 (0.01)	1.46 - 1.53	7 (71.4 %)	1.43 (0.08)	1.31 - 1.52	0.1	
R Thalamus – R Hippocampus <sup>a</sup>	9 (44.4 %)	1.50 (0.04)	1.43 - 1.69	7 (71.4 %)	1.53 (0.05)	1.46 - 1.74	0.2	
R Caudate – R Putamen <sup>a</sup>	7 (14.3 %)	1.41 (0.02)	1.35 - 1.50	8 (75.0 %)	1.45 (0.06)	1.34 - 1.51	0.09	
R Caudate – R Pallidum <sup>a</sup>	8 (25.0 %)	1.41 (0.03)	1.37 - 1.53	7 (71.4 %)	1.46 (0.06)	1.35 - 1.52	0.06	
<b>R Putamen – R Pallidum<sup>a</sup></b>	8 (37.5 %)	<b>1.39 (0.01)</b>	1.37- 1.51	7 (71.4 %)	<b>1.42 (0.02)</b>	1.29 - 1.45	<b>0.002</b>	<b>0.003</b>

SD: Standard deviation; n: Total number of participants

Independent samples T-test (p)

ANCOVA was used to adjust for potential confounding by total intracranial volume (TIV) and postnatal age at scan (p')

No outliers were removed unless stated otherwise

<sup>a</sup>One outlier was removed from the choline group

<sup>b</sup>Two outliers were removed from the choline group

<sup>c</sup>Three outliers were removed from the choline group

<sup>d</sup>One outlier was removed from the placebo group

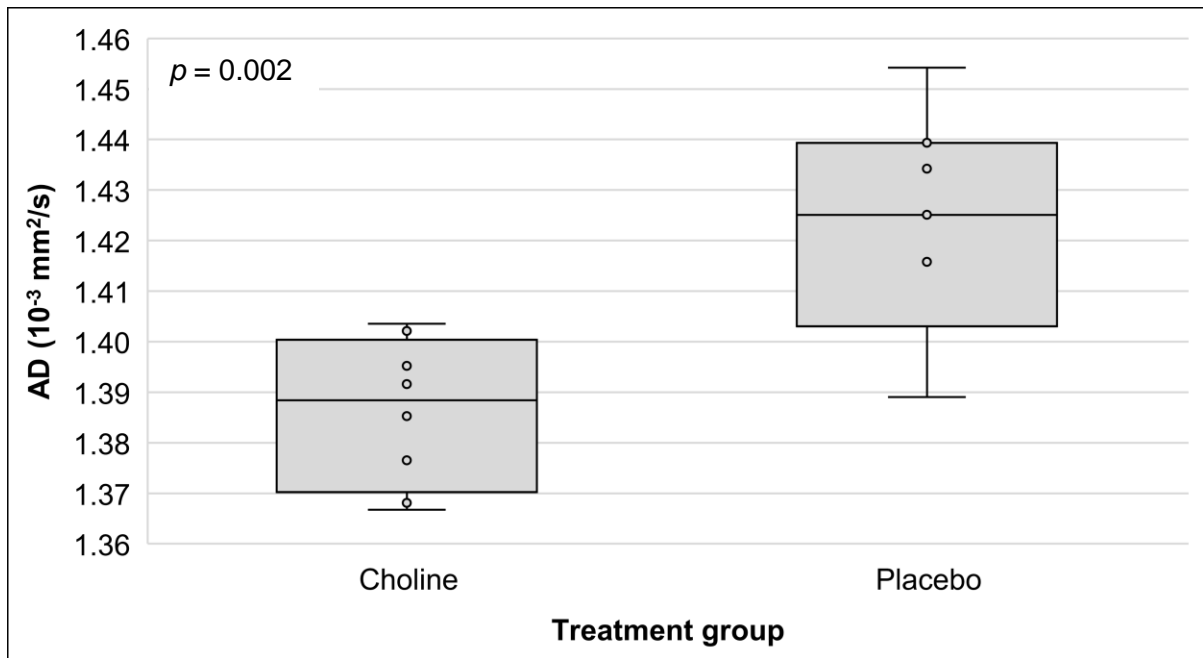


**Figure 17:** Participants in the choline-treated group demonstrated lower axial diffusivity (AD) than those in the placebo-treated group in the WM connection between the R putamen and R pallidum. This difference remained significant after adjusting for potential confounding by total intracranial volume a (TIV) and postnatal age at scan.

**Table 17:** Comparisons by treatment group of the mean radial diffusivity (RD) in the 15 WM connections found in  $\geq 85\%$  of participants.

WM connections	RD							
	Choline (n = 10)			Placebo (n = 8)			Statistics	
	n (% males)	Mean (SD)	Range	n (% males)	Mean (SD)	Range	p	p'
L Thalamus – L Caudate <sup>a</sup>	8 (37.5 %)	0.96 (0.10)	0.84 - 1.19	8 (75.0 %)	1.51 (0.20)	1.34 - 1.77	0.9	
L Thalamus – L Putamen <sup>a</sup>	9 (33.3 %)	0.84 (0.03)	0.78 - 0.92	8 (75.0 %)	1.46 (0.06)	1.35 - 1.54	1.0	
L Thalamus – L Pallidum	10 (40.0 %)	0.82 (0.04)	0.78 - 0.91	8 (75.0 %)	1.46 (0.08)	1.32 - 1.52	0.5	
L Thalamus – L Hippocampus	10 (40.0 %)	0.91 (0.04)	0.85 - 0.97	8 (75.0 %)	1.52 (0.05)	1.47 - 1.78	0.7	
L Thalamus – R Thalamus	9 (44.4 %)	1.06 (0.05)	0.97 - 1.25	7 (71.4 %)	1.83 (0.11)	1.35 - 2.01	0.5	
L Caudate – L Putamen <sup>a</sup>	8 (37.5 %)	0.85 (0.02)	0.81 - 0.89	7 (71.4 %)	1.46 (0.06)	1.36 - 1.55	0.4	
L Caudate – L Pallidum	9 (33.3 %)	0.86 (0.02)	0.83 - 0.91	6 (83.3 %)	1.46 (0.06)	1.37 - 1.51	0.9	
<b>L Putamen – L Pallidum<sup>a</sup></b>	10 (40.0 %)	<b>0.86 (0.02)</b>	0.82 - 0.91	8 (75.0 %)	<b>0.88 (0.02)</b>	0.76 - 0.91	<b>0.046</b>	0.1
R Thalamus – R Caudate <sup>a</sup>	8 (37.5 %)	0.95 (0.06)	0.87 - 1.11	7 (71.4 %)	0.97 (0.07)	0.83 - 1.09	0.5	
R Thalamus – R Putamen	10 (40.0 %)	0.85 (0.04)	0.80 - 0.92	8 (75.0 %)	0.85 (0.03)	0.80 - 0.90	0.7	
R Thalamus – R Pallidum	9 (33.3 %)	0.8 (0.03)	0.75 - 0.84	7 (71.4 %)	0.8 (0.04)	0.73 - 0.86	0.8	
R Thalamus – R Hippocampus	10 (40.0 %)	0.91 (0.04)	0.85 - 1.03	7 (71.4 %)	0.9 (0.05)	0.81 - 1.06	0.4	
R Caudate – R Putamen	8 (25.0 %)	0.85 (0.03)	0.80 - 0.91	8 (75.0 %)	0.86 (0.04)	0.81 - 0.94	0.6	
R Caudate – R Pallidum <sup>a</sup>	8 (25.0 %)	0.84 (0.03)	0.80 - 0.96	7 (71.4 %)	0.85 (0.03)	0.77 - 0.90	0.7	
R Putamen – R Pallidum <sup>b</sup>	9 (33.3 %)	0.86 (0.04)	0.81 - 0.93	6 (83.3 %)	0.89 (0.02)	0.81 - 0.92	0.2	

SD: Standard deviation; n: Total number of participants

Independent samples T-test (p)

ANCOVA was used to adjust for potential confounding by total intracranial volume (TIV) and postnatal age at scan (p')

No outliers were removed unless stated otherwise

<sup>a</sup>One outlier was removed from the choline group

<sup>a</sup>One outlier was removed from the placebo group

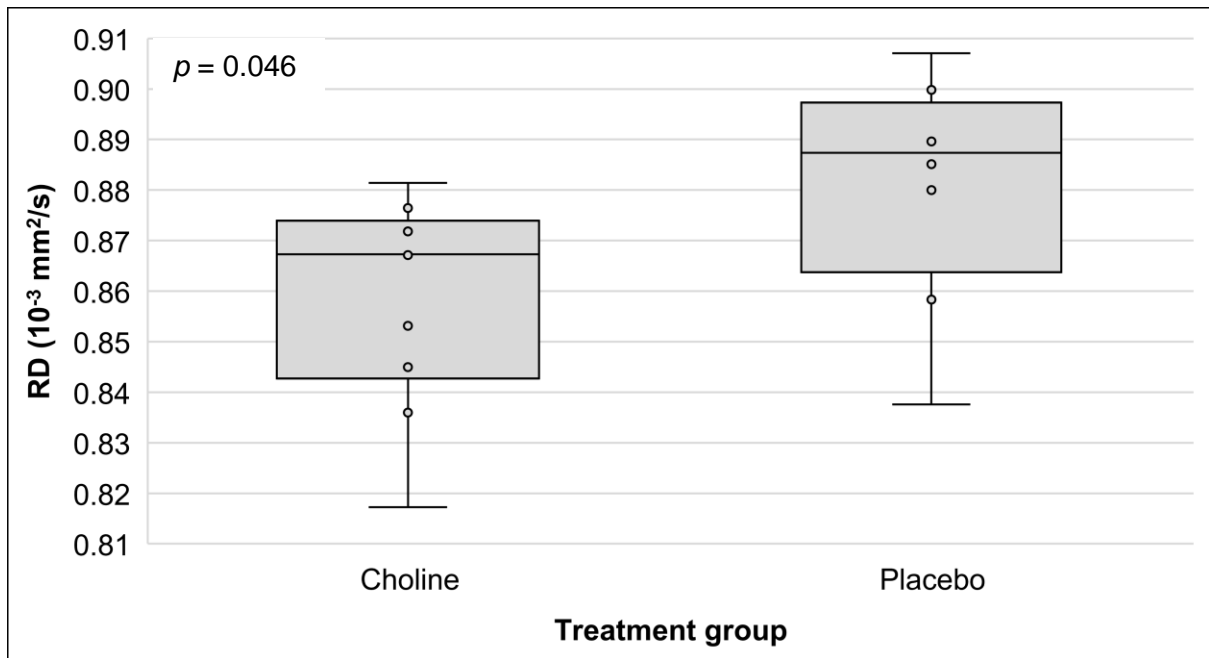


**Figure 18:** Neonates in the choline group demonstrated significantly lower radial diffusivity (RD) than those in the placebo group in the WM connection between the L putamen and L pallidum.

#### 4.5.2. Associations with choline dose

As mentioned previously, we examined associations of WM microstructure with choline dose approximated by either maternal choline treatment adherence or the total amount of choline consumed (in grams) by the mother from enrolment through delivery.

##### Choline dose approximated by treatment adherence

Using maternal choline treatment adherence as a proxy for choline dose (in % choline packets consumed), and after adjusting for infant sex, postnatal age at scan and TIV, as well as a possible dose-by-sex interaction effect, increasing choline dose was found to be associated with lower FA in the WM connection between R caudate and R pallidum (Table 18). The correlation of this association is illustrated in Figure 19.

**Table 18:** Associations of fractional anisotropy (FA) in each WM connection with choline treatment adherence (in % choline packets consumed) as a proxy for choline dose while controlling for potential confounding by infant sex and postnatal age at scan, total intracranial volume (TIV), and a possible dose-by-sex interaction effect.

WM connections	$\beta_{dose}$ ( $\epsilon_{dose}$ )	$\rho_{dose}$	$\beta_{infant\ sex}$ ( $\epsilon_{infant\ sex}$ )	$\beta_{age}$ ( $\epsilon_{age}$ )	$\beta_{TIV}$ ( $\epsilon_{TIV}$ )	$\beta_{dose*sex}$ ( $\epsilon_{dose*sex}$ )	$\rho_{dose*sex}$
L Thalamus – L Caudate	-0.29 (0.15)	0.08	0.06 (0.15)	-0.28 (0.19)	0.18 (0.18)	0.17 (0.15)	0.3
L Thalamus – L Putamen	-0.26 (0.22)	0.3	-0.22 (0.22)	-0.22 (0.29)	0.14 (0.28)	0.22 (0.23)	0.4
L Thalamus – L Pallidum	-0.12 (0.26)	0.7	-0.28 (0.25)	-0.45 (0.34)	0.19 (0.33)	0.15 (0.27)	0.6
L Thalamus – L Hippocampus	-0.09 (0.13)	0.5	-0.28 (0.12)	0.92 (0.16)	-0.08 (0.16)	-0.05 (0.13)	0.7
L Thalamus – R Thalamus	-0.07 (0.20)	0.7	0.56 (0.19)	-0.31 (0.26)	0.31 (0.25)	0.14 (0.20)	0.5
L Caudate – L Putamen	-0.19 (0.27)	0.5	0.04 (0.27)	-0.36 (0.34)	0.22 (0.33)	-0.22 (0.28)	0.4
L Caudate – L Pallidum	-0.42 (0.27)	0.2	-0.12 (0.28)	-0.6 (0.35)	0.48 (0.35)	-0.45 (0.29)	0.2
L Putamen – L Pallidum	0.06 (0.29)	0.8	0.02 (0.29)	0.27 (0.38)	-0.08 (0.37)	-0.02 (0.31)	1.0
R Thalamus – R Caudate	0.03 (0.25)	0.9	0.05 (0.24)	0.24 (0.31)	-0.37 (0.31)	0.39 (0.26)	0.2
R Thalamus – R Putamen	-0.38 (0.22)	0.1	0.07 (0.21)	0.73 (0.29)	-0.51 (0.28)	0.13 (0.23)	0.6
R Thalamus – R Pallidum	-0.06 (0.20)	0.8	-0.53 (0.20)	0.62 (0.25)	-0.02 (0.25)	-0.29 (0.20)	0.2
R Thalamus – R Hippocampus	-0.26 (0.17)	0.2	-0.22 (0.17)	0.56 (0.22)	0.10 (0.22)	0.25 (0.18)	0.2
R Caudate – R Putamen	-0.34 (0.24)	0.2	0.19 (0.24)	0.38 (0.30)	0.09 (0.30)	0.22 (0.25)	0.4
<b>R Caudate – R Pallidum</b>	<b>-0.55 (0.20)</b>	<b>0.016</b>	0.34 (0.19)	0.52 (0.25)	-0.22 (0.24)	0.27 (0.20)	0.2
R Putamen – R Pallidum	-0.37 (0.22)	0.1	0.55 (0.21)	0.13 (0.28)	0.33 (0.27)	-0.25 (0.22)	0.3

$\beta$ : Standardized regression coefficients;  $\epsilon$ : Standardized standard errors.

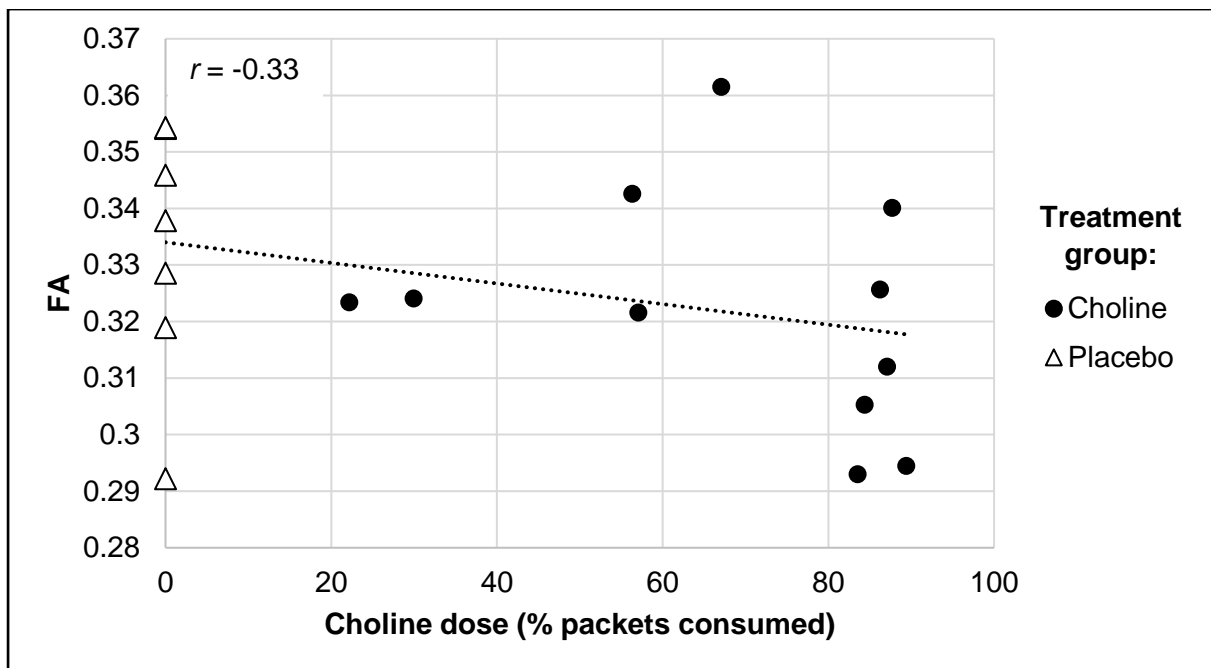


**Figure 19:** Increasing choline dose was associated with lower FA in the WM connection between the R caudate and R pallidum. The correlation coefficient shown is Pearson  $r$ .

In addition, Table 19 shows that increasing choline dose was associated with lower AD in 2 WM connections: between R putamen and R pallidum, and R caudate and R putamen, with a significant dose-by-sex interaction effect in the latter (underlined in Table 19). Correlations between choline dose and AD for these WM connections are illustrated in Figures 20 and 21.

In contrast, we did not find associations of choline treatment adherence with RD in any WM connections (all  $p$ 's > 0.05; Table C.1.1 in Appendix C).

**Table 19:** Associations of axial diffusivity (AD) in each WM with maternal choline treatment adherence (in % packets consumed as a proxy for choline dose), controlling for infant sex, postnatal age at scan , total intracranial volume (TIV) and after and a dose-by-sex interaction effect.

WM connections	$\beta_{dose}$ ( $\epsilon_{dose}$ )	$\rho_{dose}$	$\beta_{infant\ sex}$ ( $\epsilon_{infant\ sex}$ )	$\beta_{age}$ ( $\epsilon_{age}$ )	$\beta_{TIV}$ ( $\epsilon_{TIV}$ )	$\beta_{dose*sex}$ ( $\epsilon_{dose*sex}$ )	$\rho_{dose*sex}$
L Thalamus – L Caudate	-0.05 (0.23)	0.8	0.23 (0.22)	-0.44 (0.28)	0.04 (0.27)	-0.02 (0.23)	0.9
L Thalamus – L Putamen	-0.005 (0.14)	1.0	-0.52 (0.14)	-0.34 (0.18)	-0.25 (0.18)	0.11 (0.15)	0.5
L Thalamus – L Pallidum	0.03 (0.18)	0.9	-0.38 (0.18)	-0.57 (0.23)	0.001 (0.23)	0.29 (0.19)	0.2
L Thalamus – L Hippocampus	-0.09 (0.26)	0.7	-0.02 (0.25)	0.43 (0.34)	-0.5 (0.33)	-0.08 (0.27)	0.8
L Thalamus – R Thalamus	-0.10 (0.13)	0.5	0.52 (0.13)	0.14 (0.18)	0.05 (0.17)	0.18 (0.14)	0.3
L Caudate – L Putamen	-0.08 (0.19)	0.7	-0.34 (0.18)	-0.49 (0.24)	-0.22 (0.23)	0.15 (0.19)	0.4
L Caudate – L Pallidum	-0.04 (0.12)	0.8	-0.45 (0.12)	-0.76 (0.16)	0.35 (0.16)	-0.16 (0.13)	0.3
L Putamen – L Pallidum	0.09 (0.3)	0.8	-0.28 (0.29)	0.01 (0.39)	-0.15 (0.38)	0.13 (0.32)	0.7
R Thalamus – R Caudate	-0.07 (0.15)	0.7	0.05 (0.15)	0.16 (0.19)	-0.74 (0.19)	-0.03 (0.16)	0.9
R Thalamus – R Putamen	-0.17 (0.13)	0.2	-0.41 (0.13)	-0.400 (0.17)	-0.09 (0.17)	0.21 (0.14)	0.1
R Thalamus – R Pallidum	-0.01 (0.14)	1.0	-0.74 (0.13)	0.16 (0.17)	-0.28 (0.17)	0.28 (0.14)	0.07
R Thalamus – R Hippocampus	0.12 (0.19)	0.6	-0.19 (0.19)	-0.25 (0.25)	0.43 (0.25)	0.43 (0.20)	0.05
<b>R Caudate – R Putamen</b>	<b>-0.50 (0.15)</b>	<b>0.006</b>	0.04 (0.15)	-0.32 (0.19)	-0.08 (0.19)	0.36 (0.16)	<u>0.041</u>
R Caudate – R Pallidum	-0.13 (0.24)	0.6	-0.45 (0.24)	0.31 (0.30)	-0.41 (0.29)	0.21 (0.25)	0.4
<b>R Putamen – R Pallidum</b>	<b>-0.66 (0.14)</b>	<b>0.0003</b>	0.37 (0.13)	-0.40 (0.17)	0.37 (0.17)	-0.04 (0.14)	0.8

$\beta$ : Standardized regression coefficients;  $\epsilon$ : Standardized standard errors

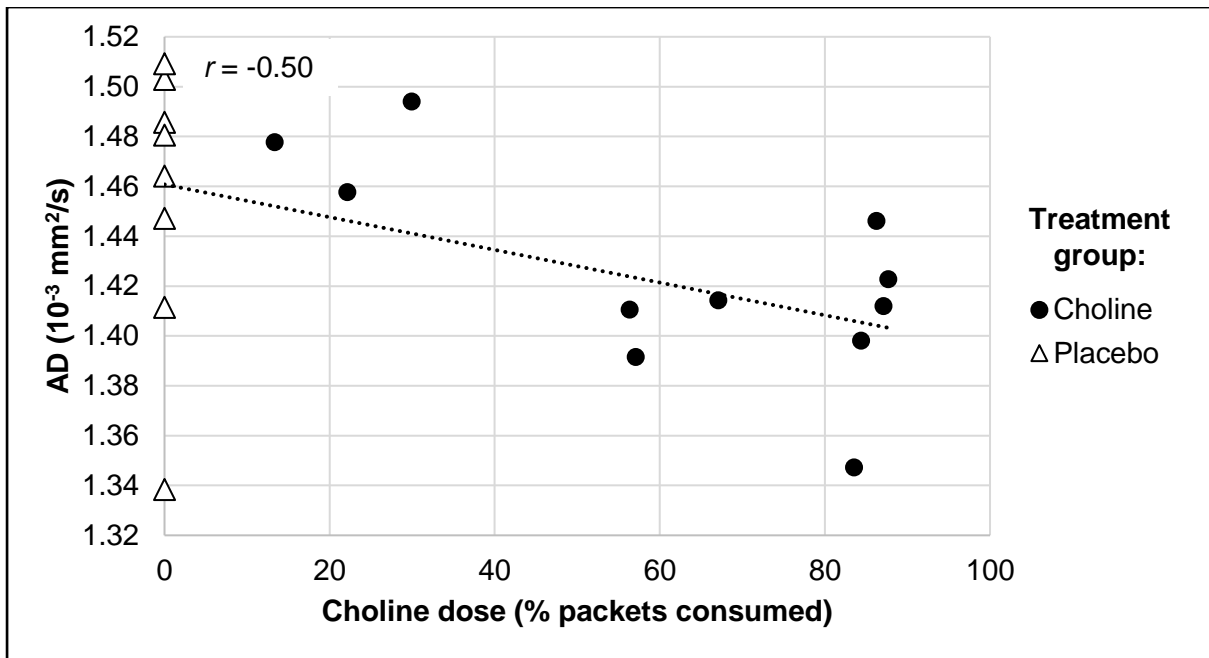


**Figure 20:** Increasing choline dose was associated with lower axial diffusivity (AD) in the WM connection between the R caudate and R putamen. The correlation coefficient shown is Pearson  $r$ .

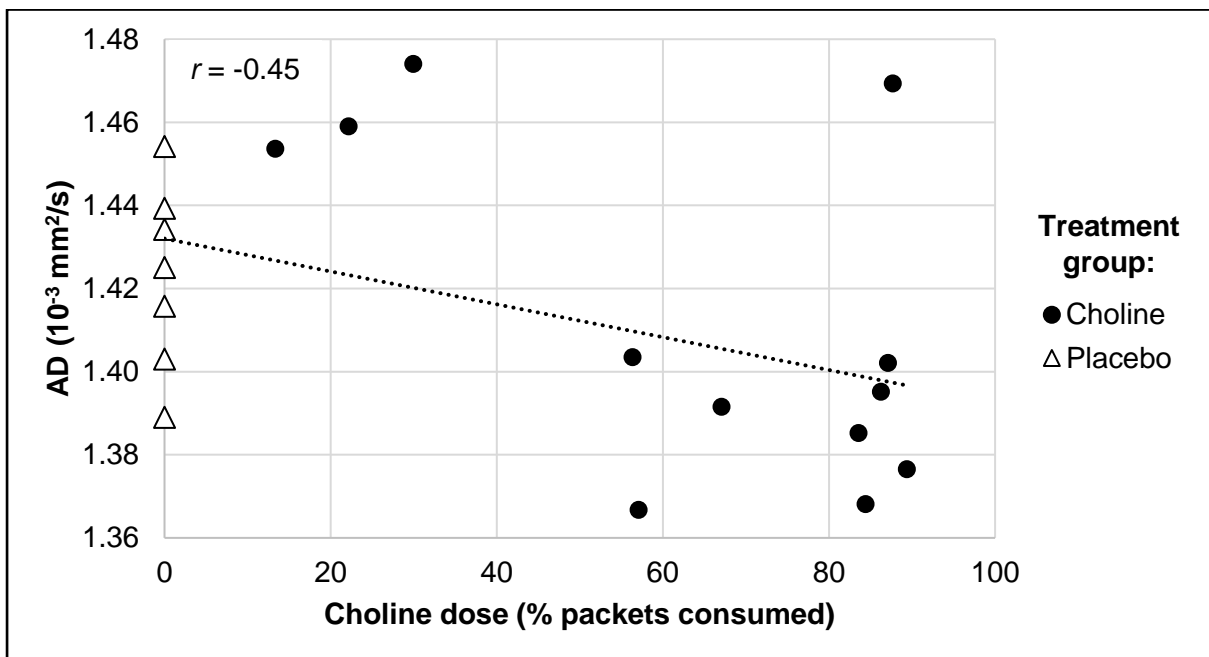


**Figure 21:** Increasing choline dose was associated with lower axial diffusivity (AD) in the WM connection from the R putamen to the R pallidum. The correlation coefficient shown is Pearson  $r$ .

### **Choline dose approximated by total grams consumed from enrolment through delivery**

Cumulative choline dose across pregnancy showed associations with FA and AD in the same WM connections that showed associations with choline treatment adherence (Tables C.2.1 and C.2.2; Figures C.2.1-C.2.3 in Appendix C). Again, no significant associations were observed with RD in any connections (Table C.2.3 in Appendix C).

#### **4.5.3. Summary of WM connections showing choline treatment effects**

In summary, after controlling for confounders, 4 WM connections between the caudate, pallidum and putamen showed choline treatment effects. Choline-related FA decreases were observed in the bilateral connection between the caudate and pallidum, and AD decreases in WM connections between the R putamen and R pallidum or R caudate. Figure 22 is an illustration of these WM connections:

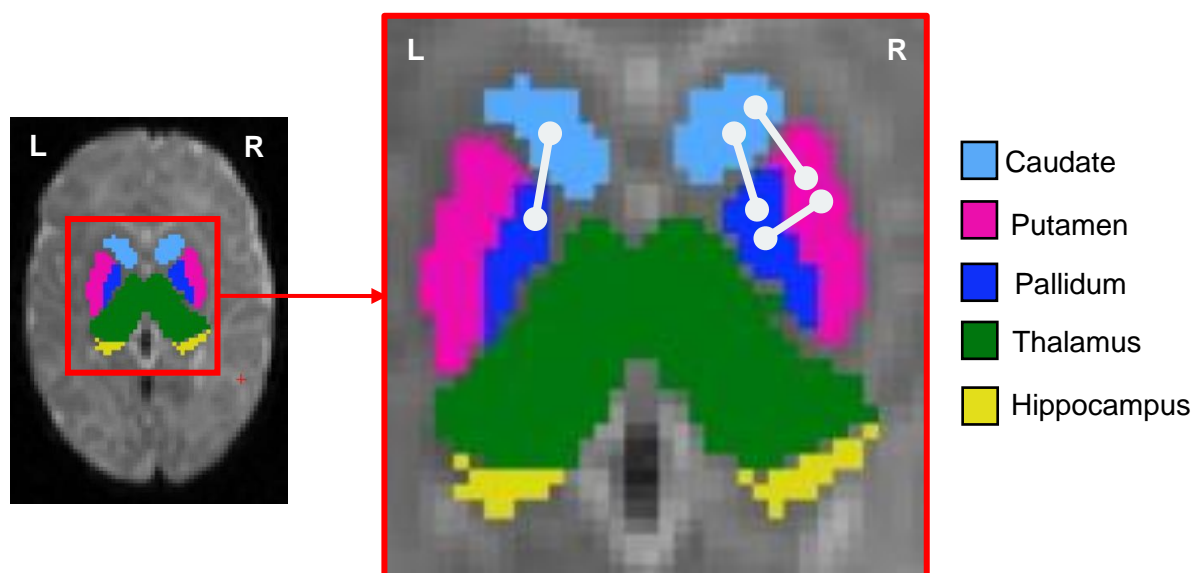


**Figure 22:** A zoomed-in axial view of the WM connections where choline-treated neonates demonstrated either lower FA or lower AD. L denotes the left-hand side of the brain and R denotes the right-hand side of the brain.

#### **4.6. Associations of WM integrity with visual recognition memory on the FTII**

The RCT from which the participants of the current sub-study were recruited found associations of choline treatment with visual recognition memory on the FTII (Jacobson et al., 2018b). Here we examined associations of WM microstructural integrity with visual recognition memory.

Given that the DTI measures were included in this analysis, the choline-treated participant for whom using only AP data resulted in bias on the DTI measures was excluded. Of the 21 neonates with non-biased DTI data, FTII data were only available for 14 neonates (8 choline-treated, 6 placebo-treated).

We found no significant associations of FA or AD in any of our WM connections with visual recognition memory on the FTII (Table 20). Increasing RD in the WM connection between the L and R thalami was, however, associated with poorer visual recognition memory, while increasing RD in the connection between the R caudate and R putamen was associated with better visual recognition memory (Figures 23 and 24). Notably, the latter is the same WM connection where we found choline treatment-related reductions in AD. Given that the DTI measure (RD) showing associations with visual recognition memory differed from that showing choline treatment effects (AD), we did not perform a mediation analysis.

**Table 20:** Associations of microstructural measures in each WM connection with visual recognition memory on the FTII.

WM connections	FA		AD		RD	
	$\beta$ ( $\epsilon$ )	$p$	$\beta$ ( $\epsilon$ )	$p$	$\beta$ ( $\epsilon$ )	$p$
L Thalamus – L Caudate	0.25 (0.32)	0.4	0.15 (0.29)	0.6	-0.07 (0.31)	0.8
L Thalamus – L Putamen	0.22 (0.32)	0.5	0.35 (0.28)	0.2	-0.001 (0.29)	1.0
L Thalamus – L Pallidum	0.33 (0.31)	0.3	0.47 (0.28)	0.1	-0.01 (0.29)	1.0
L Thalamus – L Hippocampus	-0.34 (0.27)	0.2	0.28 (0.28)	0.3	0.63 (0.31)	0.1
<b>L Thalamus – R Thalamus</b>	-0.04 (0.35)	0.9	-0.25 (0.34)	0.5	<b>-0.62 (0.27)</b>	<b>0.038</b>
L Caudate – L Putamen	-0.17 (0.34)	0.6	0.28 (0.31)	0.4	0.41 (0.27)	0.2
L Caudate – L Pallidum	0.22 (0.33)	0.5	0.38 (0.29)	0.2	0.07 (0.35)	0.9
L Putamen – L Pallidum	-0.32 (0.27)	0.3	-0.22 (0.28)	0.5	0.37 (0.27)	0.2
R Thalamus – R Caudate	-0.02 (0.32)	0.9	0.36 (0.3)	0.3	0.34 (0.30)	0.3
R Thalamus – R Putamen	0.04 (0.29)	0.9	-0.19 (0.28)	0.5	-0.18 (0.31)	0.6
R Thalamus – R Pallidum	-0.04 (0.3)	0.9	0.07 (0.3)	0.8	0.14 (0.30)	0.6
R Thalamus – R Hippocampus	-0.28 (0.32)	0.4	-0.48 (0.32)	0.2	-0.07 (0.32)	0.8
<b>R Caudate – R Putamen</b>	-0.07 (0.3)	0.8	0.44 (0.29)	0.2	<b>0.54 (0.18)</b>	<b>0.009</b>
R Caudate – R Pallidum	0.38 (0.29)	0.2	0.20 (0.31)	0.5	-0.19 (0.31)	0.5
R Putamen – R Pallidum	0.34 (0.28)	0.3	0.25 (0.38)	0.5	-0.32 (0.29)	0.3

$\beta$ : Standardized regression coefficient;  $\epsilon$ : Standardized standard errors

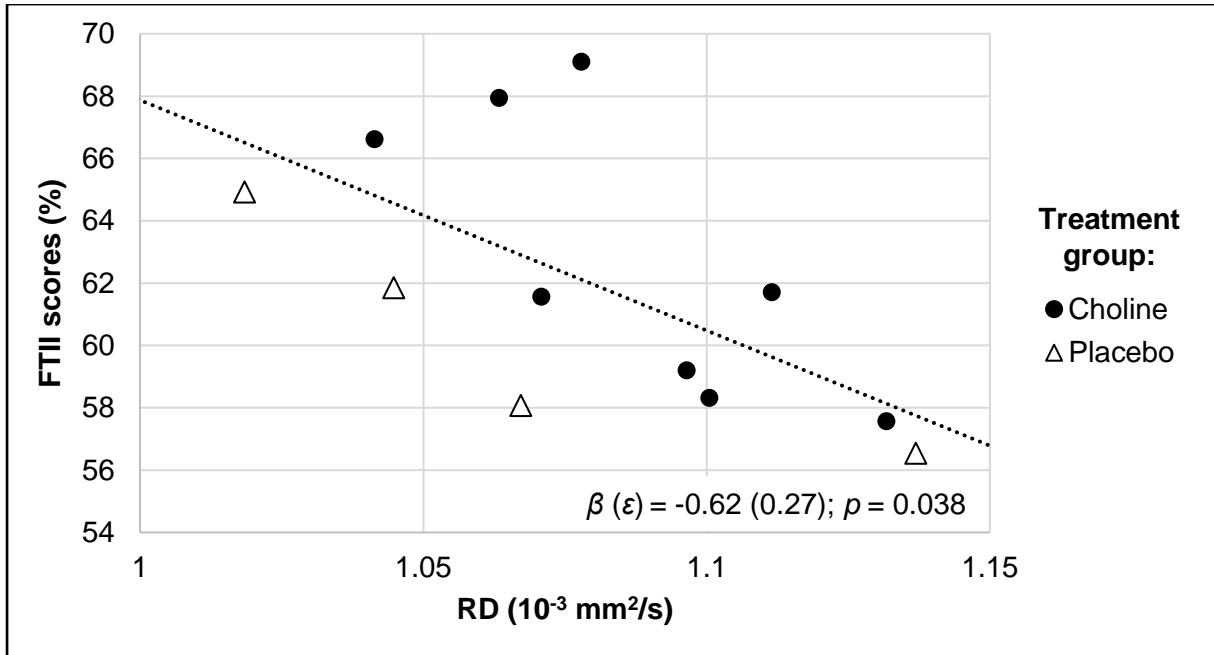


**Figure 23:** Lower radial diffusivity (RD) in the WM connection between the L and R thalami was associated with better visual recognition memory on the FTII.  $\beta$  is the standardized regression coefficient and  $\epsilon$  is the standardized standard error.

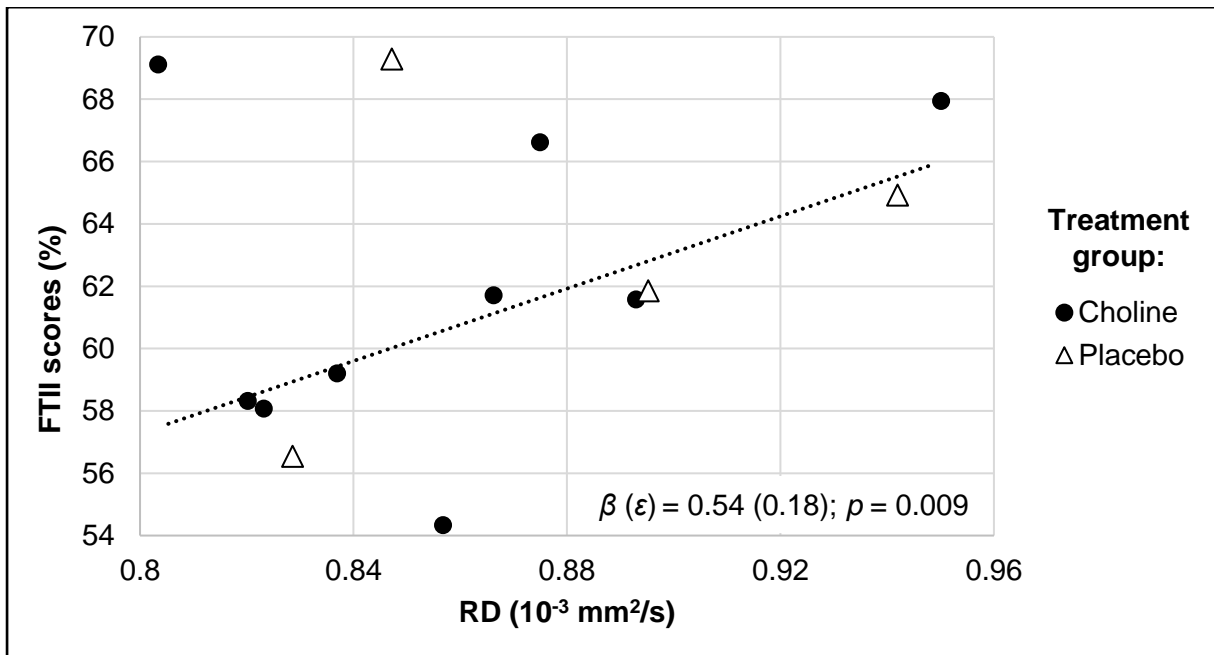


**Figure 24:** Increasing radial diffusivity (RD) in the WM connection between the R caudate and R putamen with better visual recognition memory on the FTII.  $\beta$  denotes the standardized regression coefficient and  $\epsilon$  denotes the standardized standard error.

## 5. Discussion

To our knowledge, this is the first study to investigate the effects of high-dose prenatal maternal choline supplementation on the microstructure of WM connecting select subcortical regions in neonates exposed to alcohol prenatally. We also evaluated the relationship between measures of WM microstructure in these WM connections and recognition memory on the FTII at 12 months.

### 5.1. Treatment effects on WM microstructure

We used group differences and associations with choline dose, approximated by either maternal treatment adherence in the choline group or cumulative choline dose consumed by the mother from enrolment through delivery, to examine the effects of choline on the WM microstructure of neonates exposed to alcohol prenatally.

Given that maturing axons and pre-myelination of WM fibres are characterised by stable FA and decreasing radial and axial diffusivity (Dubois et al., 2008), we had hypothesised that neonates born to mothers who received choline supplementation would demonstrate lower radial and axial diffusivities than those in the placebo group in WM connections between selected subcortical seeds.

As hypothesised, we observed choline-related decreases in AD on the right in the WM connecting the putamen to both the caudate and pallidum (Figure 25), but the choline-related decrease in RD seen on the left in the connection between the putamen and pallidum did not survive after controlling for confounders. We also found choline-related reductions in FA bilaterally in WM connecting the caudate and pallidum (Figure 25), and choline-related effects in the connection between the L caudate and L thalamus that did not survive after confounders were controlled.

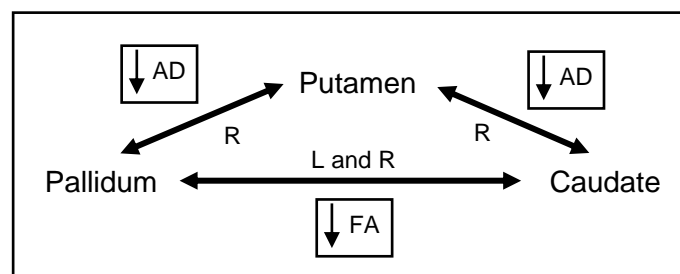


**Figure 25:** The WM connections showing choline-related reductions in either axial diffusivity (AD) or fractional anisotropy (FA). L denotes the WM connections on the left-hand side of the brain and R on the right-hand side.

Anatomically the caudate, putamen, pallidum and thalamus are separated by a V-shaped WM structure known as the internal capsule. Specifically, the anterior limb of the internal capsule separates the caudate from the putamen and pallidum and contains the thalamocortical-corticothalamic and frontopontine fibres, to name a few (Haines and Mihailoff, 2018). The posterior limb of the internal capsule separates the thalamus from the pallidum and putamen, and among others, contains pallidothalamic fibres, fibres of the corticospinal and corticonigral tracts, and the optic and auditory radiations (Haines and Mihailoff, 2018).

Three of the 4 WM connections where choline-related changes were observed were on the right-hand side of the brain (see Figure 25). Liu et al. (2021) showed that in the first six postnatal months deep brain regions, such as the thalamus, pallidum, putamen and posterior limb of the internal capsule demonstrate rightward asymmetry based on MD measures. Given that MD can be explained using AD and/or RD, this asymmetry in development suggests and explains why the alterations we observed in the microstructure of subcortical WM connected to the putamen and pallidum were predominantly on the right-hand side of the brain with AD being the detectable DTI measure.

Additionally, the 4 WM connections show choline-related changes between 3 basal ganglia (BG) seeds (caudate, putamen and pallidum; Figure 25), one of which plays a role in one of the functional domains in which infants in the choline arm of the Jacobson and colleagues RCT showed improvements – the putamen played a role in visual recognition memory (FTII) (Jacobson et al., 2018b, Warton et al., 2021). While the caudate and pallidum have not been directly linked to this functional domain, both are involved in hearing (Chavez and Zaborszky, 2017) and the pallidum is involved in motor functions (Alexander et al., 1986) and coordination (Debaere et al., 2004), which are all key aspects of eyeblink conditioning response, the other functional domain where choline related improvements were observed in the RCT (Jacobson et al., 2018b).

Moreover, the caudate and putamen, which form part of the neostriatum, are input structures of the BG (Lanciego et al., 2012, Haines and Mihailoff, 2018). The striatum receives input from cortical and subcortical structures (Lanciego et al., 2012). Notably, functionally distinct cortical regions project to different parts of the striatum. In 1986, Alexander et al. (1986) proposed that the putamen and caudate are BG input structures for motor, oculomotor, dorsolateral prefrontal and lateral orbitofrontal circuits.

More recently, Tziortzi et al. (2014) showed using probabilistic tractography that the frontal lobe projects to around 82 % of the total striatal volume, including almost the entire caudate and pre-commissural putamen. The parietal lobe projects primarily to the post-commissural caudate and putamen, making up around 11 % of the total striatal volume; the temporal lobe

to small, interspersed parts of the pre-commissural caudate, nucleus accumbens and ventral post-commissural putamen making up about 5 % of the striatal volume, and the occipital lobe only to the ventral post-commissural putamen. Moreover, the authors showed that distinct regions within the caudate and pre-commissural putamen receive projections from limbic, executive, rostral-motor and caudal-motor regions of the frontal lobe. After receiving inputs, the striatum then projects to the pallidum (comprising the globus pallidus and ventral pallidum), which is an output structure of the BG, and the pallidum projects back to the cortex via the thalamus thereby completing the cortico-BG-thalamo-cortical circuit (Haber, 2016, Mole, 2018). The caudate-pallidum and putamen-pallidum connections where we found lower FA and AD, respectively, in the choline-treated neonates form part of the cortico-BG-thalamo-cortical circuit (Chakravarthy and Balasubramani, 2022).

Interestingly, no choline-related changes were observed in WM connecting to the rest of the seeds included in the analysis, namely, the nucleus accumbens, amygdala, cerebellar vermis and hemispheres, thalamus and hippocampus. There is variability in the development of each of these seeds. For example, the formation of the hippocampus begins at 8 weeks GA (Glenn, 2009) and starts resembling an adult hippocampus by 18-20 weeks GA (Kier et al., 1997); cells of the amygdala are visible by 12 weeks GA and the major nuclei is fully formed by 15 weeks GA (Nikolić and Kostović, 1986); the main/dorsal thalamus enlarges and is separated from the diencephalon by 6-7 weeks GA (Cooper, 1950) with major groups of the adult thalamic nuclei being easily delineated by 12-15 weeks GA using Nissl-staining (Kostovic and Goldman-Rakic, 1983); the cerebellar vermis and hemispheres have their neonatal shape by 22 weeks GA (Prayer et al., 2006); and neurons in the nucleus accumbens are generated in 36-85 embryonic days in monkeys (approximately 8-20 weeks GA in humans) (Brand and Rakic, 1980).

The 3 BG seeds (caudate, putamen and pallidum) where we found choline-related changes develop later than the seeds mentioned above. Essentially these three regions are distinguishable by 16 weeks GA (Meng et al., 2012). However, they only split from each other to form distinct and separate regions, namely the caudate and lenticular nucleus (putamen and pallidum), by 17 weeks GA (Mtui et al., 2020). Given that the mothers in our study were enrolled at approximately 18.6 weeks GA, WM connected to earlier developing regions may be irreversibly damaged by the alcohol consumed prior to treatment initiation and, therefore, no choline effects were identified in those connections.

### **5.1.1. Effects of prenatal alcohol exposure (PAE)**

Considerable research has been conducted on the effects of PAE on the brain using various MRI techniques. The caudate, putamen and pallidum have consistently been among the deep

grey matter regions shown to be affected by PAE (Mattson et al., 1994, Lebel et al., 2008, Astley et al., 2009, Roussotte et al., 2012, Long and Lebel, 2022).

Several studies have also examined the effects of PAE on WM microstructure. The majority of these studies have been conducted in children, adolescents or adults, and have found that PAE results in regional FA reductions and MD increases (Ma et al., 2005, Fryer et al., 2009, Li et al., 2009, Santhanam et al., 2011, O'Conaill et al., 2015, Paolozza et al., 2017), increases in RD (Li et al., 2009, Santhanam et al., 2011, Spottiswoode et al., 2011, Fan et al., 2016) and/or decreases in AD (Donald et al., 2015, Taylor et al., 2015, Fan et al., 2016, Kar et al., 2021);

In contrast, one recent study reported lower MD in the right superior longitudinal fasciculus in children aged 7-15 years with PAE compared with non-exposed controls (Gomez et al., 2022). Another by the same group reported higher FA and/or lower MD (with lower AD and RD) in the genu of the corpus callosum and bilateral uncinate fasciculus in children with PAE aged 2-7 years (Kar et al., 2021). A different study by Paolozza et al. (2014) on 7- to 18-year-olds reported higher AD in the splenium of the FASD group. Lebel et al. (2008) reported lower MD in the genu of the corpus callosum in 5- to 13-year-old children with FASD compared to controls.

Notably, an earlier voxel-based study by Fryer et al. (2009) that observed lower FA in the frontal, parietal and occipital lobes, and in the corpus callosum, in 8- to 18-year-old individuals with PAE, also found two regions in the right posterior limb of the internal capsule and one region in the cingulum with higher FA in the individuals with PAE than controls. This result suggests that effects of PAE on WM development may be different in different brain regions, and by implication that the neuroprotective benefits of choline may present different in different brain regions. Interpreting the directionality of treatment-related differences is therefore not straightforward.

The only 2 studies to date examining effects of PAE on neonatal WM both reported lower AD in neonates with PAE compared to unexposed controls (Donald et al., 2015, Taylor et al., 2015). Donald et al. (2015) using an atlas-based approach, found lower AD in neonates with PAE in the right superior longitudinal fasciculus. No group differences on DTI measures were found in any of the other tracts examined, namely superior fronto-occipital fasciculus, uncinate fasciculus, cerebellar peduncles, corticospinal tract, cerebral peduncles, posterior thalamic radiation, fornix, cingulum nor corpus callosum.

Using tractography, Taylor et al. (2015) reported PAE-related AD reduction in all the transcallosal fibres identified in their study, and in 11 of the 15 (73 %) cortical-cortical association fibres that were present in all neonates. In contrast, only 50 % of the 24 projection

fibres found in all neonates showed PAE-related reduction in AD. Notably, only 6 (3 in each hemisphere) of the seeds used to identify projection fibres in that paper correspond to subcortical regions studied in the present work. Additionally, only one of the 5 WM connections found between those 6 subcortical seeds demonstrated lower AD in neonates with PAE. Among the projections fibres present in all neonates in that study, PAE-related AD reductions were mostly observed in connections to cortical seeds. Therefore, while these two neonatal studies together provide evidence of PAE-related reductions in AD around birth in the corpus callosum, as well as in some associations and projection fibres, the effects of PAE on striatal and basal ganglia WM connections have not been established. Given the rapid and differing rates of WM development in different regions across the perinatal and early postnatal period, caution should be exercised in applying findings from specific brain regions to other regions.

### **5.1.2. Connections between the caudate & pallidum**

We found that treatment resulted in lower FA bilaterally in the WM connection between the caudate and pallidum. This was unexpected since FA remains constant in neonates during pre-myelination occurring from 30-40 weeks (Oishi et al., 2019) and, at the same stage, the maturation and proliferation of the axonal cytoskeleton (Dubois et al., 2008). Moreover, in children, adolescents and adults, lower FA is usually an indicator of de- or dysmyelination, degenerated, damaged or less densely packed axons. However, regional FA increases have been observed in Williams syndrome (WS) (Hoeft et al., 2007) and attention deficit hyperactivity disorder (ADHD) (Silk et al., 2009, Li et al., 2010, Peterson et al., 2011), the latter being a behavioural deficit frequently seen in individuals with FASD (Burd et al., 2003). Although not focused on WM between subcortical regions, these studies highlight that lower FA may not always indicate an adverse effect.

In the above studies, higher FA was attributed to lower levels of axonal branching (Hoeft et al., 2007, Silk et al., 2009, Li et al., 2010, Peterson et al., 2011). Axonal branching is a crucial process in establishing complex and extensive interconnectivity in a neural circuit (Bodakuntla et al., 2021). Interestingly, choline is the main substrate in the biosynthesis of phosphatidylcholine (PC) – a membrane phospholipid that is abundant in plant and animal cells (Fagone and Jackowski, 2013). Rodent models have demonstrated the importance of PC for axonal growth and branching (Posse de Chaves et al., 1995b, Carter et al., 2008). The lower FA observed in the choline-treated neonates in our study may therefore be a consequence of accelerated axonal branching due to the increased availability of choline for the biosynthesis of PC. This increase in branching may increase brain connectivity and assist in mitigating certain behavioural conditions.

Notably, the anterior limb of the internal capsule, which separates the caudate and pallidum, is rich in crossing fibres (Oishi et al., 2011, Haines and Mihailoff, 2018). The presence of crossing fibres causes the diffusion tensor to become more oblate, thereby reducing the FA (Winston, 2012). Since increased axonal branching in this region would result in more crossing fibres, this may explain the lower FA observed in the choline-treated neonates.

### **5.1.3. Previous studies examining effects of choline on WM**

As mentioned before, two studies previously reported beneficial effects of choline on WM. In the one, neurite orientation dispersion and density imaging (NODDI) in children aged 11 years with PAE who had received postnatal choline at ages 2.5 to 5 years demonstrated more coherent axons in the splenium of the corpus callosum (Gimbel et al., 2022). Greater axonal coherence would presumably result in higher AD. Given the differences between neonatal and childhood WM development and microstructural properties, as well as the different regions and outcomes examined in that paper compared to here, it is not clear how those findings would translate to neonates or could be related to the present findings.

In another study, voxel-based morphometry (VBM) demonstrated more WM in 30-day-old non-alcohol-exposed prenatal-choline-sufficient pigs compared to prenatal-choline-deficient pigs in the putamen-pallidum region, the internal capsule and right cortex (Mudd et al., 2018). The authors attributed the reduction in WM in the prenatal-choline-deficient pigs to (1) the breaking down of phospholipid products (such as PC) due to a lack of choline; and (2) altered myelination. However, given that no significant findings were observed in any of the DTI parameters (FA, MD, AD or RD) evaluated with tract-based spatial statistics (TBSS) (Mudd et al., 2018), the authors speculated that changes in myelination may have been too small to observe the DTI. It is striking that the two subcortical regions where prenatal-choline-sufficient pigs exhibited greater WM than prenatal-choline-deficient pigs in that study, are the exact same regions that the WM connections in which we observed choline-related AD reduction are located, i.e. between the putamen and pallidum. These results suggest that greater availability of choline during gestation may be particularly beneficial for WM development within the basal ganglia region, thereby mitigating the damaging effects of PAE.

### **5.1.4. Connections between the putamen & caudate and putamen & pallidum**

The choline-related reductions in AD observed on the right in the connections between the putamen and both the caudate and pallidum are consistent with our hypothesis. In contrast to older children, adolescents and adults in whom lower AD is generally attributed to a lack of axonal integrity or orientation, lower AD in neonates and infant's points to accelerated (pre-) myelination or axonal maturation/growth.

Studies of postnatal WM development until age 6 years have consistently shown that the biggest changes in WM microstructural development occur during the first postnatal year, and are characterised by FA increases, and decreases in RD and AD, in most major WM tracts (Gao et al., 2009, Geng et al., 2012, Stephens et al., 2020). Notably, AD shows smaller age-related changes than FA and RD (Stephens et al., 2020), which have been shown to be more strongly associated with myelination (Dubois et al., 2008). Myelination comprises two processes – membrane proliferation that may cause decreases in AD and RD, and ‘true’ myelination synthesis that may decrease RD but leave AD unchanged (Dubois et al., 2008). This may account for the greater age-related decreases typically seen in RD compared to AD. Given that no choline-related decreases in RD were found in the present study, the observed AD decreases are likely not due to accelerated pre-myelination in choline-treated neonates.

Given that AD is a marker of axonal organization and integrity (Dubois et al., 2014), age-related decreases in AD have also been attributed to increases in axonal growth/maturation (Dubois et al., 2008, Gao et al., 2009, Geng et al., 2012) through increases in axonal diameter. This is supported by findings from Liu et al. (2021) who demonstrated increases in the cross-sections of fibres in the first 6 months of life suggesting increased phosphorylation of neurofilaments which are responsible for the axonal diameter and calibre size during WM development (Xu et al., 1996). Combining this with evidence from rodent models that greater availability of choline promotes the synthesis of PC required for axonal growth or elongation (Posse de Chaves et al., 1995a), the choline-related AD decreases observed in the present study are likely a consequence of increased axonal growth through increases in axonal diameter.

Axonal pruning, which is the refinement of neural systems through the removal of extra synapses and neurons, and maturational decreases in brain water content may also contribute to AD decreases during the first years of life. However, decreases in brain water content would affect RD and AD equally (Dubois et al., 2008).

## **5.2. Associations of WM integrity with visual recognition memory on the FTII**

Recognition memory on the FTII is known to predict future intellectual ability in infants (Fagan III and Detterman, 1992). Given that the RCT by Jacobson and colleagues observed choline-related improvements in visual recognition memory on the FTII at age 12 months (Jacobson et al., 2018b), and regional choline-related volume increases were associated with improved visual recognition memory, we examined associations of WM microstructural measures with visual recognition memory on the FTII. We had hypothesised that lower AD and RD would be associated with better visual recognition memory.

As per our hypothesis, lower RD in the WM connection between the left and right thalami was associated with better visual recognition memory. However, in the connection on the right between the caudate and putamen where we observed choline-related decreases in AD, higher RD was associated with better visual recognition memory.

### **5.2.1. Connection between the left & right thalami**

Although no choline treatment-related benefit was observed in the connection between the left and right thalami, lower RD in this connection around birth was associated with better visual recognition memory performance at age 12 months. This result is consistent with several studies performed on individuals of various ages.

Studies in healthy individuals (Sullivan et al., 2001, Beaulieu et al., 2005, Farah et al., 2020) and individuals exposed to alcohol prenatally (Sowell et al., 2008, Wozniak et al., 2009) have consistently shown an association of higher FA (Sullivan et al., 2001, Beaulieu et al., 2005, Sowell et al., 2008, Wozniak et al., 2009) with better cognitive function in children (Beaulieu et al., 2005, Sowell et al., 2008, Wozniak et al., 2009, Farah et al., 2020), and adults (Sullivan et al., 2001). Since higher FA is ordinarily attributed to increases in AD and/or decreases in RD, our result is consistent with these findings.

Due to the challenges performing and non-predictive validity of cognitive assessments within the first year of life, it is common to examine associations of neonatal imaging outcomes with later cognitive performance. Similar to the findings found in children and adults, higher FA in premature infants at term equivalent age (TEA) have, for example, been associated with better scores on Bayley's Scale of Infant Development (BSID; Bayley (2006)) and on Differential Ability Scales (DAS; Elliott et al. (1990)) at 36 months of age (Parikh et al., 2021), and in healthy infants with better scores on BSID at age 24 months (Feng et al., 2019).

Of the infant studies that have evaluated associations of cognitive outcomes with RD, lower RD at TEA in areas of the medial prefrontal cortex, sections of the inferior fronto-occipital fasciculus and the genu of corpus callosum were associated with better scores on BSID at approximately 18 months of age (Duerden et al., 2015); and lower RD at TEA was associated with better motor scores on the BSID at 12 months of age in the bilateral posterior thalamic radiations as well as better cognitive scores on the BSID at age 24 months in the right posterior limb of the internal capsule and right posterior and superior corona radiata with (Pannek et al., 2020). Additionally, lower RD in the right superior longitudinal fasciculus of a combined sample of full-term and preterm infants (at TEA) has also been correlated with improved receptive language scores on the Mullen Scales of Early Learning (MSEL) at 12 months of age (Girault et al., 2019). These studies demonstrate that WM integrity around birth may be predictive of future cognitive performance.

However, cognitive performance has also been related to imaging outcomes around the age of assessment. For example, Girault et al. (2019) found that lower RD at age 12 months (included full-term and preterm infants) in several WM tracts such as the genu of the corpus callosum, bilateral uncinate fasciculus, cingulum, inferior fronto-occipital fasciculus and corticothalamic prefrontal, premotor and motor tracts, to name a few, was significantly correlated with higher scores in general cognitive ability, gross motor and fine motor functions at 12 months of age. Similarly, Short et al. (2013) demonstrated associations of lower RD in healthy 12-month-old infants in the genu of the corpus callosum, left anterior cingulum and right superior and bilateral anterior thalamic radiations with better non-verbal and verbal developmental quotients (on the MSEL) and improved visuospatial working memory at age 12 months.

Notably, in the above studies, associations of cognitive performance and WM measures were found in different regions to those examined in the present study – mostly in the corpus callosum and/or fibre bundles that connect cortical lobes. In contrast, we found an association in WM connecting the left and right thalami.

Nevertheless, some studies have found significant associations of cognitive outcomes with DTI measures in WM connecting subcortical regions. For example, neonatal studies by Feng et al. (2019) in healthy infants and Pannek et al. (2020) in premature infants at TEA found associations of higher FA and lower RD, respectively, in the right posterior limb of the internal capsule (which is where the fibres connecting the thalamus and pallidum pass through (Haines and Mihailoff, 2018)). However, the WM connecting the bilateral thalami, known as the interthalamic adhesion or massa intermedia, does not form part of the internal capsule (Standring, 2021). Instead, it is a midline commissural fibre, functioning similarly to the corpus callosum and the anterior and posterior commissural fibres (Borghei et al., 2021). Furthermore, the thalamus is considered the relay station of the brain, meaning that all information from the rest of the body and brain is relayed to the cerebral cortex via the thalamus (Standring, 2021).

Our study has, therefore, provided evidence of an association of lower neonatal RD in the WM connecting the relay station of the brain with future cognitive outcomes.

### **5.2.2. Connection between the caudate & putamen**

Our finding of an association of increasing RD in the pathways between the right caudate and right putamen with better visual recognition memory in the FTII at 12 months is opposite to most previous studies.

Since the caudate-putamen connection is one where we found choline-related AD decreases, this unexpected result may be due to choline effects in this connection. Choline-related accelerated axonal growth in this tract could result in larger axonal diameters, which would manifest as lower AD and higher RD (Barazany et al., 2009, Harkins et al., 2021). Our findings of an association of RD in this pathway with recognition memory therefore suggests that choline-related increases in axonal diameter in this tract may, in part, mediate the effects of choline treatment on visual recognition memory. This requires validation in a larger sample.

### **5.3. Limitations and future work**

The sample size in our study was relatively small with only 21 participants providing usable, non-biased data and there were no non-alcohol-exposed controls. The small sample size limited our ability to control for potential confounding by infant sex and we did not have sufficient power to perform corrections for multiple comparisons. Due to this, future studies should aim to reproduce these findings in a larger sample, and including participants who were not exposed to alcohol and did not receive treatment. Inclusion of non-alcohol-exposed infants would provide a baseline of WM measures in normally developing neonates against which to compare the WM measures found in the neonates with PAE.

Given that only subcortical regions were delineated, we were not able to examine the effects of choline on cortical WM microstructures. Later developing WM tracts to cortical regions may, however, show greater choline treatment-related benefits, compared to developing brain regions where damage that occurred before choline treatment initiation may be irreversible. Whole-brain tractography should therefore be performed to examine treatment-related benefits on the microstructural integrity of cortical WM. Given that the Wozniak et al. (2015) postnatal choline supplementation study demonstrated treatment-related benefits at a 4-year follow-up, following the participants in the current study into early childhood could elucidate potential future benefits.

## 6. Conclusion

In conclusion, our study is one of only a few imaging studies in neonates exposed to alcohol prenatally, and the only one examining the effects of prenatal choline supplementation intervention on subcortical neonatal WM integrity.

We have demonstrated preliminary evidence on the potential protective nature of high-dose prenatal maternal choline supplementation on the microstructure of subcortical WM, specifically between the caudate, putamen and pallidum which are regions known to be affected by PAE.

We found that high-dose prenatal maternal choline supplementation in heavy-drinking women is associated with lower FA and/or AD in the subcortical WM between 3 BG seeds (caudate, putamen and pallidum), which point to accelerated branching, pruning and/or growth of the axons.

Furthermore, we found associations of increasing RD in the connections between the right caudate and right putamen (where we observed choline-related AD decreases) with better visual recognition memory on the FTII at 12 months of age. Assuming that the RD increases are a consequence of increased axonal diameter due to choline-related accelerated axonal growth, increased axonal diameter (reflected by lower AD and higher RD) may mediate, in part, the effect of choline on visual recognition memory. In contrast, lower RD in the connection between the left and right thalami was associated with better visual recognition memory. Given that this is a midline commissural fibre, functioning similarly to the corpus callosum and with different developing trajectory to unilateral subcortical pathways, a different result is perhaps surprising. Notably, this finding is consistent with various studies that have demonstrated an association of lower RD in the corpus callosum with 12-month cognitive performance.

While this study provides preliminary evidence of an effect of prenatal maternal choline supplementation in heavy drinking women on the microstructural integrity of subcortical WM of their offspring, these results require validation in a larger sample and should be extended to examine WM tracts to cortical regions.

## Appendix A: Sample characteristics

### Comparing the included (n = 22) and excluded (n = 21) participants

**Table A.1.1** : Maternal characteristics between the 22 included and 21 excluded participants.

Sample characteristics	Included (n = 22)		Excluded (n = 21)		Statistics
	Mean (SD) or Median [IQR]	Range	Mean (SD) or Median [IQR]	Range	<i>p</i>
Maternal age at delivery (years)	28.9 [25.1; 31.2]	19.1 - 37.1	27.8 [21.5; 32.5]	19.4 - 36.1	0.7 <sup>a</sup>
Education (highest grade passed)	9 [8; 10]	5 - 12	9 [8; 11]	6 - 12	0.6 <sup>a</sup>
No. married	11 (52.4 %)		5 (23.8 %)		0.1 <sup>b</sup>
Socioeconomic status <sup>d</sup>	19 (5.9)	9.5 - 30.5	19.4 (5.6)	11 - 30.5	0.8
Parity	2 (1)	0 - 6	1 (1)	0 - 4	0.7 <sup>b</sup>
<b>Treatment adherence (%)</b>	<b>86.7 [64.6; 90.2]</b>	13.4 - 99.6	<b>65.9 [50.2; 80.7]</b>	1.7 - 99.6	<b>0.025<sup>a</sup></b>
<b>Gestational age (GA) at enrolment (weeks)</b>	<b>18.6 (3.3)</b>	9.9 - 23.6	<b>21.6 (2.7)</b>	14.7 - 26.1	<b>0.002</b>
<b>Duration from enrolment through delivery (weeks)</b>	<b>20.1 (4.0)</b>	12.0 - 31.0	<b>17.6 (2.6)</b>	12.0 - 23.0	<b>0.019<sup>c</sup></b>
Cumulative choline dose (grams) <sup>e,f</sup>	184.2 (81.3)	43.0 - 307.2	137.1 (83.7)	38.0 - 274.8	0.2

Values are mean (SD) or Median [IQR]; SD: Standard deviation; IQR: Interquartile range

Independent samples T-test unless stated otherwise

<sup>a</sup>Mann-Whitney U test

<sup>b</sup>Fisher exact test

<sup>c</sup>Welch's T-test

<sup>d</sup>Hollingshead scale (Adams and Weakliem, 2011)

<sup>e</sup>Estimated as a product of maternal choline treatment adherence (with neonates in the placebo arm being set to 0), weeks from enrolment through delivery and weekly dosage (2 grams/day x 7 days/week = 14 grams/week)

<sup>f</sup>Median, IQR, range and statistics are based only on participants who used the respective substances: Participants in the included group who were in the choline arm 14 (67; participants in the excluded group who were in the choline arm 7 (33 %).

**Table A.1.2:** Maternal substance use between the 22 included and 21 excluded participants.

Sample characteristics	Included (n = 22)		Excluded (n = 21)		Statistics
	Mean (SD) or Median [IQR]	Range	Mean (SD) or Median [IQR]	Range	<i>p</i>
oz AA/day at conception <sup>d</sup>	1.1 [0.7; 2.4]	0 - 9.8	1.3 [1.0; 1.9]	0 - 3.5	0.9 <sup>a,e</sup>
oz AA/drinking day at conception <sup>d</sup>	4 .0 [2.4; 7.2]	0 - 13.7	3.5 [3.0; 4.8]	0 - 8.1	0.8 <sup>b,e</sup>
Frequency of drinking at conception (days/week)	2.0 [2.0; 3.0]	0 - 6.0	3.0 [2.0; 3.0]	0 - 4.0	0.3 <sup>c</sup>
oz AA/day during pregnancy <sup>d</sup>	0.6 [0.2; 1]	0 - 2.8	0.7 [0.4; 0.8]	0 - 2.2	0.7 <sup>c,e</sup>
oz AA/drinking day during pregnancy <sup>d</sup>	3.1 [2.5; 5.2]	1.7 - 12.5	3.2 [2.5; 3.7]	0 - 8.4	0.4 <sup>e</sup>
Frequency of drinking during pregnancy (days/week)	1.2 (0.9)	0.1 - 3.8	1.4 (0.7)	0 - 2.8	0.5
Smoking (cigarettes/day) <sup>f</sup>	5.0 [3.5; 8.0]	2.3 - 20.0	4.7 [3.0; 8.0]	2.0 - 13.5	0.6 <sup>e</sup>
Marijuana use (days/month) <sup>f</sup>	10.0 (11.5)	0.1 - 30.1	10.3 (9.3)	1.3 - 23.3	1.0
Methamphetamine use (days/month) <sup>f</sup>	2.1 (N/A)	N/A	6.7 (N/A)	N/A	N/A
No. of mandrax users	0		0		N/A

Values are mean (SD) or Median [IQR]; SD: Standard deviation; IQR: Interquartile range

Independent samples T-test unless stated otherwise

<sup>a</sup>Yuen test

<sup>b</sup>Welch's T-test

<sup>c</sup>Mann-Whitney U test

<sup>d</sup>Ounces (oz) of absolute alcohol (AA) consumed

<sup>f</sup>Logarithmic transform was used for the statistics

<sup>f</sup>Median, IQR, range and statistics are based only on participants who used the respective substances: Participants in the included group who were smokers *n* = 21 (95 %), marijuana users *n* = 6 (27 %) and methamphetamine users *n* = 1 (5 %); participants in the excluded group who were smokers *n* = 15 (71 %), marijuana users *n* = 4 (19 %) and methamphetamine users *n* = 1 (5 %)

**Table A.1.3:** Neonatal birth characteristics and FASD diagnosis between the 22 included and 21 excluded participants.

Sample characteristics		Included (n = 22)		Excluded (n = 21)		Statistics
		Mean (SD) or Median [IQR]	Range	Mean (SD) or Median [IQR]	Range	<i>p</i>
FASD diagnosis (2019 clinic)	No. of FAS <sup>a</sup>	5 (22.7 %)		6 (28.6 %)		0.9 <sup>b</sup>
	No. of PFAS <sup>a</sup>	2 (9.1 %)		2 (9.5 %)		
	No. of HE <sup>a</sup>	15 (68.2 %)		13 (61.9 %)		
No. of males		11 (52.4 %)		12 (57.1 %)		0.8 <sup>b</sup>
No. of choline-treated neonates		14 (66.7%)		7 (33.3%)		0.07 <sup>b</sup>
Gestational age (GA) at birth (weeks)		38.8 (1.5)	35.6 - 41.3	39.2 (1.4)	37.1 - 41.3	0.3
Birthweight (g)		2690.5 (365)	2180 - 3360	2906 (580)	1750 - 3870	0.2 <sup>c</sup>
<b>Birth length (cm)<sup>e</sup></b>		<b>47.3 (3.3)</b>	40 - 53	<b>49.3 (2.5)</b>	45 - 55	<b>0.035</b>
<b>Birth head circumference (cm)</b>		<b>32.6 [31.0; 33.6]</b>	30 - 36	<b>33.0 [33.0; 34.0]</b>	30 - 36	<b>0.040<sup>d</sup></b>

Values are mean (SD) or Median [IQR]; SD: Standard deviation; IQR: Interquartile range

Independent samples T-test unless stated otherwise

<sup>a</sup>FAS = Fetal Alcohol Syndrome, PFAS = Partial Fetal Alcohol Syndrome and HE = Non-syndromal Heavily Exposed

<sup>b</sup>Fisher exact test

<sup>c</sup>Welch's T-test

<sup>d</sup>Mann-Whitney U test

<sup>e</sup>Missing data for n = 1 included participant

**Table A.1.4:** Neonatal scan characteristics between the 22 included and 21 excluded participants.

Sample characteristics	Included (n = 22)		Excluded (n = 21)		Statistics
	Mean (SD) or Median [IQR]	Range	Mean (SD) or Median [IQR]	Range	<i>p</i>
Postnatal age at scan (weeks)	2.9 [2.5; 3.2]	1.3 - 6.1	2.7 [2.1; 3.8]	1.0 - 5.0	0.7 <sup>a</sup>
Gestational age (GA) equivalent at scan (weeks)	41.8 (2.0)	37.7 - 47.0	42.1 (1.9)	38.7 - 45.3	0.5
Weight at scan (g) <sup>d</sup>	3170 (644)	2280 - 5100	3394 (630)	1780 - 4500	0.3
Length at scan (cm) <sup>d</sup>	48.5 [46.5; 50.2]	45.0 - 53.4	49.8 [48.1; 52]	36.2 - 54.4	0.2 <sup>b</sup>
Head circumference at scan (cm) <sup>d</sup>	34.7 [33.6; 36.6]	31.8 - 39.0	35.4 [34.7; 36.6]	31.0 - 53.0	0.5 <sup>b</sup>
Total intracranial volume (mm <sup>3</sup> )	492 954 (66 679)	393 000 - 655 300	507 686 (56 021)	436 800 - 622 000	0.4
Total cerebral white matter volume (mm <sup>3</sup> ) <sup>e</sup>	123 137 (20 174)	99 000 - 172 092	131 367 (14 657)	107 646 - 162 006	0.1
<b>No. of navigated sequence scans</b>	<b>22 (100.0 %)</b>		<b>15 (71.4 %)</b>		<b>0.009<sup>c</sup></b>

Values are mean (SD) or Median [IQR]; SD: Standard deviation; IQR: Interquartile range

Independent samples T-test unless stated otherwise

<sup>a</sup>Logarithmic transform was used for the statistics

<sup>b</sup>Mann-Whitney U test

<sup>c</sup>Fisher exact test

<sup>d</sup>Missing data for n = 3 included participants

<sup>e</sup>Missing data for n = 1 included participant

## Comparing the included (n = 21) and excluded (n = 22) participants

**Table A.2.1:** Maternal characteristics compared between the 21 participants who had usable DTI data and did not introduce bias on the DTI measures, and the 22 participants who were excluded.

Sample characteristics	Included (n = 21)		Excluded (n = 22)		Statistics
	Mean (SD) or Median [IQR]	Range	Mean (SD) or Median [IQR]	Range	p
Maternal age at delivery (years)	28.8 [24.8; 31.2]	19.1 - 37.1	28.2 [21.6; 32.5]	19.4 - 36.1	0.9 <sup>a</sup>
Education (highest grade passed)	9 [8; 10]	5 - 12	9 [8; 11]	6 - 12	0.8 <sup>a</sup>
No. married	11 (52.4 %)		5 (22.7 %)		0.06 <sup>b</sup>
Socioeconomic status <sup>c</sup>	19.4 (5.8)	9.5 - 30.5	19.0 (5.7)	11.0 - 30.5	0.8
Parity	2 (1)	0 - 4	2 (1)	0 - 6	0.7 <sup>b</sup>
<b>Treatment adherence (%)</b>	<b>86.3 [62.1; 91.0]</b>	13.3 - 99.6	<b>67.0 [50.5; 85.5]</b>	1.7 - 99.6	<b>0.042<sup>a</sup></b>
<b>Gestational age (GA) at enrolment (weeks)</b>	<b>18.4 (3.2)</b>	9.9 - 22.4	<b>21.7 (2.7)</b>	14.7 - 26.1	<b>&lt; 0.001</b>
<b>Duration from enrolment through delivery (weeks)</b>	<b>20.5 (3.7)</b>	16.0 - 31.0	<b>17.4 (2.8)</b>	12.0 - 23.0	<b>0.03</b>
Cumulative choline dose (grams) <sup>d,e</sup>	187.1 (83.9)	43.0 - 307.2	138.3 (77.6)	38.0 - 274.8	0.2

Values are mean (SD) or Median [IQR]; SD: Standard deviation; IQR: Interquartile range

Independent samples T-test unless stated otherwise

<sup>a</sup>Mann-Whitney U test

<sup>b</sup>Fisher exact test

<sup>c</sup>Hollingshead scale (Adams and Weakliem, 2011)

<sup>d</sup>Estimated as a product of maternal choline treatment adherence (with neonates in the placebo arm being set to 0), weeks from enrolment through delivery and weekly dosage (2 grams/day x 7 days/week = 14 grams/week)

<sup>e</sup>Median, IQR, range and statistics are based only on participants who used the respective substances: Participants in the included group who were in the choline arm 13 (62 %); participants in the excluded group who were in the choline arm 8 (36 %).

**Table A.2.2:** Maternal substance use compared between the 21 participants who had usable DTI data and did not introduce bias on the DTI measures, and the 22 participants who were excluded.

Sample characteristics	Included (n = 21)		Excluded (n = 22)		Statistics
	Mean (SD) or Median [IQR]	Range	Mean (SD) or Median [IQR]	Range	<i>p</i>
oz AA/day at conception <sup>a</sup>	1.1 [0.7; 2.2]	0 - 9.8	1.3 [1.0; 1.9]	0 - 4.4	0.5 <sup>b,c</sup>
oz AA/drinking day at conception <sup>a</sup>	4.0 [2.4; 7.3]	0 - 13.7	3.6 [3.1; 5.1]	2.1 - 8.1	1.0 <sup>d,c</sup>
Frequency of drinking at conception (days/week)	2.0 [2.0; 3.0]	0 - 5.0	3.0 [2.0; 3.0]	1.0 - 6.0	0.1 <sup>b</sup>
oz AA/day during pregnancy <sup>a</sup>	0.5 [0.2; 0.9]	0.04 - 2.8	0.7 [0.4; 0.9]	0 - 2.8	0.3 <sup>b,c</sup>
oz AA/drinking day during pregnancy <sup>a</sup>	3.0 [2.5; 5.1]	1.6 - 12.4	3.2 [2.5; 3.9]	0 - 8.4	0.6 <sup>c</sup>
Frequency of drinking during pregnancy (days/week)	1.1 (0.7)	0.09 - 2.1	1.5 (0.9)	0 - 3.8	0.09
Smoking (cigarettes/day) <sup>e</sup>	5.0 [3.9; 8.7]	2.3 - 20.0	4.3 [3.0; 7.9]	2.0 - 13.5	1.0 <sup>c</sup>
Marijuana use (days/month) <sup>e</sup>	10.0 (11.5)	0.1 - 30.1	10.4 (9.3)	1.3 - 23.3	1.0
Methamphetamine use (days/month) <sup>e</sup>	2.1 (N/A)	N/A	6.7 (N/A)	N/A	N/A
No. of mandrax users	0		0		N/A

Values are mean (SD) or Median [IQR]; SD: Standard deviation; IQR: Interquartile range

Independent samples T-test unless stated otherwise

<sup>a</sup>Ounces (oz) of absolute alcohol (AA) consumed

<sup>b</sup>Mann-Whitney U test

<sup>c</sup>Logarithmic transform was used for the statistics

<sup>d</sup>Welch's T-test

<sup>e</sup>Median, IQR, range and statistics are based only on participants who used the respective substances: Participants in the included group who were smokers *n* = 20 (95 %), marijuana users *n* = 6 (29 %) and methamphetamine users *n* = 1 (5 %); participants in the excluded group who were smokers *n* = 16 (73 %), marijuana users *n* = 4 (18 %) and methamphetamine users *n* = 1 (5 %)

**Table A.2.3:** Comparison of the neonatal birth characteristics and FASD diagnosis between the included 21 participants with usable DTI data and did not introduce bias on the DTI measures, and the excluded 22 participants.

Sample characteristics		Included (n = 21)		Excluded (n = 22)		Statistics
		Mean (SD) or Median [IQR]	Range	Mean (SD) or Median [IQR]	Range	p
FASD diagnosis (2019 clinic)	No. of FAS <sup>a</sup>	5 (21.8 %)		6 (27.3%)		1.0 <sup>b</sup>
	No. of PFAS <sup>a</sup>	2 (9.5 %)		2 (9.1 %)		
	No. of HE <sup>a</sup>	14 (66.7 %)		14 (63.6 %)		
No. of males		11 (52.4 %)		12(54.5 %)		1.0 <sup>b</sup>
No. of choline-treated neonates		13 (61.9 %)		8(36.4 %)		0.1 <sup>b</sup>
Gestational age (GA) at birth (weeks)		38.9 (1.3)	37.1 - 41.3	39.1 (1.5)	35.6- 41.3	0.8
Birthweight (g)		2670 (361)	2180 - 3360	2916 (568)	1750 - 3870	0.1 <sup>c</sup>
<b>Birth length (cm)<sup>e</sup></b>		<b>47.2 (3.3)</b>	<b>40.0 - 53.0</b>	<b>49.2 (2.4)</b>	<b>45.0 - 55.0</b>	<b>0.028</b>
Birth head circumference (cm)		33.0 [31.0; 33.8]	30.0 - 36.0	33.0 [33.0; 34.0]	30.0 - 36.0	0.07 <sup>d</sup>

Values are mean (SD) or Median [IQR]; SD: Standard deviation; IQR: Interquartile range

Independent samples T-test unless stated otherwise

<sup>a</sup>FAS = Fetal Alcohol Syndrome, PFAS = Partial Fetal Alcohol Syndrome and HE = Non-syndromal Heavily Exposed

<sup>b</sup>Fisher exact test

<sup>c</sup>Welch's T-test

<sup>d</sup>Mann-Whitney U test

<sup>e</sup>Missing data for n = 1 included participant

**Table A.2.4:** Comparing the neonatal scan characteristics between the 21 participants who had usable DTI data and did not introduce bias on the DTI measures, and the 22 participants who were excluded.

Sample characteristics	Included (n = 21)		Excluded (n = 22)		Statistics
	Mean (SD) or Median [IQR]	Range	Mean (SD) or Median [IQR]	Range	<i>p</i>
Postnatal age at scan (weeks)	3.0 [2.6; 3.2]	1.3 - 6.1	2.6 [2.1; 3.4]	1.0 - 5.0	0.6 <sup>a</sup>
Gestational age (GA) equivalent at scan (weeks)	41.9 (1.8)	38.8 - 47.0	41.9 (2.0)	37.7 - 45.3	1.0
Weight at scan (g) <sup>c</sup>	3182 (660)	2280 - 5100	3373 (622)	1780 - 500	0.4
Length at scan (cm) <sup>c</sup>	48.5 [46.4; 50.4]	45.0 - 53.4	49.7 [48.1; 52.0]	36.2 - 54.4	0.2 <sup>b</sup>
Head circumference at scan (cm) <sup>c</sup>	35.0 [33.6; 36.7]	31.8 - 39.0	35.4 [34.3; 36.5]	31.0 - 53.0	0.7 <sup>b</sup>
Total intracranial volume (mm <sup>3</sup> )	496 005 (66 734)	393 000 - 655 300	504 104 (57 193)	428 900 - 622 000	0.3
Total cerebral white matter volume (mm <sup>3</sup> ) <sup>d</sup>	124 344 (19 905)	101 013 - 172 092	129 896 (15 881)	99 001 - 162 006	0.1
<b>No. of navigated sequence scans</b>	<b>21 (100.0 %)</b>		<b>16 (72.7 %)</b>		<b>0.021<sup>e</sup></b>

Values are mean (SD) or Median [IQR]; SD: Standard deviation; IQR: Interquartile range

Independent samples T-test unless stated otherwise

<sup>a</sup>Logarithmic transform was used for the statistics

<sup>b</sup>Mann-Whitney U test

<sup>c</sup>Missing data for n = 3 included participants

<sup>d</sup>Missing data for n = 1 included participant

<sup>e</sup>Fisher exact test

## Comparing the choline- and placebo-treated groups for the 21 included participants

**Table A.3.1:** Maternal characteristics between the treatment groups after excluding the one choline-treated participant for whom using only AP data resulted in bias on the DTI measures (n = 21).

Sample characteristics	Choline (n = 13)		Placebo (n = 8)		Statistics
	Mean (SD) or Median [IQR]	Range	Mean (SD) or Median [IQR]	Range	p
Maternal age at delivery (years)	27.4 (4.3)	19.1 - 33.8	28.8 (5.7)	20.7 - 37.1	0.5
Education (highest grade passed)	9 [8; 10]	5 - 12	10 [7; 10]	6 - 12	0.9 <sup>a</sup>
No. married	7 (53.8 %)		4 (50.0 %)		1.0 <sup>b</sup>
Socioeconomic status <sup>c</sup>	20.3 (6.4)	9.5 - 30.5	17.9 (4.5)	9.5 - 24.0	0.4
Parity	1.8 (1.3)	0 - 4	1.8 (1.0)	1 - 3	0.1 <sup>b</sup>
<b>Treatment adherence (%) (n = 21)</b>	<b>83.5 [43.1; 87.4]</b>	13.4 - 89.4	<b>94.3 [83.0; 98.9]</b>	75.3 - 99.6	<b>0.033<sup>d</sup></b>
<b>Treatment adherence (%) (n = 18)<sup>e</sup></b>	<b>85.3 [64.6; 87.9]</b>	56.3 - 89.4	<b>94.3 [83.0; 98.9]</b>	75.3 - 99.6	<b>0.029<sup>a</sup></b>
Gestational age (GA) at enrolment (weeks)	18.1 (2.8)	13.7 - 22.4	18.8 (3.9)	9.9 - 22.1	0.6
Duration from enrolment through delivery (weeks)	21.0 [18.0; 23.0]	16.0 - 26.0	19.5 [16.3; 22.0]	13.0 - 31.0	0.5 <sup>a</sup>
<b>Cumulative choline dose (grams)<sup>f</sup></b>	<b>205.3 [107.9; 253.2]</b>	43.0 - 307.2	<b>0</b>	0	<b>&lt; 0.0001<sup>d</sup></b>

Values are mean (SD) or Median [IQR]; SD: Standard deviation; IQR: Interquartile range

Independent samples T-test was used unless stated otherwise

<sup>a</sup>Mann-Whitney U test

<sup>b</sup>Fisher exact test

<sup>c</sup>Hollingshead scale (Adams and Weakliem, 2011)

<sup>d</sup>Yuen test

<sup>e</sup>Excluding 3 mothers from the choline arm with adherences < 50.0 % (adherences of 13.4 %, 22.2 % and 29.9 %, respectively)

<sup>f</sup>Estimated as a product of maternal choline treatment adherence (with neonates in the placebo arm being set to 0), weeks from enrolment through delivery and weekly dosage (2 grams/day x 7 days/week = 14 grams/week)

**Table A.3.2:** Maternal substance use between the treatment groups after excluding the one choline-treated participant for whom using only AP data resulted in bias on the DTI measures (n = 21).

Sample characteristics	Choline (n = 13)		Placebo (n = 8)		Statistics
	Mean (SD) or Median [IQR]	Range	Mean (SD) or Median [IQR]	Range	p
oz AA/day at conception <sup>a</sup>	1.1 [0.6; 1.9]	0 - 9.8	1.5 [0.7; 2.9]	0 - 3.2	0.9 <sup>b</sup>
oz AA/drinking day at conception <sup>a</sup>	4.4 (3.6)	0 - 13.7	5.1 (3.3)	0 - 9.6	0.6 <sup>b</sup>
Frequency of drinking at conception (days/week)	2.0 [2.0; 3.0]	0 - 5.0	2.0 [1.5; 2.8]	0 - 3.0	0.9 <sup>c</sup>
oz AA/day during pregnancy <sup>a</sup>	0.5 [0.2; 0.9]	0.04 - 2.8	0.7 [0.2; 0.9]	0.05 - 1.0	0.7 <sup>c,b</sup>
oz AA/drinking day during pregnancy <sup>a</sup>	3.0 [2.3; 3.8]	1.6 - 12.5	0.5 [0.1; 0.7]	2.5 - 7.0	0.3 <sup>b</sup>
Frequency of drinking during pregnancy (days/week)	1.2 (0.7)	0.1 - 3.8	0.8 (0.4)	0.1 - 1.5	0.2
Smoking (cigarettes/day) <sup>d</sup>	5.0 [4.6; 7.7]	2.3 - 20.0	5.0 [3.3; 11.7]	3.0 - 15.0	1.0 <sup>b</sup>
Marijuana use (days/month) <sup>d</sup>	11.0 (12.6)	0.1 - 30.1	5.0 (N/A)	N/A	N/A
Methamphetamine use (days/month) <sup>d</sup>	2.1 (N/A)	N/A	N/A	N/A	N/A
Number of mandrax users	0		0		N/A

Values are mean (SD) or Median [IQR]; SD: Standard deviation; IQR: Interquartile range

Independent samples T-test was used unless stated otherwise

<sup>a</sup>Ounces (oz) of absolute alcohol (AA) consumed

<sup>b</sup>Log transform was used for the statistics

<sup>c</sup>Mann-Whitney U test

<sup>d</sup>Median, IQR, range and statistics are based only on participants who used the respective substances: Participants in the choline group who were smokers n = 13 (100 %), marijuana users n = 5 (38 %) and methamphetamine users n = 1 (8 %); participants in the placebo group who were smokers n = 7 (88 %), marijuana users n = 1 (13 %) and methamphetamine users n = 0 (0 %)

**Table A.3.3:** Neonatal birth characteristics and FASD diagnosis between the treatment groups excluding the one choline-treated for whom using only AP data resulted in bias on the DTI measures (n = 21).

Sample characteristics		Choline (n = 13)		Placebo (n = 8)		Statistics
		Mean (SD) or Median [IQR]	Range	Mean (SD) or Median [IQR]	Range	p
FASD diagnosis (2019 clinic)	No. of FAS <sup>a</sup>	4 (30.8 %)		1 (12.5 %)		0.8 <sup>b</sup>
	No. of PFAS <sup>a</sup>	1 (7.7 %)		1 (12.5%)		
	No. of HE <sup>a</sup>	8 (61.5 %)		6 (75.0%)		
No. of males		5 (38.5 %)		6 (75.0 %)		0.2 <sup>b</sup>
Gestational age (GA) at birth (weeks)		38.7 (1.0)	37.1 - 40.6	39.2 (1.7)	37.3 - 41.3	0.4
Birthweight (g)		2668 (363)	2180 - 3230	2672 (382)	2240 - 3360	1.0
Birth length (cm) <sup>c</sup>		46.8 (3.5)	40.0 - 53.0	48.1 (2.9)	43.0 - 52.0	0.4
Birth head circumference (cm)		32.0 (1.6)	30.0 - 34.0	33.1 (1.9)	30.0 - 36.0	0.2

Values are mean (SD) or Median [IQR]; SD: Standard deviation; IQR: Interquartile range

Independent samples T-test unless stated otherwise

<sup>a</sup>FAS = Fetal Alcohol Syndrome, PFAS = Partial Fetal Alcohol Syndrome and HE = Non-syndromal Heavily Exposed

<sup>b</sup>Fisher exact test

<sup>c</sup>Missing data for n = 1 placebo-treated participant

**Table A.3.4:** Neonatal scan characteristics between the treatment groups excluding the one choline-treated for whom using only AP data resulted in bias on the DTI measures ( $n = 21$ ).

Sample characteristics	Choline (n = 13)		Placebo (n = 8)		Statistics
	Mean (SD) or Median [IQR]	Range	Mean (SD) or Median [IQR]	Range	<i>p</i>
Postnatal age at scan (weeks)	3.0 [2.9; 3.4]	1.6 - 5.1	2.7 [1.5; 3.3]	1.3 - 6.1	0.3 <sup>a</sup>
Gestational age (GA) equivalent at scan (weeks)	41.9 (1.2)	38.9 - 43.6	42.0 (2.6)	39.3 - 47.0	0.9 <sup>b</sup>
Weight at scan (g) <sup>c</sup>	3176 (458)	2340 - 3960	3198 (1104)	2280 - 5100	1.0 <sup>b</sup>
Length at scan (cm) <sup>c</sup>	48.7 (2.3)	45.5 - 52.2	48.5 (3.4)	45.0 - 53.4	0.9
Head circumference at scan (cm) <sup>c</sup>	35.1 (1.6)	31.8 - 37.7	35.6 (3.1)	32.8 - 39.0	0.6
Total intracranial volume (mm <sup>3</sup> )	497 123 (59 836)	393 000 - 579 400	494 188 (81 18)	420 000 - 655 300	0.9
Total cerebral white matter volume (mm <sup>3</sup> ) <sup>d</sup>	126 214 (17 599)	101 039 - 156 142	121 538 (23 953)	101 013 - 172 092	0.6
Average head motion (mm)	0.4 (0.1)	0.2 - 0.7	0.3 (0.1)	0.2 - 0.6	0.3

Values are mean (SD) or Median [IQR]; SD: Standard deviation; IQR: Interquartile range

Independent samples T-test unless stated otherwise

<sup>a</sup>Mann-Whitney U test

<sup>b</sup>Welch's T-test

<sup>c</sup>Missing data for  $n = 3$  placebo-treated participants

<sup>d</sup>Missing data for  $n = 1$  choline-treated participant

## Appendix B: Potential confounders

**Table B.1:** The process of removing linearly dependent variables.

Variable 1	Variable 2	<i>r</i>	Correlation with FA		Correlation with MD		Final Variable <sup>c</sup>
			Variable 1	Variable 2	Variable 1	Variable 2	
Parity	Maternal age at delivery	0.7	<b>-0.3</b>	-0.2	<b>0.4</b>	0.3	<b>Parity</b>
Gestational age (GA) at birth	Gestational age (GA) equivalent at scan	0.8	-0.031	<b>0.1</b>	-0.4	<b>-0.6</b>	Gestational age (GA) equivalent at scan
Postnatal age at scan	GA equivalent at scan	0.6 <sup>a</sup>	<b>0.2</b>	0.1	<b>-0.6</b>	-0.6	Postnatal age at scan
Birth weight	Weight at scan	0.8	0.004	<b>0.1</b>	-0.2	<b>-0.4</b>	Weight at scan
Postnatal age at scan	Weight at scan	0.6 <sup>a</sup>	<b>0.2</b>	0.1	<b>-0.6</b>	-0.4	<b>Postnatal age at scan</b>
Head circumference at scan	Birth head circumference	0.7	<b>0.041</b>	0.037	<b>-0.4</b>	-0.2	Head circumference at scan
Head circumference at scan	Total cerebral white matter volume	0.7	0.041	<b>0.3</b>	-0.4	<b>-0.5</b>	<b>Total cerebral white matter volume</b>
Head circumference at scan	Total intracranial volume	0.7	0.041	<b>0.2</b>	-0.4	<b>-0.6</b>	<b>Total intracranial volume</b>
Total intracranial volume	Total cerebral white matter volume	0.9	0.2	<b>0.3</b>	<b>-0.6</b>	-0.5	Investigated further <sup>b</sup>
Socioeconomic status	Marriage status	0.6	-0.004	<b>-0.2</b>	<b>-0.4</b>	-0.2	Investigated further <sup>b</sup>
Socioeconomic status	Maternal education level	0.5 <sup>a</sup>	-0.004	<b>-0.048</b>	<b>-0.4</b>	-0.1	Investigated further <sup>b</sup>

*Excludes the one choline-treated participant whose AP acquisition was used due to it introducing bias on the DTI measures (n = 21)*

<sup>a</sup>Spearman rank

<sup>b</sup>Neither of these variables had larger correlations with FA **and** MD over their respective counterparts. Due to this, their association with the outcomes was used to decide which of the variables in each pair were included as potential confounders.

<sup>c</sup>The variables in bold are those whose associations with the outcomes were evaluated.

## Appendix C: Treatment effects

### Choline dose approximated by treatment adherence

**Table C.1.1:** Associations of radial diffusivity (RD) in each WM connection with choline dose (proxied by maternal choline treatment adherence in % packets consumed) while controlling for infant sex, total intracranial volume (TIV) and postnatal age at scan; and after including a dose-by-sex interaction effect.

WM connections	$\beta_{dose}$ ( $\epsilon_{dose}$ )	$\rho_{dose}$	$\beta_{infant\ sex}$ ( $\epsilon_{infant\ sex}$ )	$\beta_{age}$ ( $\epsilon_{age}$ )	$\beta_{TIV}$ ( $\epsilon_{TIV}$ )	$\beta_{dose*sex}$ ( $\epsilon_{dose*sex}$ )	$\rho_{dose*sex}$
L Thalamus – L Caudate	0.08 (0.24)	0.7	0.29 (0.23)	-0.25 (0.29)	0.01 (0.28)	-0.05 (0.24)	0.8
L Thalamus – L Putamen	0.22 (0.23)	0.3	-0.13 (0.22)	0.01 (0.30)	-0.44 (0.29)	-0.14 (0.24)	0.6
L Thalamus – L Pallidum	-0.01 (0.19)	1.0	0.02 (0.19)	0.34 (0.25)	-0.55 (0.24)	-0.03 (0.20)	0.9
L Thalamus – L Hippocampus	0.02 (0.18)	0.9	0.34 (0.18)	-0.24 (0.23)	-0.54 (0.23)	0.04 (0.19)	0.8
L Thalamus – R Thalamus	0.13 (0.28)	0.6	-0.09 (0.27)	0.60 (0.37)	-0.18 (0.36)	0.22 (0.29)	0.5
L Caudate – L Putamen	0.09 (0.21)	0.7	-0.22 (0.20)	0.01 (0.26)	-0.55 (0.25)	0.40 (0.21)	0.08
L Caudate – L Pallidum	0.13 (0.21)	0.5	-0.23 (0.22)	-0.02 (0.27)	-0.52 (0.27)	0.47 (0.22)	0.05
L Putamen – L Pallidum	-0.17 (0.19)	0.4	-0.25 (0.18)	-0.53 (0.24)	0.06 (0.24)	0.38 (0.20)	0.05
R Thalamus – R Caudate	-0.16 (0.30)	0.6	0.11 (0.29)	-0.12 (0.37)	-0.28 (0.36)	-0.10 (0.30)	0.7
R Thalamus – R Putamen	0.32 (0.16)	0.07	-0.49 (0.16)	-0.71 (0.21)	0.30 (0.20)	-0.07 (0.17)	0.7
R Thalamus – R Pallidum	0.19 (0.22)	0.4	-0.16 (0.21)	-0.44 (0.27)	-0.14 (0.26)	0.45 (0.22)	0.1
R Thalamus – R Hippocampus	0.36 (0.23)	0.1	0.06 (0.22)	-0.65 (0.30)	0.15 (0.30)	0.15 (0.24)	0.5
R Caudate – R Putamen	0.12 (0.21)	0.6	-0.36 (0.21)	-0.32 (0.26)	-0.24 (0.25)	0.14 (0.21)	0.5
R Caudate – R Pallidum	0.39 (0.18)	0.06	-0.67 (0.18)	-0.31 (0.23)	-0.05 (0.22)	-0.05 (0.19)	0.8
R Putamen – R Pallidum	0.21 (0.20)	0.3	-0.51 (0.19)	-0.48 (0.25)	-0.02 (0.24)	0.26 (0.20)	0.2

$\beta$ : Standardized regression coefficients;  $\epsilon$ : Standardized standard errors

## Choline dose approximated by total grams consumed from enrolment through delivery

**Table C.2.1:** Associations of fractional anisotropy (FA) in each WM connection with choline dose approximated by total grams consumed from enrolment through delivery, controlling for after infant sex, postnatal age at scan, total intracranial volume (TIV) and dose-by-sex interactions.

WM connections	$\beta_{dose}$ ( $\epsilon_{dose}$ )	$p_{dose}$	$\beta_{infant\ sex}$ ( $\epsilon_{infant\ sex}$ )	$\beta_{age}$ ( $\epsilon_{age}$ )	$\beta_{TIV}$ ( $\epsilon_{TIV}$ )	$\beta_{dose*sex}$ ( $\epsilon_{dose*sex}$ )	$p_{dose*sex}$
L Thalamus – L Caudate	-0.26 (0.16)	0.1	0.04 (0.15)	-0.28 (0.19)	0.21 (0.19)	0.12 (0.17)	0.5
L Thalamus – L Putamen	-0.19 (0.24)	0.4	-0.24 (0.23)	-0.21 (0.31)	0.16 (0.30)	0.15 (0.26)	0.6
L Thalamus – L Pallidum	-0.11 (0.28)	0.7	-0.29 (0.26)	-0.44 (0.36)	0.20 (0.35)	0.10 (0.30)	0.7
L Thalamus – L Hippocampus	-0.07 (0.13)	0.6	-0.29 (0.12)	0.91 (0.16)	-0.06 (0.16)	-0.07 (0.14)	0.6
L Thalamus – R Thalamus	-0.001 (0.21)	1.0	0.56 (0.19)	-0.32 (0.26)	0.31 (0.25)	0.18 (0.22)	0.4
L Caudate – L Putamen	-0.23 (0.28)	0.4	0.04 (0.25)	-0.35 (0.33)	0.25 (0.32)	-0.32 (0.28)	0.3
L Caudate – L Pallidum	-0.38 (0.29)	0.2	-0.20 (0.27)	-0.62 (0.35)	0.52 (0.35)	-0.45 (0.30)	0.2
L Putamen – L Pallidum	0.15 (0.28)	0.6	0.001 (0.26)	0.28 (0.36)	-0.10 (0.35)	0.03 (0.3)	0.9
R Thalamus – R Caudate	0.10 (0.26)	0.7	0.07 (0.24)	0.26 (0.31)	-0.37 (0.30)	0.32 (0.26)	0.2
R Thalamus – R Putamen	-0.30 (0.24)	0.2	0.01 (0.22)	0.69 (0.30)	-0.44 (0.29)	0.04 (0.26)	0.9
R Thalamus – R Pallidum	-0.14 (0.24)	0.6	-0.48 (0.22)	0.59 (0.29)	-0.18 (0.28)	-0.21 (0.24)	0.4
R Thalamus – R Hippocampus	-0.19 (0.18)	0.3	-0.26 (0.17)	0.56 (0.23)	0.12 (0.22)	0.21 (0.19)	0.3
R Caudate – R Putamen	-0.33 (0.25)	0.2	0.15 (0.23)	0.40 (0.30)	0.09 (0.29)	0.16 (0.25)	0.5
<b>R Caudate – R Pallidum</b>	<b>-0.51 (0.20)</b>	<b>0.024</b>	0.32 (0.18)	0.55 (0.24)	-0.18 (0.23)	0.19 (0.20)	0.4
R Putamen – R Pallidum	-0.46 (0.21)	0.06	0.53 (0.19)	0.12 (0.26)	0.37 (0.25)	-0.36 (0.21)	0.1

$\beta$ : Standardized regression coefficients;  $\epsilon$ : Standardized standard errors.

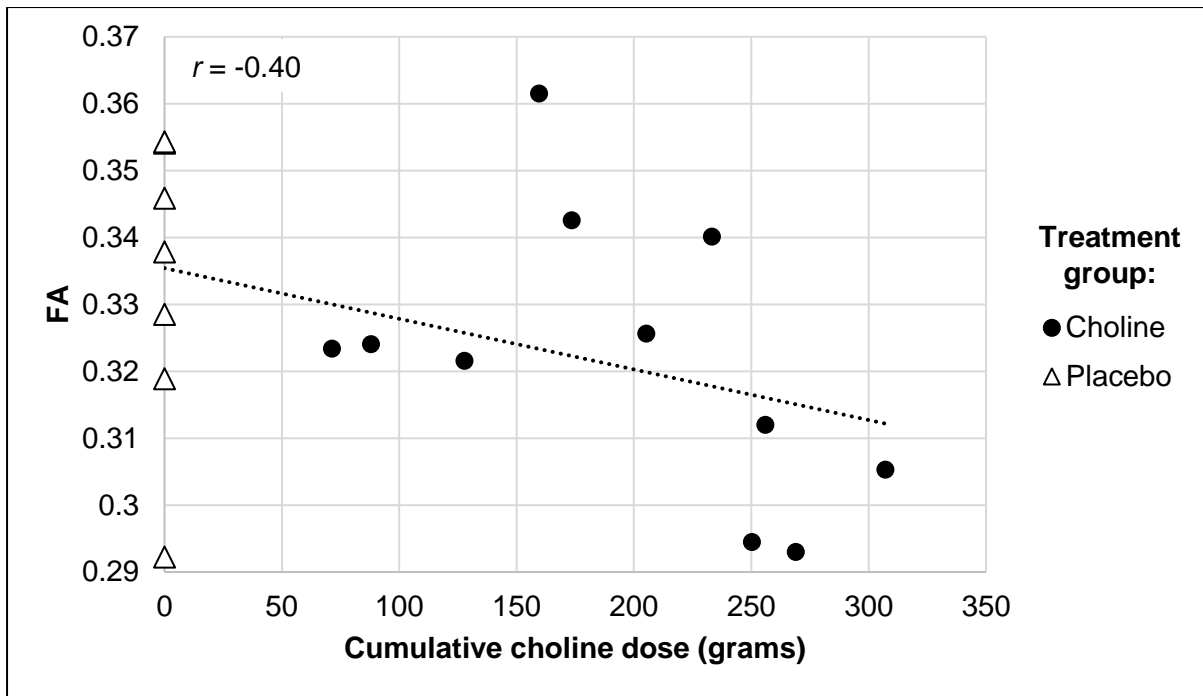


**Figure C.2.1:** Increasing cumulative choline dose (estimated by total grams consumed from enrolment through delivery) was associated with lower fractional anisotropy (FA) in the WM connection between the R caudate and R pallidum. Pearson  $r$  is the correlation coefficient shown.

**Table C.2.2:** Associations of axial diffusivity (AD) in each WM connection with the amount of choline (in grams) consumed in grams from enrolment through delivery, controlling for infant sex, postnatal age at scan, total intracranial volume (TIV), and dose-by-sex interactions.

WM connections	$\beta_{dose}$ ( $\epsilon_{dose}$ )	$\rho_{dose}$	$\beta_{infant\ sex}$ ( $\epsilon_{infant\ sex}$ )	$\beta_{age}$ ( $\epsilon_{age}$ )	$\beta_{TIV}$ ( $\epsilon_{TIV}$ )	$\beta_{dose*sex}$ ( $\epsilon_{dose*sex}$ )	$\rho_{dose*sex}$
L Thalamus – L Caudate	-0.06 (0.24)	0.8	0.24 (0.22)	-0.45 (0.29)	0.05 (0.28)	-0.04 (0.25)	0.9
L Thalamus – L Putamen	0.04 (0.14)	0.8	-0.52 (0.13)	-0.35 (0.18)	-0.25 (0.18)	0.13 (0.15)	0.4
L Thalamus – L Pallidum	0.04 (0.19)	0.8	-0.36 (0.17)	-0.57 (0.23)	-0.01 (0.23)	0.29 (0.20)	0.2
L Thalamus – L Hippocampus	-0.11 (0.27)	0.7	-0.02 (0.25)	0.43 (0.34)	-0.5 (0.33)	-0.06 (0.28)	0.8
L Thalamus – R Thalamus	-0.05 (0.13)	0.7	0.51 (0.12)	0.13 (0.16)	0.07 (0.15)	0.2 (0.14)	0.2
L Caudate – L Putamen	-0.06 (0.2)	0.8	-0.35 (0.18)	-0.49 (0.24)	-0.22 (0.23)	0.12 (0.2)	0.6
L Caudate – L Pallidum	-0.05 (0.12)	0.7	-0.45 (0.12)	-0.76 (0.15)	0.36 (0.15)	-0.16 (0.13)	0.3
L Putamen – L Pallidum	0.16 (0.35)	0.6	-0.28 (0.33)	0.01 (0.44)	-0.16 (0.43)	0.18 (0.38)	0.6
R Thalamus – R Caudate	-0.14 (0.17)	0.4	0.05 (0.15)	0.19 (0.20)	-0.75 (0.19)	-0.10 (0.17)	0.5
R Thalamus – R Putamen	-0.09 (0.14)	0.6	-0.42 (0.13)	-0.42 (0.18)	-0.1 (0.17)	0.29 (0.15)	0.08
R Thalamus – R Pallidum	0.06 (0.12)	0.6	-0.76 (0.11)	0.17 (0.15)	-0.31 (0.14)	0.32 (0.12)	0.022
R Thalamus – R Hippocampus	0.24 (0.19)	0.3	-0.15 (0.18)	-0.3 (0.24)	0.45 (0.24)	0.55 (0.20)	0.023
<b>R Caudate – R Putamen</b>	<b>-0.41 (0.16)</b>	<b>0.027</b>	-0.07 (0.15)	-0.32 (0.20)	-0.09 (0.19)	0.28 (0.16)	0.1
R Caudate – R Pallidum	-0.13 (0.25)	0.6	-0.46 (0.22)	0.3 (0.29)	-0.41 (0.29)	0.25 (0.25)	0.3
<b>R Putamen – R Pallidum</b>	<b>-0.53 (0.24)</b>	<b>0.049</b>	0.24 (0.22)	-0.48 (0.29)	0.55 (0.28)	0.04 (0.24)	0.9

$\beta$ : Standardized regression coefficients;  $\epsilon$ : Standardized standard errors

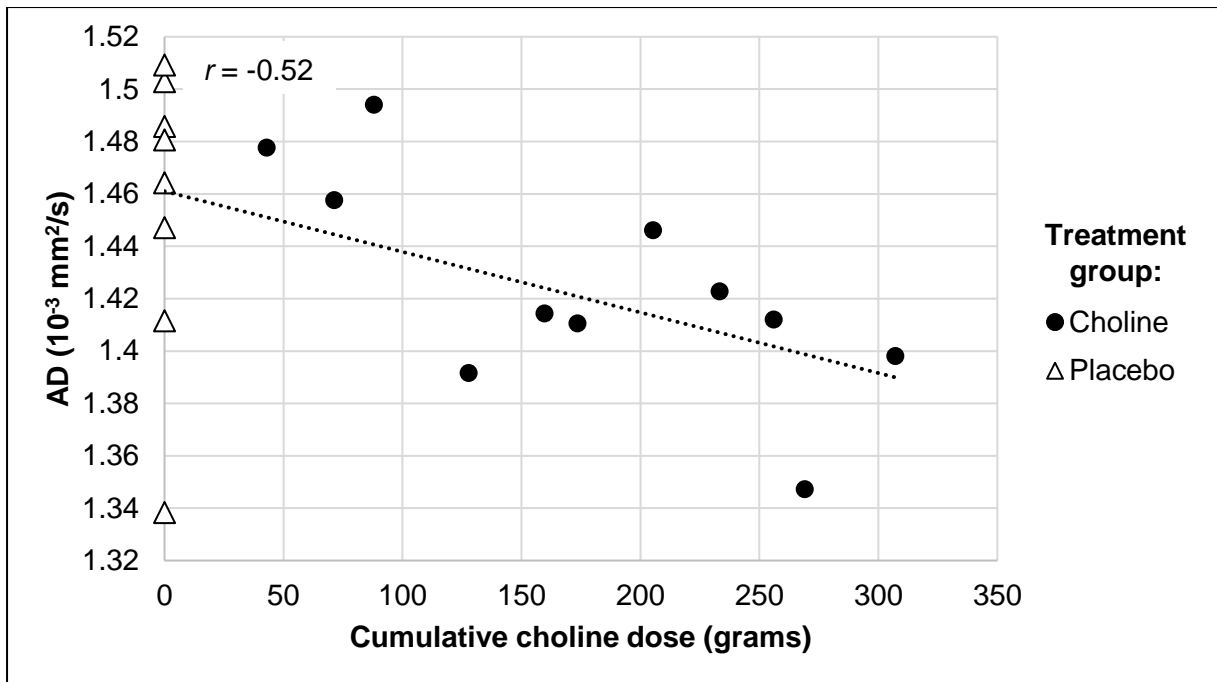


**Figure C.2.2:** Increasing cumulative choline dose (approximated as the total grams consumed from enrolment through deliver) was associated with lower axial diffusivity (AD) in the WM connection between the R caudate and R putamen connection. The correlation coefficient shown is Pearson  $r$ .

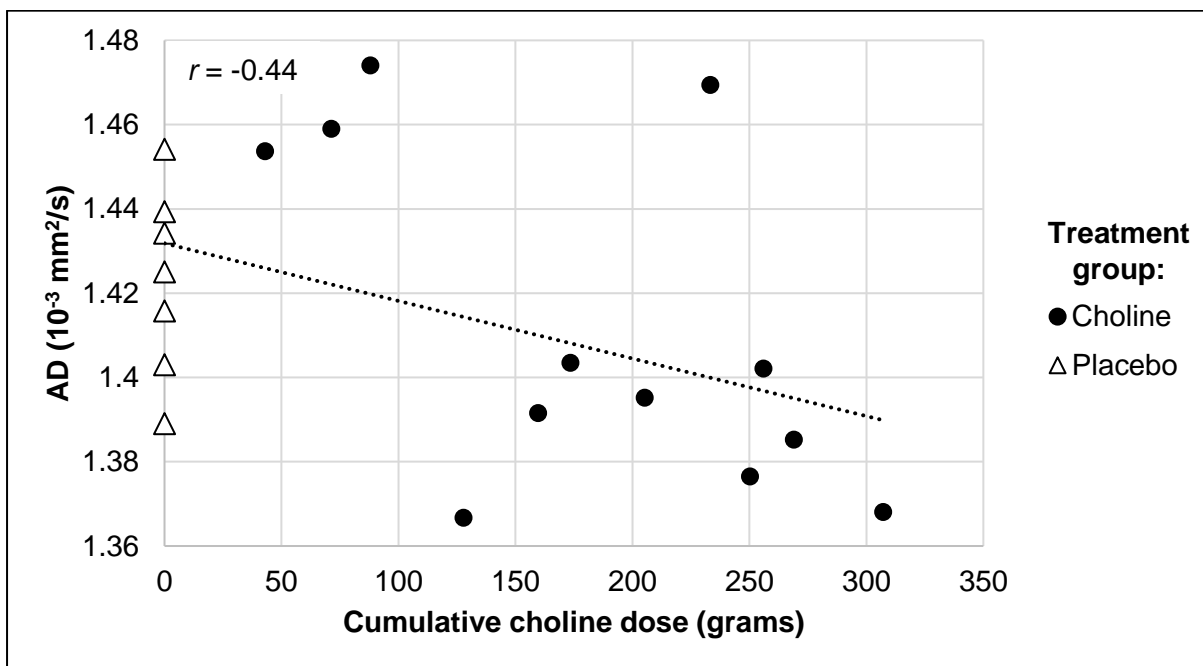


**Figure C.2.3:** Increasing cumulative choline dose (estimated by total grams consumed from enrolment through delivery) was associated with lower axial diffusivity (AD) in the WM connection from the R putamen to the R pallidum connection. Pearson  $r$  is the correlation coefficient shown.

**Table C.2.3:** Associations of radial diffusivity (RD) in each WM connection with cumulative choline dose (in grams) consumed from enrolment through delivery while controlling for infant sex, postnatal age at scan, total intracranial volume (TIV) and dose-by-sex interactions.

WM connections	$\beta_{dose}$ ( $\epsilon_{dose}$ )	$\rho_{dose}$	$\beta_{infant\ sex}$ ( $\epsilon_{infant\ sex}$ )	$\beta_{age}$ ( $\epsilon_{age}$ )	$\beta_{TIV}$ ( $\epsilon_{TIV}$ )	$\beta_{dose*sex}$ ( $\epsilon_{dose*sex}$ )	$\rho_{dose*sex}$
L Thalamus – L Caudate	0.01 (0.22)	1.0	0.34 (0.20)	-0.29 (0.26)	0.09 (0.26)	0.01 (0.23)	1.0
L Thalamus – L Putamen	0.2 (0.26)	0.5	-0.11 (0.24)	0.001 (0.32)	-0.47 (0.32)	-0.05 (0.27)	0.9
L Thalamus – L Pallidum	-0.02 (0.20)	0.9	0.020 (0.19)	0.33 (0.25)	-0.55 (0.25)	0.003 (0.21)	1.0
L Thalamus – L Hippocampus	-0.04 (0.22)	0.9	0.35 (0.2)	-0.24 (0.27)	-0.54 (0.27)	0.04 (0.23)	0.9
L Thalamus – R Thalamus	0.11 (0.30)	0.7	-0.06 (0.27)	0.59 (0.37)	-0.18 (0.36)	0.19 (0.32)	0.6
L Caudate – L Putamen	0.14 (0.25)	0.6	-0.27 (0.23)	-0.02 (0.30)	-0.55 (0.29)	0.47 (0.25)	0.08
L Caudate – L Pallidum	0.17 (0.21)	0.5	-0.19 (0.20)	-0.06 (0.26)	-0.52 (0.26)	0.57 (0.22)	0.024
L Putamen – L Pallidum	-0.21 (0.19)	0.3	-0.25 (0.17)	-0.5 (0.24)	0.05 (0.23)	0.31 (0.20)	0.1
R Thalamus – R Caudate	-0.23 (0.31)	0.5	0.10 (0.28)	-0.11 (0.37)	-0.27 (0.36)	-0.12 (0.31)	0.7
R Thalamus – R Putamen	0.26 (0.18)	0.2	-0.41 (0.17)	-0.71 (0.22)	0.24 (0.22)	0.09 (0.19)	0.7
R Thalamus – R Pallidum	0.25 (0.20)	0.2	-0.16 (0.19)	-0.43 (0.24)	-0.17 (0.24)	0.44 (0.20)	0.047
R Thalamus – R Hippocampus	0.38 (0.25)	0.1	0.13 (0.24)	-0.65 (0.32)	0.1 (0.31)	0.26 (0.27)	0.3
R Caudate – R Putamen	0.17 (0.21)	0.4	-0.37 (0.20)	-0.32 (0.25)	-0.25 (0.25)	0.17 (0.21)	0.4
R Caudate – R Pallidum	0.34 (0.18)	0.08	-0.61 (0.16)	-0.34 (0.21)	-0.04 (0.21)	0.12 (0.18)	0.5
R Putamen – R Pallidum	0.25 (0.21)	0.3	-0.49 (0.19)	-0.43 (0.26)	-0.13 (0.25)	0.33 (0.21)	0.1

$\beta$ : Standardized regression coefficients;  $\epsilon$ : Standardized standard errors

## References

- AARON, D. S. & DANIEL, K. S. 2016. Chapter 18 - Introductory Magnetic Resonance Imaging Physics. In: HERBERT, B. N. (ed.) *Handbook of Neuro-Oncology Neuroimaging (Second Edition)*. Second Edition ed. San Diego: Academic Press.
- ABE, O., TAKAO, H., GONOI, W., SASAKI, H., MURAKAMI, M., KABASAWA, H., KAWAGUCHI, H., GOTO, M., YAMADA, H. & YAMASUE, H. 2010. Voxel-based analysis of the diffusion tensor. *Neuroradiology*, 52, 699-710.
- ABEL, E. L. & HANNIGAN, J. H. 1995. Maternal risk factors in fetal alcohol syndrome: provocative and permissive influences. *Neurotoxicology and teratology*, 17, 445-462.
- ADAMS, J. & WEAKLIEM, D. L. 2011. August B. Hollingshead's "Four Factor Index of Social Status": from unpublished paper to citation classic. *Yale Journal of Sociology*, 8, 11-17.
- ADEBIYI, B. O., MUKUMBANG, F. C. & BEYTELL, A.-M. 2021. Policy Requirements for the Prevention and Management of Fetal Alcohol Spectrum Disorder in South Africa: A Policy Brief. *Frontiers in Public Health*, 9, 592726.
- ADNAMS, C. M., KODITUWAKKU, P. W., HAY, A., MOLTENO, C. D., VILJOEN, D. & MAY, P. A. 2001. Patterns of cognitive-motor development in children with fetal alcohol syndrome from a community in South Africa. *Alcoholism: Clinical and Experimental Research*, 25, 557-562.
- AKISON, L. K., KUO, J., REID, N., BOYD, R. N. & MORITZ, K. M. 2018. Effect of choline supplementation on neurological, cognitive, and behavioral outcomes in offspring arising from alcohol exposure during development: a quantitative systematic review of clinical and preclinical studies. *Alcoholism: Clinical and Experimental Research*, 42, 1591-1611.
- AKOGLU, H. 2018. User's guide to correlation coefficients. *Turkish journal of emergency medicine*, 18, 91-93.
- ALEXANDER, A. L., LEE, J. E., LAZAR, M. & FIELD, A. S. 2007. Diffusion tensor imaging of the brain. *Neurotherapeutics*, 4, 316-329.
- ALEXANDER, G. E., DELONG, M. R. & STRICK, P. L. 1986. Parallel organization of functionally segregated circuits linking basal ganglia and cortex. *Annual review of neuroscience*, 9, 357-381.
- ALHAMUD, A., TISDALL, M. D., HESS, A. T., HASAN, K. M., MEINTJES, E. M. & VAN DER KOUWE, A. J. 2012. Volumetric navigators for real-time motion correction in diffusion tensor imaging. *Magnetic resonance in medicine*, 68, 1097-1108.

- ALMA, Ö. G. 2011. Comparison of robust regression methods in linear regression. *Int. J. Contemp. Math. Sciences*, 6, 409-421.
- ANAND, K. S. & DHIKAV, V. 2012. Hippocampus in health and disease: An overview. *Annals of Indian Academy of Neurology*, 15, 239.
- ANN-CHRISTINE, D. & RIMA SESTOKAS, R. 2015. Chapter 15 - Special considerations in infants and children. In: JORDAN, G. & ANDRES, M. S. (eds.) *Traumatic Brain Injury, Part I*. Elsevier.
- ARCHIBALD, S. L., FENNEMA-NOTESTINE, C., GAMST, A., RILEY, E. P., MATTSON, S. N. & JERNIGAN, T. L. 2001. Brain dysmorphology in individuals with severe prenatal alcohol exposure. *Developmental medicine and child neurology*, 43, 148-154.
- ASTLEY, S. J., RICHARDS, T., AYLWARD, E. H., OLSON, H. C., KERNS, K., BROOKS, A., COGGINS, T. E., DAVIES, J., DORN, S. & GENDLER, B. 2009. Magnetic resonance spectroscopy outcomes from a comprehensive magnetic resonance study of children with fetal alcohol spectrum disorders. *Magnetic resonance imaging*, 27, 760-778.
- BAILEY, R. L., PAC, S. G., FULGONI, V. L., REIDY, K. C. & CATALANO, P. M. 2019. Estimation of total usual dietary intakes of pregnant women in the United States. *JAMA network open*, 2, e195967-e195967.
- BAKKER, A., KIRWAN, C. B., MILLER, M. & STARK, C. E. 2008. Pattern separation in the human hippocampal CA3 and dentate gyrus. *science*, 319, 1640-1642.
- BALIYAN, V., DAS, C. J., SHARMA, R. & GUPTA, A. K. 2016. Diffusion weighted imaging: technique and applications. *World journal of radiology*, 8, 785.
- BARAZANY, D., BASSER, P. J. & ASSAF, Y. 2009. In vivo measurement of axon diameter distribution in the corpus callosum of rat brain. *Brain*, 132, 1210-1220.
- BARKOVICH, A. J. 2002. Normal development of the neonatal and infant brain, skull, and spine. *Pediatric neuroimaging*, 13-71.
- BASSER, P. J., MATTIELLO, J. & LEBIHAN, D. 1994. MR diffusion tensor spectroscopy and imaging. *Biophysical journal*, 66, 259-267.
- BASSER, P. J., PAJEVIC, S., PIERPAOLI, C., DUDA, J. & ALDROUBI, A. 2000. In vivo fiber tractography using DT-MRI data. *Magnetic resonance in medicine*, 44, 625-632.
- BASSER, P. J. & PIERPAOLI, C. 1996. Microstructural and Physiological Features of Tissues Elucidated by Quantitative-Diffusion-Tensor MRI. *Journal of Magnetic Resonance, Series B*, 3, 209-219.
- BASTIANI, M., ANDERSSON, J. L., CORDERO-GRANDE, L., MURGASOVA, M., HUTTER, J., PRICE, A. N., MAKROPOULOS, A., FITZGIBBON, S. P., HUGHES, E., RUECKERT, D., VICTOR, S., RUTHERFORD, M., EDWARDS, A. D., SMITH, S., TOURNIER, J.-D., HAJNAL, J. V., JBABDI, S. & SOTIROPOULOS, S. N. 2019.

- Automated processing pipeline for neonatal diffusion MRI in the developing Human Connectome Project. *Neuroimage*, 185, 750-763.
- BAYLEY, N. 2006. Bayley scales of infant and toddler development.
- BEAULIEU, C. 2002. The basis of anisotropic water diffusion in the nervous system—a technical review. *NMR in Biomedicine: An International Journal Devoted to the Development and Application of Magnetic Resonance In Vivo*, 15, 435-455.
- BEAULIEU, C., PLEWES, C., PAULSON, L. A., ROY, D., SNOOK, L., CONCHA, L. & PHILLIPS, L. 2005. Imaging brain connectivity in children with diverse reading ability. *Neuroimage*, 25, 1266-1271.
- BEHRENS, T. E., SOTIROPOULOS, S. N. & JBABDI, S. 2014. MR diffusion tractography. *Diffusion MRI*. Elsevier.
- BEHRENS, T. E., WOOLRICH, M. W., JENKINSON, M., JOHANSEN-BERG, H., NUNES, R. G., CLARE, S., MATTHEWS, P. M., BRADY, J. M. & SMITH, S. M. 2003. Characterization and propagation of uncertainty in diffusion-weighted MR imaging. *Magnetic Resonance in Medicine: An Official Journal of the International Society for Magnetic Resonance in Medicine*, 50, 1077-1088.
- BEKDASH, R. A. 2019. Neuroprotective effects of choline and other methyl donors. *Nutrients*, 11, 2995.
- BIFFEN, S. C., DODGE, N. C., WARTON, C. M., MOLTENO, C. D., JACOBSON, J. L., MEINTJES, E. M. & JACOBSON, S. W. 2022. Compromised interhemispheric transfer of information partially mediates cognitive function deficits in adolescents with fetal alcohol syndrome. *Alcoholism: Clinical and Experimental Research*, 46, 517-529.
- BIFFEN, S. C., WARTON, C. M., LINDINGER, N. M., RANDALL, S. R., LEWIS, C. E., MOLTENO, C. D., JACOBSON, J. L., JACOBSON, S. W. & MEINTJES, E. M. 2018. Reductions in corpus callosum volume partially mediate effects of prenatal alcohol exposure on IQ. *Frontiers in neuroanatomy*, 132.
- BINGOL, N., SCHUSTER, C., FUCHS, M., IOSUB, S., TURNER, G., STONE, R. K. & GROMISCH, D. S. 1987. The influence of socioeconomic factors on the occurrence of fetal alcohol syndrome. *Advances in alcohol & substance abuse*, 6, 105-118.
- BLAIR, C. 2017. Educating executive function. *Wiley Interdisciplinary Reviews: Cognitive Science*, 8, e1403.
- BLANCHARD, B., STEINDORF, S., WANG, S., LEFEVRE, R., MANKES, R. & GLICK, S. 1993. Prenatal ethanol exposure alters ethanol-induced dopamine release in nucleus accumbens and striatum in male and female rats. *Alcoholism: Clinical and Experimental Research*, 17, 974-981.

- BODAKUNTLA, S., NEDOZRALOVA, H., BASNET, N. & MIZUNO, N. 2021. Cytoskeleton and membrane organization at axon branches. *Frontiers in Cell and Developmental Biology*, 9, 707486.
- BONNER-JACKSON, A., MAHMOUD, S., MILLER, J. & BANKS, S. J. 2015. Verbal and non-verbal memory and hippocampal volumes in a memory clinic population. *Alzheimer's Research & Therapy*, 7, 1-10.
- BOOKSTEIN, F. L., STREISSGUTH, A. P., CONNOR, P. D. & SAMPSON, P. D. 2006. Damage to the human cerebellum from prenatal alcohol exposure: the anatomy of a simple biometrical explanation. *The Anatomical Record Part B: The New Anatomist*, 289, 195-209.
- BOOTH, J. R., WOOD, L., LU, D., HOUK, J. C. & BITAN, T. 2007. The role of the basal ganglia and cerebellum in language processing. *Brain research*, 1133, 136-144.
- BORGHEI, A., KAPUCU, I., DAWE, R., KOCÁK, M. & SANI, S. 2021. Structural connectivity of the human massa intermedia: A probabilistic tractography study. *Human Brain Mapping*, 42, 1794-1804.
- BRAND, S. & RAKIC, P. 1980. Neurogenesis of the nucleus accumbens septi and neighboring septal nuclei in the rhesus monkey: a combined [<sup>3</sup>H] thymidine and electron microscopic study. *Neuroscience*, 5, 2125-2138.
- BURD, L., KLUG, M. G., MARTSOLF, J. T. & KERBESHIAN, J. 2003. Fetal alcohol syndrome: neuropsychiatric phenomics. *Neurotoxicology and Teratology*, 25, 697-705.
- BURNHAM, K. P. & ANDERSON, D. R. 2004. Model selection and multimodel inference. *A practical information-theoretic approach*, 2.
- BUXTON, R. B. 2009. Relaxation and contrast in MRI. *Introduction to functional magnetic resonance imaging: principles and techniques*. Cambridge university press.
- CAAN, M. W. 2016. DTI analysis methods: fibre tracking and connectivity. *Diffusion tensor imaging: A practical handbook*, 205-228.
- CARTER, J. M., DEMIZIEUX, L., CAMPENOT, R. B., VANCE, D. E. & VANCE, J. E. 2008. Phosphatidylcholine biosynthesis via CTP: Phosphocholine cytidyltransferase  $\beta$ 2 facilitates neurite outgrowth and branching. *Journal of Biological Chemistry*, 283, 202-212.
- CHAKRAVARTHY, V. S. & BALASUBRAMANI, P. P. 2022. Basal ganglia system as an engine for exploration. *Encyclopedia of computational neuroscience*. Springer.
- CHAMBERS, W. W. & SPRAGUE, J. M. 1955. Functional localization in the cerebellum: Somatotopic organization in cortex and nuclei. *AMA Archives of Neurology & Psychiatry*, 74, 653-680.

- CHAVEZ, C. & ZABORSZKY, L. 2017. Basal forebrain cholinergic–auditory cortical network: primary versus nonprimary auditory cortical areas. *Cerebral cortex*, 27, 2335-2347.
- COLEMAN, J., GINSBURG, A. S., MACHARIA, W. M., OCHIENG, R., CHOMBA, D., ZHOU, G., DUNSMUIR, D., KARLEN, W. & ANSERMINO, J. M. 2022. Assessment of neonatal respiratory rate variability. *Journal of Clinical Monitoring and Computing*, 36, 1869-1879.
- COLES, C. D., GOLDSTEIN, F. C., LYNCH, M. E., CHEN, X., KABLE, J. A., JOHNSON, K. C. & HU, X. 2011. Memory and brain volume in adults prenatally exposed to alcohol. *Brain and cognition*, 75, 67-77.
- COLES, C. D., KABLE, J. A., KEEN, C. L., JONES, K. L., WERTELECKI, W., GRANOVSKA, I. V., PASHTEPA, A. O., CHAMBERS, C. D. & CIFASD 2015. Dose and timing of prenatal alcohol exposure and maternal nutritional supplements: developmental effects on 6-month-old infants. *Maternal and child health journal*, 19, 2605-2614.
- CONTURO, T. E., LORI, N. F., CULL, T. S., AKBUDAK, E., SNYDER, A. Z., SHIMONY, J. S., MCKINSTRY, R. C., BURTON, H. & RAICHLE, M. E. 1999. Tracking neuronal fiber pathways in the living human brain. *Proceedings of the National Academy of Sciences*, 96, 10422-10427.
- COOPER, E. R. 1950. The development of the thalamus. *Cells Tissues Organs*, 9, 201-226.
- COX, R. W. 1996. AFNI: software for analysis and visualization of functional magnetic resonance neuroimages. *Computers and Biomedical research*, 29, 162-173.
- DAI, Y., SHI, F., WANG, L., WU, G. & SHEN, D. 2013. iBEAT: a toolbox for infant brain magnetic resonance image processing. *Neuroinformatics*, 11, 211-225.
- DE GUIO, F., MANGIN, J. F., RIVIÈRE, D., PERROT, M., MOLTENO, C. D., JACOBSON, S. W., MEINTJES, E. M. & JACOBSON, J. L. 2014. A study of cortical morphology in children with fetal alcohol spectrum disorders. *Human brain mapping*, 35, 2285-2296.
- DE MUTH, J. E. 2009. Overview of biostatistics used in clinical research. *American Journal of Health-System Pharmacy*, 66, 70-81.
- DE REUCK, J. L. 2014. White Matter. In: MICHAEL, J. A. & ROBERT, B. D. (eds.) *Encyclopedia of the Neurological Sciences*. Second ed. Oxford: Academic Press.
- DE VRIES, M. M., JOUBERT, B., CLOETE, M., ROUX, S., BACA, B. A., HASKEN, J. M., BARNARD, R., BUCKLEY, D., KALBERG, W. O., SNELL, C. L., MARAIS, A.-S., SEEDAT, S., PARRY, C. D. H. & MAY, P. A. 2016. Indicated prevention of fetal alcohol spectrum disorders in South Africa: effectiveness of case management. *International journal of environmental research and public health*, 13, 76.

- DEBAERE, F., WENDEROTH, N., SUNAERT, S., VAN HECKE, P. & SWINNEN, S. 2004. Changes in brain activation during the acquisition of a new bimanual coordination task. *Neuropsychologia*, 42, 855-867.
- DEL CAMPO, M. & JONES, K. L. 2017. A review of the physical features of the fetal alcohol spectrum disorders. *European journal of medical genetics*, 60, 55-64.
- DICKIE, D. A., SHENKIN, S. D., ANBLAGAN, D., LEE, J., BLESÁ CABEZ, M., RODRIGUEZ, D., BOARDMAN, J. P., WALDMAN, A., JOB, D. E. & WARDLAW, J. M. 2017. Whole brain magnetic resonance image atlases: a systematic review of existing atlases and caveats for use in population imaging. *Frontiers in neuroinformatics*, 11, 1.
- DOBBING, J. & SANDS, J. 1973. Quantitative growth and development of human brain. *Archives of disease in childhood*, 48, 757-767.
- DONALD, K. A., ROOS, A., FOUICHE, J.-P., KOEN, N., HOWELLS, F. M., WOODS, R. P., ZAR, H. J., NARR, K. L. & STEIN, D. J. 2015. A study of the effects of prenatal alcohol exposure on white matter microstructural integrity at birth. *Acta neuropsychiatrica*, 27, 197-205.
- DRAKE, R. L., VOGL, A. W. & MITCHELL, A. W. M. 2023. Neuroanatomy. *Gray's Basic Anatomy*. Third ed. Philadelphia: Jeremy Bowes.
- DU PLESSIS, A. J., LIMPEROPOULOS, C. & VOLPE, J. J. 2018. Cerebellar development. In: VOLPE, J. J., INDER, T. E., DARRAS, B. T., DE VRIES, L. S., DU PLESSIS, A. J., NEIL, J. J. & PERLMAN, J. M. (eds.) *Volpe's Neurology of the Newborn*. Sixth ed. Philadelphia: Elsevier.
- DUBOIS, J., ADIBPOUR, P., POUPON, C., HERTZ-PANNIER, L. & DEHAENE-LAMBERTZ, G. 2016. MRI and M/EEG studies of the white matter development in human fetuses and infants: review and opinion. *Brain Plasticity*, 2, 49-69.
- DUBOIS, J., ALISON, M., COUNSELL, S. J., HERTZ-PANNIER, L., HÜPPI, P. S. & BENDERS, M. J. 2021. MRI of the neonatal brain: a review of methodological challenges and neuroscientific advances. *Journal of Magnetic Resonance Imaging*, 53, 1318-1343.
- DUBOIS, J., DEHAENE-LAMBERTZ, G., KULIKOVA, S., POUPON, C., HÜPPI, P. S. & HERTZ-PANNIER, L. 2014. The early development of brain white matter: a review of imaging studies in fetuses, newborns and infants. *Neuroscience*, 276, 48-71.
- DUBOIS, J., DEHAENE-LAMBERTZ, G., PERRIN, M., MANGIN, J. F., COINTEPAS, Y., DUCHESNAY, E., LE BIHAN, D. & HERTZ-PANNIER, L. 2008. Asynchrony of the early maturation of white matter bundles in healthy infants: quantitative landmarks revealed noninvasively by diffusion tensor imaging. *Human brain mapping*, 29, 14-27.

- DUBOIS, J., HERTZ-PANNIER, L., DEHAENE-LAMBERTZ, G., COINTEPAS, Y. & LE BIHAN, D. 2006. Assessment of the early organization and maturation of infants' cerebral white matter fiber bundles: a feasibility study using quantitative diffusion tensor imaging and tractography. *Neuroimage*, 30, 1121-1132.
- DUERDEN, E., FOONG, J., CHAU, V., BRANSON, H., POSKITT, K., GRUNAU, R., SYNNESE, A., ZWICKER, J. & MILLER, S. 2015. Tract-based spatial statistics in preterm-born neonates predicts cognitive and motor outcomes at 18 months. *American Journal of Neuroradiology*, 36, 1565-1571.
- ELENBAAS, R. M., ELENBAAS, J. K. & CUDDY, P. G. 1983. Evaluating the medical literature part II: statistical analysis. *Annals of emergency medicine*, 12, 610-620.
- ELLIOTT, C. D., MURRAY, G. & PEARSON, L. 1990. Differential ability scales. *San Antonio, Texas*.
- FAGAN III, J. F. & DETTERMAN, D. K. 1992. The Fagan test of infant intelligence: A technical summary. *Journal of applied developmental psychology*, 13, 173-193.
- FAGAN, J. F. & SINGER, L. T. 1983. Infant recognition memory as a measure of intelligence. *Advances in infancy research*.
- FAGONE, P. & JACKOWSKI, S. 2013. Phosphatidylcholine and the CDP–choline cycle. *Biochimica et Biophysica Acta (BBA)-Molecular and Cell Biology of Lipids*, 1831, 523-532.
- FAN, J., JACOBSON, S. W., TAYLOR, P. A., MOLTENO, C. D., DODGE, N. C., STANTON, M. E., JACOBSON, J. L. & MEINTJES, E. M. 2016. White matter deficits mediate effects of prenatal alcohol exposure on cognitive development in childhood. *Human brain mapping*, 37, 2943-2958.
- FARAH, R., TZAFRIR, H. & HOROWITZ-KRAUS, T. 2020. Association between diffusivity measures and language and cognitive-control abilities from early toddler's age to childhood. *Brain Structure and Function*, 225, 1103-1122.
- FELDMAN, H. M., YEATMAN, J. D., LEE, E. S., BARDE, L. H. & GAMAN-BEAN, S. 2010. Diffusion tensor imaging: a review for pediatric researchers and clinicians. *Journal of developmental and behavioral pediatrics: JDBP*, 31, 346.
- FENG, K., ROWELL, A. C., ANDRES, A., BELLANDO, B. J., LOU, X., GLASIER, C. M., RAMAKRISHNAIAH, R. H., BADGER, T. M. & OU, X. 2019. Diffusion tensor MRI of white matter of healthy full-term newborns: relationship to neurodevelopmental outcomes. *Radiology*, 292, 179-187.
- FILLARD, P., DESCOTEAUX, M., GOH, A., GOUTTARD, S., JEURISSEN, B., MALCOLM, J., RAMIREZ-MANZANARES, A., REISERT, M., SAKAIE, K., TENSAOUTI, F., YO,

- T., MANGIN, J.-F. & POUPON, C. 2011. Quantitative evaluation of 10 tractography algorithms on a realistic diffusion MR phantom. *Neuroimage*, 56, 220-234.
- FOX, J. & WEISBERG, S. 2002. Robust regression. *An R and S-Plus companion to applied regression*, 91, 6.
- FROELING, M., PULLENS, P. & LEEMANS, A. 2016. DTI analysis methods: region of interest analysis. *Diffusion tensor imaging: a practical handbook*, 175-182.
- FRYER, S. L., SCHWEINSBURG, B. C., BJORKQUIST, O. A., FRANK, L. R., MATTSON, S. N., SPADONI, A. D. & RILEY, E. P. 2009. Characterization of white matter microstructure in fetal alcohol spectrum disorders. *Alcoholism: Clinical and Experimental Research*, 33, 514-521.
- GADDIS, G. M. & GADDIS, M. L. 1990. Introduction to biostatistics: Part 5, Statistical inference techniques for hypothesis testing with nonparametric data. *Annals of emergency medicine*, 19, 1054-1059.
- GAO, W., LIN, W., CHEN, Y., GERIG, G., SMITH, J., JEWELLS, V. & GILMORE, J. 2009. Temporal and spatial development of axonal maturation and myelination of white matter in the developing brain. *American journal of neuroradiology*, 30, 290-296.
- GASTWIRTH, J. L., GEL, Y. R. & MIAO, W. 2009. The impact of Levene's test of equality of variances on statistical theory and practice.
- GENG, X., GOUTTARD, S., SHARMA, A., GU, H., STYNER, M., LIN, W., GERIG, G. & GILMORE, J. H. 2012. Quantitative tract-based white matter development from birth to age 2 years. *Neuroimage*, 61, 542-557.
- GERWIG, M., KOLB, F. & TIMMANN, D. 2007. The involvement of the human cerebellum in eyeblink conditioning. *The Cerebellum*, 6, 38-57.
- GHAZI SHERBAF, F., AARABI, M. H., HOSEIN YAZDI, M. & HAGHSHOMAR, M. 2019. White matter microstructure in fetal alcohol spectrum disorders: A systematic review of diffusion tensor imaging studies. *Human brain mapping*, 40, 1017-1036.
- GIBBY, W. A. 2005. Basic principles of magnetic resonance imaging. *Neurosurgery Clinics*, 16, 1-64.
- GIMBEL, B. A., ANTHONY, M. E., ERNST, A. M., ROEDIGER, D. J., DE WATER, E., ECKERLE, J. K., BOYS, C. J., RADKE, J. P., MUELLER, B. A., FUGLESTAD, A. J., GEORGIEFF, M. K. & WOZNIAK, J. R. 2022. Long-term follow-up of a randomized controlled trial of choline for neurodevelopment in fetal alcohol spectrum disorder: corpus callosum white matter microstructure and neurocognitive outcomes. *Journal of neurodevelopmental disorders*, 14, 59.

- GIRAULT, J. B., CORNEA, E., GOLDMAN, B. D., KNICKMEYER, R. C., STYNER, M. & GILMORE, J. H. 2019. White matter microstructural development and cognitive ability in the first 2 years of life. *Human Brain Mapping*, 40, 1195-1210.
- GLENN, O. A. Normal development of the fetal brain by MRI. *Seminars in perinatology*, 2009. Elsevier, 208-219.
- GOMEZ, M. J. C., BEAULIEU, C., MCMORRIS, C. A., GIBBARD, B., TORTORELLI, C. & LEBEL, C. 2022. Frontoparietal and temporal white matter diffusion MRI in children and youth with prenatal alcohol exposure. *Alcoholism: Clinical and Experimental Research*, 46, 1808-1818.
- GREGOR, K., PETER, C. B., MICHAEL, W., MARTIN, K., ELISABETH, K., CHRISTIAN, H. & DANIELA, P. 2008. In utero tractography of fetal white matter development. *NeuroImage*, 43, 213-224.
- HABER, S. N. 2016. Corticostriatal circuitry. *Dialogues in clinical neuroscience*, 18, 7-21.
- HAINES, D. E. & MIHAIOFF, G. A. 2018. Chapter 16 - The Telencephalon. *In: DUANE, E. H. & GREGORY, A. M. (eds.) Fundamental Neuroscience for Basic and Clinical Applications*. Fifth ed.: Elsevier.
- HALVERSON, H. E., POREMBA, A. & FREEMAN, J. H. 2008. Medial auditory thalamus inactivation prevents acquisition and retention of eyeblink conditioning. *Learning & memory*, 15, 532-538.
- HARKINS, K. D., BEAULIEU, C., XU, J., GORE, J. C. & DOES, M. D. 2021. A simple estimate of axon size with diffusion MRI. *Neuroimage*, 227, 117619.
- HASEGAWA, M., HOUDOU, S., MITO, T., TAKASHIMA, S., ASANUMA, K. & OHNO, T. 1992. Development of myelination in the human fetal and infant cerebrum: a myelin basic protein immunohistochemical study. *Brain and Development*, 14, 1-6.
- HAUSER, M. F., HEBA, S., SCHMIDT-WILCKE, T., TEGENTHOFF, M. & MANAHAN-VAUGHAN, D. 2020. Cerebellar-hippocampal processing in passive perception of visuospatial change: An ego-and allocentric axis? *Human brain mapping*, 41, 1153-1166.
- HAZRA, A. & GOGTAY, N. 2016. Biostatistics series module 6: correlation and linear regression. *Indian journal of dermatology*, 61, 593.
- HEEMSKERK, A., LEEMANS, A., PLAISIER, A., PIETERMAN, K., LEQUIN, M. & DUDINK, J. 2013. Acquisition guidelines and quality assessment tools for analyzing neonatal diffusion tensor MRI data. *American Journal of Neuroradiology*, 34, 1496-1505.
- HOEFT, F., BARNEA-GORALY, N., HAAS, B. W., GOLARAI, G., NG, D., MILLS, D., KORENBERG, J., BELLUGI, U., GALABURDA, A. & REISS, A. L. 2007. More is not always better: increased fractional anisotropy of superior longitudinal fasciculus

- associated with poor visuospatial abilities in Williams syndrome. *Journal of Neuroscience*, 27, 11960-11965.
- HORGOS, B., MECEA, M., BOER, A., SZABO, B., BURUIANA, A., STAMATIAN, F., MIHU, C.-M., FLORIAN, I. Ş., SUSMAN, S. & PASCALAU, R. 2020. White matter dissection of the fetal brain. *Frontiers in Neuroanatomy*, 14, 584266.
- HOYME, H. E., MAY, P. A., KALBERG, W. O., KODITUWAKKU, P., GOSSAGE, J. P., TRUJILLO, P. M., BUCKLEY, D. G., MILLER, J. H., ARAGON, A. S., KHAOLE, N., VILJOEN, D. L., JONES, K. L. & ROBINSON, L. K. 2005. A practical clinical approach to diagnosis of fetal alcohol spectrum disorders: clarification of the 1996 institute of medicine criteria. *Pediatrics*, 115, 39-47.
- HUANG, H., XUE, R., ZHANG, J., REN, T., RICHARDS, L. J., YAROWSKY, P., MILLER, M. I. & MORI, S. 2009. Anatomical characterization of human fetal brain development with diffusion tensor magnetic resonance imaging. *Journal of Neuroscience*, 29, 4263-4273.
- HUANG, H., ZHANG, J., WAKANA, S., ZHANG, W., REN, T., RICHARDS, L. J., YAROWSKY, P., DONOHUE, P., GRAHAM, E., VAN ZIJL, P. C. & MORI, S. 2006. White and gray matter development in human fetal, newborn and pediatric brains. *Neuroimage*, 33, 27-38.
- HUBER, P. J. 1964. Robust Estimation of a Location Parameter. *The Annals of Mathematical Statistics*, 73-101.
- HUISMAN, T. 2010. Diffusion-weighted and diffusion tensor imaging of the brain, made easy. *Cancer Imaging*, 10, S163.
- IDRUS, N. M., BREIT, K. R. & THOMAS, J. D. 2017. Dietary choline levels modify the effects of prenatal alcohol exposure in rats. *Neurotoxicology and Teratology*, 59, 43-52.
- INDER, T. E. & HUPPI, P. S. 2000. In vivo studies of brain development by magnetic resonance techniques. *Mental retardation and developmental disabilities research reviews*, 6, 59-67.
- INSTITUTE OF MEDICINE STANDING COMMITTEE ON THE SCIENTIFIC EVALUATION OF DIETARY REFERENCE INTAKES AND ITS PANEL ON FOLATE, O. B. V., AND CHOLINE 1998. Choline. *Dietary reference intakes for thiamin, riboflavin, niacin, vitamin B6, folate, vitamin B12, pantothenic acid, biotin, and choline*. National Academies Press (US).
- IRFANOGLU, M. O., NAYAK, A., JENKINS, J. & PIERPAOLI, C. TORTOISE v3: Improvements and new features of the NIH diffusion MRI processing pipeline. Program and proceedings of the ISMRM 25th annual meeting and exhibition, Honolulu, HI, USA, 2017.

- JACOBSON, S. W., CARTER, R. C., MOLTENO, C. D., MEINTJES, E. M., SENEKAL, M. S., LINDINGER, N. M., DODGE, N. C., ZEISEL, S. H., DUGGAN, C. P. & JACOBSON, J. L. 2018a. Feasibility and acceptability of maternal choline supplementation in heavy drinking pregnant women: a randomized, double-blind, placebo-controlled clinical trial. *Alcoholism: Clinical and Experimental Research*, 42, 1315-1326.
- JACOBSON, S. W., CARTER, R. C., MOLTENO, C. D., STANTON, M. E., HERBERT, J. S., LINDINGER, N. M., LEWIS, C. E., DODGE, N. C., HOYME, H. E., ZEISEL, S. H., MEINTJES, E. M., DUGGAN, C. P. & JACOBSON, J. L. 2018b. Efficacy of maternal choline supplementation during pregnancy in mitigating adverse effects of prenatal alcohol exposure on growth and cognitive function: a randomized, double-blind, placebo-controlled clinical trial. *Alcoholism: Clinical and Experimental Research*, 42, 1327-1341.
- JACOBSON, S. W., JACOBSON, J. L., MOLTENO, C. D., WARTON, C. M., WINTERMARK, P., HOYME, H. E., DE JONG, G., TAYLOR, P., WARTON, F. & LINDINGER, N. M. 2017. Heavy prenatal alcohol exposure is related to smaller corpus callosum in newborn MRI scans. *Alcoholism: Clinical and Experimental Research*, 41, 965-975.
- JACOBSON, S. W., JACOBSON, J. L., SOKOL, R. J., MARTIER, S. S. & AGER, J. W. 1993. Prenatal alcohol exposure and infant information processing ability. *Child development*, 64, 1706-1721.
- JACOBSON, S. W., STANTON, M. E., MOLTENO, C. D., BURDEN, M. J., FULLER, D. S., HOYME, H. E., ROBINSON, L. K., KHAOLE, N. & JACOBSON, J. L. 2008. Impaired eyeblink conditioning in children with fetal alcohol syndrome. *Alcoholism: Clinical and Experimental Research*, 32, 365-372.
- JANELLE, F., IORIO-MORIN, C., D'AMOUR, S. & FORTIN, D. 2022. Superior longitudinal fasciculus: a review of the anatomical descriptions with functional correlates. *Frontiers in Neurology*, 13, 794618.
- JELLISON, B. J., FIELD, A. S., MEDOW, J., LAZAR, M., SALAMAT, M. S. & ALEXANDER, A. L. 2004. Diffusion tensor imaging of cerebral white matter: a pictorial review of physics, fiber tract anatomy, and tumor imaging patterns. *American Journal of Neuroradiology*, 25, 356-369.
- JEURISSEN, B., DESCOTEAUX, M., MORI, S. & LEEMANS, A. 2019. Diffusion MRI fiber tractography of the brain. *NMR in Biomedicine*, 32, e3785.
- JONES, K. & SMITH, D. 1973. Recognition of the fetal alcohol syndrome in early infancy. *The Lancet*, 302, 999-1001.
- KABLE, J., COLES, C., KEEN, C. L., URIU-ADAMS, J., JONES, K., YEVTUSHOK, L., KULIKOVSKY, Y., WERTELECKI, W., PEDERSEN, T., CHAMBERS, C. & CIFASD

2015. The impact of micronutrient supplementation in alcohol-exposed pregnancies on information processing skills in Ukrainian infants. *Alcohol*, 49, 647-656.
- KABLE, J. A. & COLES, C. D. 2004. The impact of prenatal alcohol exposure on neurophysiological encoding of environmental events at six months. *Alcoholism: Clinical and Experimental Research*, 28, 489-496.
- KALIYADAN, F. & KULKARNI, V. 2019. Types of variables, descriptive statistics, and sample size. *Indian dermatology online journal*, 10, 82.
- KAR, P., REYNOLDS, J. E., GROHS, M. N., GIBBARD, W. B., MCMORRIS, C., TORTORELLI, C. & LEBEL, C. 2021. White matter alterations in young children with prenatal alcohol exposure. *Developmental Neurobiology*, 81, 400-410.
- KATTI, G., ARA, S. A. & SHIREEN, A. 2011. Magnetic resonance imaging (MRI)—A review. *International journal of dental clinics*, 3, 65-70.
- KEHOR, E. J. 2012. Eyeblick Conditioning *In*: SEEL, N. M. (ed.) *Encyclopedia of the Sciences of Learning*. First ed. Boston, MA: Springer US.
- KEVENAAR, J. T. & HOOGENRAAD, C. C. 2015. The axonal cytoskeleton: from organization to function. *Frontiers in molecular neuroscience*, 8, 44.
- KHAN, D. M., ALI, M., AHMAD, Z., MANZOOR, S. & HUSSAIN, S. 2021. A new efficient redescending M-estimator for robust fitting of linear regression models in the presence of outliers. *Mathematical Problems in Engineering*, 2021, 1-11.
- KHAN, S., VASUNG, L., MARAMI, B., ROLLINS, C. K., AFACAN, O., ORTINAU, C. M., YANG, E., WARFIELD, S. K. & GHOLIPOUR, A. 2019. Fetal brain growth portrayed by a spatiotemporal diffusion tensor MRI atlas computed from in utero images. *Neuroimage*, 185, 593-608.
- KIER, E. L., KIM, J. H., FULBRIGHT, R. K. & BRONEN, R. A. 1997. Embryology of the human fetal hippocampus: MR imaging, anatomy, and histology. *American journal of neuroradiology*, 18, 525-532.
- KLEIN, A., ULMER, J., QUINET, S., MATHEWS, V. & MARK, L. 2016. Nonmotor functions of the cerebellum: an introduction. *American Journal of Neuroradiology*, 37, 1005-1009.
- KOSTOVIC, I. & GOLDMAN-RAKIC, P. S. 1983. Transient cholinesterase staining in the mediodorsal nucleus of the thalamus and its connections in the developing human and monkey brain. *Journal of Comparative Neurology*, 219, 431-447.
- KOZANIAN, O. O., ROHAC, D. J., BAVADIAN, N., CORCHES, A., KORZUS, E. & HUFFMAN, K. J. 2018. Long-lasting effects of prenatal ethanol exposure on fear learning and development of the amygdala. *Frontiers in Behavioral Neuroscience*, 12, 200.
- KRZYSZTOF BLUSZTAJN, J. & J MELLOTT, T. 2012. Choline nutrition programs brain development via DNA and histone methylation. *Central Nervous System Agents in*

*Medicinal Chemistry (Formerly Current Medicinal Chemistry-Central Nervous System Agents)*, 12, 82-94.

- KYLLERMAN, M., ARONSON, M., SABEL, K. G., KARLBERG, E., SANDIN, B. & OLEGÅRD, R. 1985. Children of alcoholic mothers: Growth and motor performance compared to matched controls. *Acta Pædiatrica*, 74, 20-26.
- LANCIEGO, J. L., LUQUIN, N. & OBESO, J. A. 2012. Functional neuroanatomy of the basal ganglia. *Cold Spring Harbor perspectives in medicine*, 2, a009621.
- LANGE, S., PROBST, C., GMEL, G., REHM, J., BURD, L. & POPOVA, S. 2018. Global prevalence of fetal alcohol spectrum disorder among children and youth: a systematic review and meta-analysis. *Obstetrical & Gynecological Survey*, 73, 189-191.
- LAROBINA, M. & MURINO, L. 2014. Medical image file formats. *Journal of digital imaging*, 27, 200-206.
- LASSER, M., TIBER, J. & LOWERY, L. A. 2018. The role of the microtubule cytoskeleton in neurodevelopmental disorders. *Frontiers in cellular neuroscience*, 12, 165.
- LE BIHAN, D., MANGIN, J. F., POUPON, C., CLARK, C. A., PAPPATA, S., MOLKO, N. & CHABRIAT, H. 2001. Diffusion tensor imaging: concepts and applications. *Journal of Magnetic Resonance Imaging: An Official Journal of the International Society for Magnetic Resonance in Medicine*, 13, 534-546.
- LEBEL, C., RASMUSSEN, C., WYPER, K., ANDREW, G. & BEAULIEU, C. 2010. Brain microstructure is related to math ability in children with fetal alcohol spectrum disorder. *Alcoholism: Clinical and experimental research*, 34, 354-363.
- LEBEL, C., RASMUSSEN, C., WYPER, K., WALKER, L., ANDREW, G., YAGER, J. & BEAULIEU, C. 2008. Brain diffusion abnormalities in children with fetal alcohol spectrum disorder. *Alcoholism: Clinical and Experimental Research*, 32, 1732-1740.
- LEBEL, C., ROUSSOTTE, F. & SOWELL, E. R. 2011. Imaging the impact of prenatal alcohol exposure on the structure of the developing human brain. *Neuropsychology review*, 21, 102-118.
- LEE, T. & KIM, J. J. 2004. Differential effects of cerebellar, amygdalar, and hippocampal lesions on classical eyeblink conditioning in rats. *Journal of Neuroscience*, 24, 3242-3250.
- LEMIEUX, L., HAGEMANN, G., KRAKOW, K. & WOERMANN, F. G. 1999. Fast, accurate, and reproducible automatic segmentation of the brain in T1-weighted volume MRI data. *Magnetic Resonance in Medicine: An Official Journal of the International Society for Magnetic Resonance in Medicine*, 42, 127-135.
- LETOURNEAU, P. C. 2009. Actin in axons: stable scaffolds and dynamic filaments. *Cell Biology of the Axon*, 265-290.

- LEWIS, E. D., SUBHAN, F. B., BELL, R. C., MCCARGAR, L. J., CURTIS, J. M., JACOBS, R. L. & FIELD, C. J. 2014. Estimation of choline intake from 24 h dietary intake recalls and contribution of egg and milk consumption to intake among pregnant and lactating women in Alberta. *British journal of nutrition*, 112, 112-121.
- LEWIS, S. J., DOVE, A., ROBBINS, T. W., BARKER, R. A. & OWEN, A. M. 2004. Striatal contributions to working memory: a functional magnetic resonance imaging study in humans. *European Journal of Neuroscience*, 19, 755-760.
- LI, G., WANG, L., YAP, P.-T., WANG, F., WU, Z., MENG, Y., DONG, P., KIM, J., SHI, F. & REKIK, I. 2019. Computational neuroanatomy of baby brains: A review. *NeuroImage*, 185, 906-925.
- LI, L., COLES, C. D., LYNCH, M. E. & HU, X. 2009. Voxelwise and skeleton-based region of interest analysis of fetal alcohol syndrome and fetal alcohol spectrum disorders in young adults. *Human brain mapping*, 30, 3265-3274.
- LI, Q., SUN, J., GUO, L., ZANG, Y., FENG, Z., HUANG, X., YANG, H., LV, Y., HUANG, M. & GONG, Q. 2010. Increased fractional anisotropy in white matter of the right frontal region in children with attention-deficit/hyperactivity disorder: a diffusion tensor imaging study. *Neuroendocrinology Letters*, 31, 747.
- LI, X., MORGAN, P. S., ASHBURNER, J., SMITH, J. & RORDEN, C. 2016. The first step for neuroimaging data analysis: DICOM to NIfTI conversion. *Journal of neuroscience methods*, 264, 47-56.
- LIU, T., GAO, F., ZHENG, W., YOU, Y., ZHAO, Z., LV, Y., CHEN, W., ZHANG, H., JI, C. & WU, D. 2021. Diffusion MRI of the infant brain reveals unique asymmetry patterns during the first-half-year of development. *Neuroimage*, 242, 118465.
- LLANO, D. A. 2013. Functional imaging of the thalamus in language. *Brain and Language*, 126, 62-72.
- LOGAN, C. G. & GRAFTON, S. T. 1995. Functional anatomy of human eyeblink conditioning determined with regional cerebral glucose metabolism and positron-emission tomography. *Proceedings of the National Academy of Sciences*, 92, 7500-7504.
- LONDON, L. 1999. The 'dop' system, alcohol abuse and social control amongst farm workers in South Africa: a public health challenge. *Social Science & Medicine*, 48, 1407-1414.
- LONG, X. & LEBEL, C. 2022. Evaluation of brain alterations and behavior in children with low levels of prenatal alcohol exposure. *JAMA Network Open*, 5, e225972-e225972.
- MA, X., COLES, C. D., LYNCH, M. E., LACONTE, S. M., ZURKIYA, O., WANG, D. & HU, X. 2005. Evaluation of corpus callosum anisotropy in young adults with fetal alcohol syndrome according to diffusion tensor imaging. *Alcoholism: Clinical and Experimental Research*, 29, 1214-1222.

- MAIER, S. E. & WEST, J. R. 2001. Drinking patterns and alcohol-related birth defects. *Alcohol Research & Health*, 25, 168.
- MAKROPOULOS, A., ROBINSON, E. C., SCHUH, A., WRIGHT, R., FITZGIBBON, S., BOZEK, J., COUNSELL, S. J., STEINWEG, J., VECCHIATO, K., PASSERAT-PALMBACH, J., LENZ, G., MORTARI, F., TENEV, T., DUFF, E. P., BASTIANI, M., CORDERO-GRANDE, L., HUGHES, E., TUSOR, N., TOURNIER, J.-D., HUTTER, J., PRICE, A. N., TEIXEIRA, R. P. A. G., MURGASOVA, M., VICTOR, S., KELLY, C., RUTHERFORD, M. A., SMITH, S. M., EDWARDS, A. D., HAJNAL, J. V., JENKINSON, M. & RUECKERT, D. 2018. The developing human connectome project: A minimal processing pipeline for neonatal cortical surface reconstruction. *Neuroimage*, 173, 88-112.
- MANN, H. B. & WHITNEY, D. R. 1947. On a test of whether one of two random variables is stochastically larger than the other. *The annals of mathematical statistics*, 50-60.
- MANTO, M., BOWER, J. M., CONFORTO, A. B., DELGADO-GARCÍA, J. M., DA GUARDA, S. N. F., GERWIG, M., HABAS, C., HAGURA, N., IVRY, R. B. & MARIËN, P. 2012. Consensus paper: roles of the cerebellum in motor control—the diversity of ideas on cerebellar involvement in movement. *The Cerebellum*, 11, 457-487.
- MATTSON, S. N., JERNIGAN, T. L. & RILEY, E. P. 1994. MRI and prenatal alcohol exposure: Images provide insight into FAS. *Alcohol Health and Research World*, 18, 49.
- MATTSON, S. N. & RILEY, E. P. 2000. Parent ratings of behavior in children with heavy prenatal alcohol exposure and IQ-matched controls. *Alcoholism: Clinical and Experimental Research*, 24, 226-231.
- MATTSON, S. N., RILEY, E. P., DELIS, D. C., STERN, C. & JONES, K. L. 1996a. Verbal learning and memory in children with fetal alcohol syndrome. *Alcoholism: Clinical and Experimental Research*, 20, 810-816.
- MATTSON, S. N., RILEY, E. P., GRAMLING, L., DELIS, D. C. & JONES, K. L. 1998. Neuropsychological comparison of alcohol-exposed children with or without physical features of fetal alcohol syndrome. *Neuropsychology*, 12, 146.
- MATTSON, S. N., RILEY, E. P., SOWELL, E. R., JERNIGAN, T. L., SOBEL, D. F. & JONES, K. L. 1996b. A decrease in the size of the basal ganglia in children with fetal alcohol syndrome. *Alcoholism: Clinical and Experimental Research*, 20, 1088-1093.
- MATTSON, S. N., SCHOENFELD, A. M. & RILEY, E. P. 2001. Teratogenic effects of alcohol on brain and behavior. *Alcohol Research & Health*, 25, 185.
- MAY, P. A., DE VRIES, M. M., MARAIS, A. S., KALBERG, W. O., BUCKLEY, D., HASKEN, J. M., ABDUL-RAHMAN, O., ROBINSON, L. K., MANNING, M. A. & SEEDAT, S. 2022. The prevalence of fetal alcohol spectrum disorders in rural communities in South

- Africa: A third regional sample of child characteristics and maternal risk factors. *Alcoholism: Clinical and Experimental Research*, 46, 1819-1836.
- MAY, P. A. & GOSSAGE, J. P. 2011. Maternal risk factors for fetal alcohol spectrum disorders: not as simple as it might seem. *Alcohol Research & Health*, 34, 15.
- MAY, P. A., MARAIS, A.-S., DE VRIES, M., HASKEN, J. M., STEGALL, J. M., HEDRICK, D. M., SNELL, C. L., SEEDAT, S. & PARRY, C. D. 2019. The Dop System of Alcohol Distribution is Dead, but It's Legacy Lives On.... *International journal of environmental research and public health*, 16, 3701.
- MECK, W. H. & WILLIAMS, C. L. 2003. Metabolic imprinting of choline by its availability during gestation: implications for memory and attentional processing across the lifespan. *Neuroscience & Biobehavioral Reviews*, 27, 385-399.
- MENDOZA, J. E. 2011. Projection Pathways *Encyclopedia of Clinical Neuropsychology*. New York, NY: Springer New York.
- MENG, H., ZHANG, Z., GENG, H., LIN, X., FENG, L., TENG, G., FANG, F., ZANG, F. & LIU, S. 2012. Development of the subcortical brain structures in the second trimester: assessment with 7.0-T MRI. *Neuroradiology*, 54, 1153-1159.
- MENON, V., ANAGNOSON, R. T., GLOVER, G. H. & PFEFFERBAUM, A. 2000. Basal ganglia involvement in memory-guided movement sequencing. *Neuroreport*, 11, 3641-3645.
- MERKOW, M. B., BURKE, J. F. & KAHANA, M. J. 2015. The human hippocampus contributes to both the recollection and familiarity components of recognition memory. *Proceedings of the National Academy of Sciences*, 112, 14378-14383.
- MIALL, R. C., IMAMIZU, H. & MIYAUCHI, S. 2000. Activation of the cerebellum in co-ordinated eye and hand tracking movements: an fMRI study. *Experimental Brain Research*, 135, 22-33.
- MIKHEEV, A., NEVSKY, G., GOVINDAN, S., GROSSMAN, R. & RUSINEK, H. 2008. Fully automatic segmentation of the brain from T1-weighted MRI using Bridge Burner algorithm. *Journal of Magnetic Resonance Imaging*, 27, 1235-1241.
- MISHRA, P., SINGH, U., PANDEY, C. M., MISHRA, P. & PANDEY, G. 2019. Application of student's t-test, analysis of variance, and covariance. *Annals of cardiac anaesthesia*, 22, 407.
- MITCHELL, A. S. 2015. The mediodorsal thalamus as a higher order thalamic relay nucleus important for learning and decision-making. *Neuroscience & Biobehavioral Reviews*, 54, 76-88.
- MITCHELL, A. S. & DALRYMPLE-ALFORD, J. C. 2005. Dissociable memory effects after medial thalamus lesions in the rat. *European Journal of Neuroscience*, 22, 973-985.

- MOBLEY, A. S. 2019. Adult Neurogenesis in the Hippocampus. *Neural stem cells and adult neurogenesis*. Academic Press.
- MOLE, J. P. 2018. *The white matter microstructure of the basal ganglia circuitry and its changes in Parkinson's disease*. Cardiff University.
- MOORE, A. B., LI, Z., TYNER, C. E., HU, X. & CROSSON, B. 2013. Bilateral basal ganglia activity in verbal working memory. *Brain and language*, 125, 316-323.
- MOORE, E. M., MIGLIORINI, R., INFANTE, M. A. & RILEY, E. P. 2014. Fetal alcohol spectrum disorders: recent neuroimaging findings. *Current developmental disorders reports*, 1, 161-172.
- MOORE, E. M. & XIA, Y. 2022. Neurodevelopmental trajectories following prenatal alcohol exposure. *Frontiers in Human Neuroscience*, 15, 695855.
- MORELL, P. 2013. *Myelin*, Springer Science & Business Media.
- MORETTI, R., BAVA, A., TORRE, P., ANTONELLO, R. M. & CAZZATO, G. 2002. Reading errors in patients with cerebellar vermis lesions. *Journal of neurology*, 249, 461-468.
- MOREY, R. A., PETTY, C. M., XU, Y., HAYES, J. P., WAGNER II, H. R., LEWIS, D. V., LABAR, K. S., STYNER, M. & MCCARTHY, G. 2009. A comparison of automated segmentation and manual tracing for quantifying hippocampal and amygdala volumes. *Neuroimage*, 45, 855-866.
- MORI, S., WAKANA, S., VAN ZIJL, P. C. & NAGAE-POETSCHER, L. 2005. *MRI atlas of human white matter*, Elsevier.
- MORI, S. & ZHANG, J. 2006. Principles of diffusion tensor imaging and its applications to basic neuroscience research. *Neuron*, 51, 527-539.
- MTUI, E., GRUENER, G. & DOCKERY, P. 2020. *Fitzgerald's Clinical Neuroanatomy and Neuroscience E-Book*, Elsevier Health Sciences.
- MUDD, A. T., GETTY, C. M. & DILGER, R. N. 2018. Maternal dietary choline status influences brain gray and white matter development in young pigs. *Current developments in nutrition*, 2, nzy015.
- NGUYEN, T. T., RISBUD, R. D., MATTSON, S. N., CHAMBERS, C. D. & THOMAS, J. D. 2016. Randomized, double-blind, placebo-controlled clinical trial of choline supplementation in school-aged children with fetal alcohol spectrum disorders. *The American journal of clinical nutrition*, 104, 1683-1692.
- NIKOLIĆ, I. & KOSTOVIĆ, I. 1986. Development of the lateral amygdaloid nucleus in the human fetus: transient presence of discrete cytoarchitectonic units. *Anatomy and embryology*, 174, 355-360.

- O'CONNOR, M. J., SHAH, B., WHALEY, S., CRONIN, P., GUNDERSON, B. & GRAHAM, J. 2002. Psychiatric illness in a clinical sample of children with prenatal alcohol exposure. *The American journal of drug and alcohol abuse*, 28, 743-754.
- O'HARE, E. D., KAN, E., YOSHII, J., MATTSON, S. N., RILEY, E. P., THOMPSON, P. M., TOGA, A. W. & SOWELL, E. R. 2005. Mapping cerebellar vermal morphology and cognitive correlates in prenatal alcohol exposure. *Neuroreport*, 16, 1285-1290.
- O'CONNAILL, C. R., MALISZA, K. L., BUSS, J. L., BOLSTER, R. B., CLANCY, C., DE GERVAI, P. D., CHUDLEY, A. E. & LONGSTAFFE, S. 2015. Visual search for feature conjunctions: an fMRI study comparing alcohol-related neurodevelopmental disorder (ARND) to ADHD. *Journal of neurodevelopmental disorders*, 7, 1-18.
- OISHI, K., CHANG, L. & HUANG, H. 2019. Baby brain atlases. *Neuroimage*, 185, 865-880.
- OISHI, K., MORI, S., DONOHUE, P. K., ERNST, T., ANDERSON, L., BUCHTHAL, S., FARIA, A., JIANG, H., LI, X. & MILLER, M. I. 2011. Multi-contrast human neonatal brain atlas: application to normal neonate development analysis. *Neuroimage*, 56, 8-20.
- OLSON, H. C., FELDMAN, J. J., STREISSGUTH, A. P., SAMPSON, P. D. & BOOKSTEIN, F. L. 1998. Neuropsychological deficits in adolescents with fetal alcohol syndrome: Clinical findings. *Alcoholism: Clinical and Experimental Research*, 22, 1998-2012.
- OLSON, H. C., STREISSGUTH, A. P., SAMPSON, P. D., BARR, H. M., BOOKSTEIN, F. L. & THIEDE, K. 1997. Association of prenatal alcohol exposure with behavioral and learning problems in early adolescence. *Journal of the American Academy of Child & Adolescent Psychiatry*, 36, 1187-1194.
- OUCHI, Y., OKADA, H., YOSHIKAWA, E., NOBEZAWA, S. & FUTATSUBASHI, M. 1999. Brain activation during maintenance of standing postures in humans. *Brain*, 122, 329-338.
- PANNEK, K., GEORGE, J. M., BOYD, R. N., COLDITZ, P. B., ROSE, S. E. & FRIPP, J. 2020. Brain microstructure and morphology of very preterm-born infants at term equivalent age: associations with motor and cognitive outcomes at 1 and 2 years. *Neuroimage*, 221, 117163.
- PAOLOZZA, A., TREIT, S., BEAULIEU, C. & REYNOLDS, J. N. 2014. Response inhibition deficits in children with Fetal Alcohol Spectrum Disorder: Relationship between diffusion tensor imaging of the corpus callosum and eye movement control. *NeuroImage: Clinical*, 5, 53-61.
- PAOLOZZA, A., TREIT, S., BEAULIEU, C. & REYNOLDS, J. N. 2017. Diffusion tensor imaging of white matter and correlates to eye movement control and psychometric testing in children with prenatal alcohol exposure. *Human Brain Mapping*, 38, 444-456.

- PARAB, S. & BHALERAO, S. 2010. Choosing statistical test. *International journal of Ayurveda research*, 1, 187.
- PARIKH, M., CHEN, M., BRAIMAH, A., KLINE, J., MCNALLY, K., LOGAN, J., TAMM, L., YEATES, K., YUAN, W. & HE, L. 2021. Diffusion MRI microstructural abnormalities at term-equivalent age are associated with neurodevelopmental outcomes at 3 years of age in very preterm infants. *American Journal of Neuroradiology*, 42, 1535-1542.
- PATTEN, A. R., FONTAINE, C. J. & CHRISTIE, B. R. 2014. A comparison of the different animal models of fetal alcohol spectrum disorders and their use in studying complex behaviors. *Frontiers in pediatrics*, 2, 93.
- PETERSON, D. J., RYAN, M., RIMRODT, S. L., CUTTING, L. E., DENCKLA, M. B., KAUFMANN, W. E. & MAHONE, E. M. 2011. Increased regional fractional anisotropy in highly screened attention-deficit hyperactivity disorder (ADHD). *Journal of child neurology*, 26, 1296-1302.
- PIERPAOLI, C., WALKER, L., IRFANOGLU, M. O., BARNETT, A., BASSER, P., CHANG, L.-C., KOAY, C., PAJEVIC, S., ROHDE, G. & SARLLS, J. TORTOISE: an integrated software package for processing of diffusion MRI data. ISMRM 18th annual meeting, 2010. Stockholm.
- POPOVA, S., LANGE, S., PROBST, C., GMEL, G. & REHM, J. 2017. Estimation of national, regional, and global prevalence of alcohol use during pregnancy and fetal alcohol syndrome: a systematic review and meta-analysis. *The Lancet Global Health*, 5, e290-e299.
- POSSE DE CHAVES, E., VANCE, D., CAMPENOT, R. & VANCE, J. 1995a. Alkylphosphocholines inhibit choline uptake and phosphatidylcholine biosynthesis in rat sympathetic neurons and impair axonal extension. *Biochemical Journal*, 312, 411-417.
- POSSE DE CHAVES, E., VANCE, D. E., CAMPENOT, R. B. & VANCE, J. E. 1995b. Axonal synthesis of phosphatidylcholine is required for normal axonal growth in rat sympathetic neurons. *The Journal of cell biology*, 128, 913-918.
- PRAYER, D., KASPRIAN, G., KRAMPL, E., ULM, B., WITZANI, L., PRAYER, L. & BRUGGER, P. C. 2006. MRI of normal fetal brain development. *European journal of radiology*, 57, 199-216.
- PRICE, C. J., WISE, R., WATSON, J. D., PATTERSON, K., HOWARD, D. & FRACKOWIAK, R. 1994. Brain activity during reading The effects of exposure duration and task. *Brain*, 117, 1255-1269.
- RAFAL, R. D. & POSNER, M. I. 1987. Deficits in human visual spatial attention following thalamic lesions. *Proceedings of the National Academy of Sciences*, 84, 7349-7353.

- RASMUSSEN, C., MCAULEY, R. & ANDREW, G. 2007. Parental ratings of children with fetal alcohol spectrum disorder on the behavior rating inventory of executive function (BRIEF). *J FAS Int*, 5, 1-8.
- RINALDI, A., OLIVERIO, A. & MELE, A. 2012. Spatial memory, plasticity and nucleus accumbens. *Reviews in the Neurosciences*, 23, 527-541.
- ROEBUCK, T. M., SIMMONS, R. W., MATTSON, S. N. & RILEY, E. P. 1998. Prenatal exposure to alcohol affects the ability to maintain postural balance. *Alcoholism: Clinical and Experimental Research*, 22, 252-258.
- ROSEN, M. L., STERN, C. E., DEVANEY, K. J. & SOMERS, D. C. 2018. Cortical and subcortical contributions to long-term memory-guided visuospatial attention. *Cerebral Cortex*, 28, 2935-2947.
- ROSS, R. S., LOPRESTI, M. L., SCHON, K. & STERN, C. E. 2013. Role of the hippocampus and orbitofrontal cortex during the disambiguation of social cues in working memory. *Cognitive, Affective, & Behavioral Neuroscience*, 13, 900-915.
- ROUSSOTTE, F. F., SULIK, K. K., MATTSON, S. N., RILEY, E. P., JONES, K. L., ADNAMS, C. M., MAY, P. A., O'CONNOR, M. J., NARR, K. L. & SOWELL, E. R. 2012. Regional brain volume reductions relate to facial dysmorphology and neurocognitive function in fetal alcohol spectrum disorders. *Human brain mapping*, 33, 920-937.
- RUBIN, R. D., WATSON, P. D., DUFF, M. C. & COHEN, N. J. 2014. The role of the hippocampus in flexible cognition and social behavior. *Frontiers in human neuroscience*, 8, 742.
- SAAD, Z. S. & REYNOLDS, R. C. 2012. Suma. *Neuroimage*, 62, 768-773.
- SAAD, Z. S., REYNOLDS, R. C., ARGALL, B., JAPEE, S. & COX, R. W. SUMA: an interface for surface-based intra-and inter-subject analysis with AFNI. 2004 2nd IEEE International Symposium on Biomedical Imaging: Nano to Macro (IEEE Cat No. 04EX821), 2004. IEEE, 1510-1513.
- SALAT, D. H., LEE, S. Y., YU, P., SETTY, B., ROSAS, H. D. & GRANT, P. E. 2009. DTI in development and aging. *Diffusion MRI*, 205-236.
- SALOMON, L. & GAREL, C. 2007. Magnetic resonance imaging examination of the fetal brain. *Ultrasound in Obstetrics and Gynecology: The Official Journal of the International Society of Ultrasound in Obstetrics and Gynecology*, 30, 1019-1032.
- SANTHANAM, P., COLES, C. D., LI, Z., LI, L., LYNCH, M. E. & HU, X. 2011. Default mode network dysfunction in adults with prenatal alcohol exposure. *Psychiatry Research: Neuroimaging*, 194, 354-362.
- SARKAR, D. K., GANGISETTY, O., WOZNIAK, J. R., ECKERLE, J. K., GEORGIEFF, M. K., FOROUD, T. M., WETHERILL, L., WERTELECKI, W., CHAMBERS, C. D., RILEY, E.,

- ZYMAK-ZAKUTNY, N. & YEVTUSHOK, L. 2019. Persistent changes in stress-regulatory genes in pregnant women or children exposed prenatally to alcohol. *Alcoholism: Clinical and Experimental Research*, 43, 1887-1897.
- SCHNEIDER, R. D. & THOMAS, J. D. 2016. Adolescent choline supplementation attenuates working memory deficits in rats exposed to alcohol during the third trimester equivalent. *Alcoholism: Clinical and Experimental Research*, 40, 897-905.
- SEGER, C. A. & CINCOTTA, C. M. 2005. The roles of the caudate nucleus in human classification learning. *Journal of Neuroscience*, 25, 2941-2951.
- SETLOW, B. 1997. The nucleus accumbens and learning and memory. *Journal of neuroscience research*, 49, 515-521.
- SHORT, S. J., ELISON, J. T., GOLDMAN, B. D., STYNER, M., GU, H., CONNELLY, M., MALTBIE, E., WOOLSON, S., LIN, W. & GERIG, G. 2013. Associations between white matter microstructure and infants' working memory. *Neuroimage*, 64, 156-166.
- SILK, T. J., VANCE, A., RINEHART, N., BRADSHAW, J. L. & CUNNINGTON, R. 2009. White-matter abnormalities in attention deficit hyperactivity disorder: A diffusion tensor imaging study. *Human brain mapping*, 30, 2757-2765.
- SNOOK, L., PLEWES, C. & BEAULIEU, C. 2007. Voxel based versus region of interest analysis in diffusion tensor imaging of neurodevelopment. *Neuroimage*, 34, 243-252.
- SOTIROPOULOS, S. N. & ZALESKY, A. 2019. Building connectomes using diffusion MRI: why, how and but. *NMR in Biomedicine*, 32, e3752.
- SOWELL, E. R., JOHNSON, A., KAN, E., LU, L. H., VAN HORN, J. D., TOGA, A. W., O'CONNOR, M. J. & BOOKHEIMER, S. Y. 2008. Mapping white matter integrity and neurobehavioral correlates in children with fetal alcohol spectrum disorders. *Journal of Neuroscience*, 28, 1313-1319.
- SPOTTISWOODE, B. S., MEINTJES, E. M., ANDERSON, A. W., MOLTENO, C. D., STANTON, M. E., DODGE, N. C., GORE, J. C., PETERSON, B. S., JACOBSON, J. L. & JACOBSON, S. W. 2011. Diffusion tensor imaging of the cerebellum and eyeblink conditioning in fetal alcohol spectrum disorder. *Alcoholism: Clinical and Experimental Research*, 35, 2174-2183.
- STADELMANN, C., TIMMLER, S., BARRANTES-FREER, A. & SIMONS, M. 2019. Myelin in the central nervous system: structure, function, and pathology. *Physiological reviews*, 99, 1381-1431.
- STANDRING, S. 2021. Diencephalon. *Gray's Anatomy*. Fourth Edition ed.: Elsevier Limited.
- STEPHENS, R. L., LANGWORTHY, B. W., SHORT, S. J., GIRAULT, J. B., STYNER, M. A. & GILMORE, J. H. 2020. White matter development from birth to 6 years of age: a longitudinal study. *Cerebral Cortex*, 30, 6152-6168.

- STREISSGUTH, A. P., BARR, H. M., OLSON, H. C., SAMPSON, P. D., BOOKSTEIN, F. L. & BURGESS, D. M. 1994. Drinking during pregnancy decreases word attack and arithmetic scores on standardized tests: Adolescent data from a population-based prospective study. *Alcoholism: Clinical and Experimental Research*, 18, 248-254.
- STUDENT 1908. The probable error of a mean. *Biometrika*, 6, 1-25.
- SULLIVAN, E. V., ADALSTEINSSON, E., HEDEHUS, M., JU, C., MOSELEY, M., LIM, K. O. & PFEFFERBAUM, A. 2001. Equivalent disruption of regional white matter microstructure in ageing healthy men and women. *Neuroreport*, 12, 99-104.
- SZABO, E. F. 2015. E. In: FRED, E. S. (ed.) *The Linear Algebra Survival Guide*. Boston: Academic Press.
- TAKAHASHI, E., HAYASHI, E., SCHMAHMANN, J. D. & GRANT, P. E. 2014. Development of cerebellar connectivity in human fetal brains revealed by high angular resolution diffusion tractography. *Neuroimage*, 96, 326-333.
- TAYLOR, P. A., CHEN, G., COX, R. W. & SAAD, Z. S. 2016. Open environment for multimodal interactive connectivity visualization and analysis. *Brain connectivity*, 6, 109-121.
- TAYLOR, P. A., CHO, K.-H., LIN, C.-P. & BISWAL, B. B. 2012. Improving DTI tractography by including diagonal tract propagation.
- TAYLOR, P. A., JACOBSON, S. W., VAN DER KOUWE, A., MOLTENO, C. D., CHEN, G., WINTERMARK, P., ALHAMUD, A., JACOBSON, J. L. & MEINTJES, E. M. 2015. A DTI-based tractography study of effects on brain structure associated with prenatal alcohol exposure in newborns. *Human brain mapping*, 36, 170-186.
- TAYLOR, P. A. & SAAD, Z. S. 2013. FATCAT:(an efficient) functional and tractographic connectivity analysis toolbox. *Brain connectivity*, 3, 523-535.
- THOMAS, J. D., ABOU, E. J. & DOMINGUEZ, H. D. 2009. Prenatal choline supplementation mitigates the adverse effects of prenatal alcohol exposure on development in rats. *Neurotoxicology and teratology*, 31, 303-311.
- THOMAS, J. D., GARRISON, M. & O'NEILL, T. M. 2004. Perinatal choline supplementation attenuates behavioral alterations associated with neonatal alcohol exposure in rats. *Neurotoxicology and teratology*, 26, 35-45.
- THOMAS, J. D., LA FIETTE, M. H., QUINN, V. R. & RILEY, E. P. 2000. Neonatal choline supplementation ameliorates the effects of prenatal alcohol exposure on a discrimination learning task in rats. *Neurotoxicology and teratology*, 22, 703-711.
- TRAN, T. & THOMAS, J. Perinatal choline supplementation mitigates trace eyeblink conditioning deficits associated with 3rd trimester alcohol exposure in rodents. *Soc Neurosci Abstr*, 2007. 746.

- TREIT, S., LABEL, C., BAUGH, L., RASMUSSEN, C., ANDREW, G. & BEAULIEU, C. 2013. Longitudinal MRI reveals altered trajectory of brain development during childhood and adolescence in fetal alcohol spectrum disorders. *Journal of Neuroscience*, 33, 10098-10109.
- TZIORTZI, A. C., HABER, S. N., SEARLE, G. E., TSOUMPAS, C., LONG, C. J., SHOTBOLT, P., DOUAUD, G., JBABDI, S., BEHRENS, T. E., RABINER, E. A., JENKINSON, M. & GUNN, R. N. 2014. Connectivity-based functional analysis of dopamine release in the striatum using diffusion-weighted MRI and positron emission tomography. *Cerebral cortex*, 24, 1165-1177.
- VAN DER WERF, Y. D., SCHELTENS, P., LINDEBOOM, J., WITTER, M. P., UYLINGS, H. B. & JOLLES, J. 2003. Deficits of memory, executive functioning and attention following infarction in the thalamus; a study of 22 cases with localised lesions. *Neuropsychologia*, 41, 1330-1344.
- VAN GEUNS, R.-J. M., WIELOPOLSKI, P. A., DE BRUIN, H. G., RENSING, B. J., VAN OOIJEN, P. M., HULSHOFF, M., OUDKERK, M. & DE FEYTER, P. J. 1999. Basic principles of magnetic resonance imaging. *Progress in cardiovascular diseases*, 42, 149-156.
- VAN HECKE, W., LEEMANS, A. & EMSELL, L. 2016. DTI analysis methods: voxel-based analysis. *Diffusion tensor imaging: A practical handbook*, 183-203.
- VIÑAS-GUASCH, N. & WU, Y. J. 2017. The role of the putamen in language: a meta-analytic connectivity modeling study. *Brain Structure and Function*, 222, 3991-4004.
- VISSER, J. E. & BLOEM, B. R. 2005. Role of the basal ganglia in balance control. *Neural plasticity*, 12, 161-174.
- VOS, S. B., JONES, D. K., VIERGEVER, M. A. & LEEMANS, A. 2011. Partial volume effect as a hidden covariate in DTI analyses. *Neuroimage*, 55, 1566-1576.
- WANG, Y., HAGHPANAH, F. S., ZHANG, X., SANTAMARIA, K., DA COSTA AGUIAR ALVES, G. K., BRUNO, E., AW, N., MADDOCKS, A., DUARTE, C. S., MONK, C., LAINE, A. & POSNE, J. 2022. ID-Seg: An infant deep learning-based segmentation framework to improve limbic structure estimates. *Brain Informatics*, 9, 12.
- WARTON, F. L., MOLTENO, C. D., WARTON, C. M., WINTERMARK, P., LINDINGER, N. M., DODGE, N. C., ZÖLLEI, L., VAN DER KOUWE, A. J., CARTER, R. C., JACOBSON, J. L., JACOBSON, S. W. & MEINTJES, E. M. 2021. Maternal choline supplementation mitigates alcohol exposure effects on neonatal brain volumes. *Alcoholism: Clinical and Experimental Research*, 45, 1762-1774.
- WELCH, B. L. 1947. The generalization of 'STUDENT'S' problem when several different population variances are involved. *Biometrika*, 34, 28-35.

- WELKER, K. M. & PATTON, A. Assessment of normal myelination with magnetic resonance imaging. *Seminars in neurology*, 2012. Thieme Medical Publishers, 015-028.
- WILLIAMS, G. 2016. Slaves, workers, and wine: the 'Dop system' in the history of the Cape Wine industry, 1658–1894. *Journal of Southern African Studies*, 42, 893-909.
- WILLOUGHBY, K. A., SHEARD, E. D., NASH, K. & ROVET, J. 2008. Effects of prenatal alcohol exposure on hippocampal volume, verbal learning, and verbal and spatial recall in late childhood. *Journal of the International Neuropsychological Society*, 14, 1022-1033.
- WINSTON, G. P. 2012. The physical and biological basis of quantitative parameters derived from diffusion MRI. *Quantitative imaging in medicine and surgery*, 2, 254.
- WOZNIAK, J. R., FINK, B. A., FUGLESTAD, A. J., ECKERLE, J. K., BOYS, C. J., SANDNESS, K. E., RADKE, J. P., MILLER, N. C., LINDGREN, C., BREARLEY, A. M., ZEISEL, S. H. & GEORGIEFF, M. K. 2020. Four-year follow-up of a randomized controlled trial of choline for neurodevelopment in fetal alcohol spectrum disorder. *Journal of Neurodevelopmental Disorders*, 12, 1-13.
- WOZNIAK, J. R., FUGLESTAD, A. J., ECKERLE, J. K., FINK, B. A., HOECKER, H. L., BOYS, C. J., RADKE, J. P., KROUPINA, M. G., MILLER, N. C., BREARLEY, A. M., ZEISEL, S. H. & GEORGIEFF, M. K. 2015. Choline supplementation in children with fetal alcohol spectrum disorders: a randomized, double-blind, placebo-controlled trial. *The American journal of clinical nutrition*, 102, 1113-1125.
- WOZNIAK, J. R., FUGLESTAD, A. J., ECKERLE, J. K., KROUPINA, M. G., MILLER, N. C., BOYS, C. J., BREARLEY, A. M., FINK, B. A., HOECKER, H. L., ZEISEL, S. H. & GEORGIEFF, M. K. 2013. Choline supplementation in children with fetal alcohol spectrum disorders has high feasibility and tolerability. *Nutrition research*, 33, 897-904.
- WOZNIAK, J. R., MUELLER, B. A., CHANG, P. N., MUETZEL, R. L., CAROS, L. & LIM, K. O. 2006. Diffusion tensor imaging in children with fetal alcohol spectrum disorders. *Alcoholism: Clinical and Experimental Research*, 30, 1799-1806.
- WOZNIAK, J. R., MUETZEL, R. L., MUELLER, B. A., MCGEE, C. L., FREERKS, M. A., WARD, E. E., NELSON, M. L., CHANG, P. N. & LIM, K. O. 2009. Microstructural corpus callosum anomalies in children with prenatal alcohol exposure: an extension of previous diffusion tensor imaging findings. *Alcoholism: Clinical and Experimental Research*, 33, 1825-1835.
- XU, Z., MARSZALEK, J. R., LEE, M. K., WONG, P. C., FOLMER, J., CRAWFORD, T. O., HSIEH, S.-T., GRIFFIN, J. W. & CLEVELAND, D. W. 1996. Subunit composition of neurofilaments specifies axonal diameter. *The Journal of cell biology*, 133, 1061-1069.

- XUAN, B., MACKIE, M.-A., SPAGNA, A., WU, T., TIAN, Y., HOF, P. R. & FAN, J. 2016. The activation of interactive attentional networks. *Neuroimage*, 129, 308-319.
- YAP, B. W. & SIM, C. H. 2011. Comparisons of various types of normality tests. *Journal of Statistical Computation and Simulation*, 81, 2141-2155.
- YU, A. & TUBBS, R. S. 2023. Embryonic Development and Myelination of the Corpus Callosum. *The Corpus Callosum: Embryology, Neuroanatomy, Neurophysiology, Neuropathology, and Surgery*, 17-24.
- YUEN, K. K. 1974. The two-sample trimmed t for unequal population variances. *Biometrika*, 61, 165-170.
- ZEISEL, S. H. The supply of choline is important for fetal progenitor cells. *Seminars in cell & developmental biology*, 2011. Elsevier, 624-628.
- ZEISEL, S. H. 2013. Nutrition in pregnancy: the argument for including a source of choline. *International journal of women's health*, 193-199.
- ZEISEL, S. H., KLATT, K. C. & CAUDILL, M. A. 2018. Choline. *Advances in nutrition*, 9, 58-60.
- ZHANG, J., EVANS, A., HERMOYE, L., LEE, S.-K., WAKANA, S., ZHANG, W., DONOHUE, P., MILLER, M. I., HUANG, H. & WANG, X. 2007. Evidence of slow maturation of the superior longitudinal fasciculus in early childhood by diffusion tensor imaging. *Neuroimage*, 38, 239-247.
- ZÖLLEI, L., IGLESIAS, J. E., OU, Y., GRANT, P. E. & FISCHL, B. 2020. Infant FreeSurfer: An automated segmentation and surface extraction pipeline for T1-weighted neuroimaging data of infants 0–2 years. *Neuroimage*, 218, 116946.